



National Library  
of Canada

Bibliothèque nationale  
du Canada

Canadian Theses Service

Services des thèses canadiennes

Ottawa, Canada  
K1A 0N4

## CANADIAN THESES

## THÈSES CANADIENNES

### NOTICE

The quality of this microfiche is heavily dependent upon the quality of the original thesis submitted for microfilming. Every effort has been made to ensure the highest quality of reproduction possible.

If pages are missing, contact the university which granted the degree.

Some pages may have indistinct print especially if the original pages were typed with a poor typewriter ribbon or if the university sent us an inferior photocopy.

Previously copyrighted materials (journal articles, published tests, etc.) are not filmed.

Reproduction in full or in part of this film is governed by the Canadian Copyright Act, R.S.C. 1970, c. C-30.

**THIS DISSERTATION  
HAS BEEN MICROFILMED  
EXACTLY AS RECEIVED**

### AVIS

La qualité de cette microfiche dépend grandement de la qualité de la thèse soumise au microfilmage. Nous avons tout fait pour assurer une qualité supérieure de reproduction.

S'il manque des pages, veuillez communiquer avec l'université qui a conféré le grade.

La qualité d'impression de certaines pages peut laisser à désirer, surtout si les pages originales ont été dactylographiées à l'aide d'un ruban usé ou si l'université nous a fait parvenir une photocopie de qualité inférieure.

Les documents qui font déjà l'objet d'un droit d'auteur (articles de revue, examens publiés, etc.) ne sont pas microfilmés.

La reproduction, même partielle, de ce microfilm est soumise à la Loi canadienne sur le droit d'auteur, SRC 1970, c. C-30.

**LA THÈSE A ÉTÉ  
MICROFILMÉE TELLE QUE  
NOUS L'AVONS REÇUE**

THE UNIVERSITY OF ALBERTA

IMPLEMENTATION OF THE PETROVIC CODE WITH A SELF-SUSTAINING  
MONOSTABLE CLOCK RECOVERY CIRCUIT IN A FIBRE OPTIC SYSTEM

by

KUMAR S. VISVANATHA

A THESIS

SUBMITTED TO THE FACULTY OF GRADUATE STUDIES AND RESEARCH  
IN PARTIAL FULFILMENT OF THE REQUIREMENTS FOR THE DEGREE

OF MASTER OF SCIENCE

DEPARTMENT OF ELECTRICAL ENGINEERING

EDMONTON, ALBERTA

SPRING 1987

Permission has been granted to the National Library of Canada to microfilm this thesis and to lend or sell copies of the film.

The author (copyright owner) has reserved other publication rights, and neither the thesis nor extensive extracts from it may be printed or otherwise reproduced without his/her written permission.

L'autorisation a été accordée à la Bibliothèque nationale du Canada de microfilmer cette thèse et de prêter ou de vendre des exemplaires du film.

L'auteur (titulaire du droit d'auteur) se réserve les autres droits de publication; ni la thèse ni de longs extraits de celle-ci ne doivent être imprimés ou autrement reproduits sans son autorisation écrite.

ISBN 0-315-37807-7

THE UNIVERSITY OF ALBERTA

RELEASE FORM

NAME OF AUTHOR KUMAR S. VISVANATHA  
TITLE OF THESIS IMPLEMENTATION OF THE PETROVIC CODE  
WITH A SELF-SUSTAINING MONOSTABLE  
CLOCK RECOVERY CIRCUIT IN A  
FIBRE OPTIC SYSTEM

DEGREE FOR WHICH THESIS WAS PRESENTED MASTER OF SCIENCE  
YEAR THIS DEGREE GRANTED SPRING 1987

Permission is hereby granted to THE UNIVERSITY OF ALBERTA LIBRARY to reproduce single copies of this thesis and to lend or sell such copies for private, scholarly or scientific research purposes only.

The author reserves other publication rights, and neither the thesis nor extensive extracts from it may be printed or otherwise reproduced without the author's written permission.

(SIGNED) .. *Kumar Visvanatha* ..

PERMANENT ADDRESS:

... 1819 22<sup>nd</sup> Ave. South ...  
... Lethbridge, Alberta ...  
... T1K 1J2 .....

DATED ..... March 30 ..... 1987

THE UNIVERSITY OF ALBERTA  
FACULTY OF GRADUATE STUDIES AND RESEARCH

The undersigned certify that they have read, and recommend to the Faculty of Graduate Studies and Research, for acceptance, a thesis entitled IMPLEMENTATION OF THE PETROVIC CODE WITH A SELF-SUSTAINING MONOSTABLE CLOCK RECOVERY CIRCUIT IN A FIBRE OPTIC SYSTEM submitted by KUMAR S. VISVANATHA in partial fulfilment of the requirements for the degree of MASTER OF SCIENCE.

..... *C. G. Englefield* .....

Co-supervisor

..... *H. D. Bond* .....

Co-supervisor

..... *W. S. Young* .....

..... *W. G. ...* .....

Date..... *30<sup>th</sup> March 1987* .....

## ABSTRACT

In this thesis, the implementation of the Petrovic code with a self-sustaining monostable clock recovery circuit is described. The Petrovic code [7], which belongs to the 1B-2B family of block codes, is attractive for optical fibre communications since it has zero dc content, small low frequency content, contains frequent transitions, is bit sequence independent, and provides error detection capability. Using computer simulation, the bandwidth requirements of the Petrovic code are compared with those of the NRZ code for the case of an additive white gaussian noise channel. It was discovered that when the receiver transfer function is a first or second-order Butterworth filter, the Petrovic code requires twice the bandwidth of the NRZ code. This additional required bandwidth results in an optical power penalty of approximately 3dB, as compared to the NRZ code, and a decrease in the repeater spacing by a factor of  $3/\alpha$ , where  $\alpha$  is the fibre attenuation in dB/km, under attenuation limited situations and by a factor of two when the system is dispersion limited.

An experimental optical fibre communication system employing the Petrovic code was constructed and measurements were made. The system operated at a bit

rate of 44.736 Mb/s over multimode graded index fibre. The experimental Petrovic spectrum was found to be in close agreement with the theoretical spectrum obtained by Petrovic. In the experimental system, the Petrovic code required a bandwidth 1.9 times greater than that required by the NRZ code and it incurred a sensitivity penalty of 3.2dB.

One of the main reasons for employing a line code is to provide ease of timing recovery. In this project, a novel self-sustaining monostable clock recovery circuit [31] was used to extract the sampling clock from the incoming signal. Upon implementation of this circuit it was discovered that, at low received power levels, the recovered clock signal contained excessive jitter, resulting in reduced receiver sensitivity. A simple circuit modification was developed to reduce the clock jitter. This modification resulted in a reduction of jitter power by a factor of 15, and an increase in the receiver sensitivity of 1.4 dB. The receiver sensitivities for a BER of  $10^{-9}$ , using first the delayed transmitter clock and then the clock signal produced by the modified self-sustaining monostable clock recovery circuit, were virtually the same.

## ACKNOWLEDGEMENTS

I would like to thank Dr. C. ~~Dr. [redacted]~~field and Dr. P. A. Goud for their constant encouragement, advice, and support throughout this project. In addition, I would like to extend my gratitude to the following:

- Mr. Bert Telder, for his competent technical assistance as well as stimulating discussions.
- The members of the examining committee for reviewing this work.
- All the members of the Optical and Microwave Communications group.
- The National Science and Engineering Research Council (NSERC) for the award of a post-graduate fellowship.
- The Electrical Engineering Department at the U of A for the award of a teaching assistantship.
- The Optical Devices Group of Northern Telecom, for the use of their word processing facilities.

I would also like to express my sincere thanks to my parents, family, and friends for their encouragement and support during this project. My appreciation is also extended to all the teachers who have made it possible to complete the work reported in this thesis.



## TABLE OF CONTENTS

CHAPTER	PAGE
<b>1. INTRODUCTION</b>	<b>1</b>
1.1 Overview of Line Coding in Optical Fibre Communications	1
1.2 The Petrovic Code	6
1.3 Clock Recovery	9
1.4 Thesis Objectives and Organization	14
1.4.1 Objectives	14
1.4.2 Organization	16
<b>2. PERFORMANCE COMPARISON BETWEEN THE PETROVIC CODE AND THE NRZ CODE</b>	<b>18</b>
2.1 Bandwidth Requirements	19
2.1.1 System Model	22
2.1.2 Calculation of BER	24
2.1.3 Computer Simulation to Determine the BER	32
2.1.4 Results	33
2.1.5 Discussion of Results	34
2.2 Optical Power Penalty	39
2.3 Repeater Spacing	45
<b>3. THE SELF-SUSTAINING MONOSTABLE MULTIVIBRATOR CLOCK RECOVERY CIRCUIT</b>	<b>55</b>
3.1 Circuit Operation	57
3.2 Clock Recovery in a Petrovic System	61

3.3 Jitter Analysis	64
3.4 Circuit Modification	60
<b>4. THE EXPERIMENTAL PETROVIC SYSTEM</b>	<b>76</b>
4.1 Petrovic Encoder	78
4.2 Laser Transmitter	85
4.3 Fibre	85
4.4 Optical Preamplifier	87
4.5 Main Amplifier	92
4.6 Petrovic Decoder	93
4.7 Clock Recovery Circuit	97
4.8 Jitter Measurer	101
<b>5. EXPERIMENTAL RESULTS</b>	<b>103</b>
5.1 System Operation and Waveforms	104
5.1.1 Petrovic Encoder	104
5.1.2 Optical Receiver	104
5.1.3 Petrovic Decoder	108
5.1.4 Clock Recovery Circuit	110
5.2 Power Spectrum	111
5.3 BER Measurements	114
5.3.1 BER versus Received Power	115
5.3.2 BER versus Receiver Bandwidth	117
5.3.3 BER versus Bit Sequence	121
5.4 Jitter in the Recovered Clock	123
5.5 System BER with the Recovered Clock	131

<b>6. SUMMARY AND CONCLUSIONS</b>	<b>134</b>
<b>REFERENCES</b>	<b>140</b>
<b>APPENDIX A: COMPUTER PROGRAMS</b>	<b>145</b>

## LIST OF TABLES

Table	Page
2.1 Optical Power Penalty for the 1B-2B codes...	46
2.2 System Specifications.....	49
5.1 BER versus Source Bit Sequence for the Petrovic and the NRZ code.....	122
5.2 Jitter Power corresponding to the Jitter Spectra shown in Fig. 5.13.....	128
5.3 Jitter Power corresponding to the Jitter Spectra shown in Fig. 5.14.....	128

## LIST OF FIGURES

Figure	Page
1.1 Various binary line codes.....	5
1.2 Power Spectral Density of various binary line codes.....	8
1.3 Block diagram of the clock recovery circuit using the self-synchronization scheme.....	11
2.1 Block diagram of the system used to determine the bandwidth requirements.....	23
2.2 Various decoder configurations.....	25
2.3 System waveforms.....	27
2.4 Dependence of the noise margin on the bit pattern for large and small filter bandwidths	31
2.5 BER versus bandwidth for 1 <sup>st</sup> order Butterworth LPF.....	35
2.6 BER versus bandwidth for 2 <sup>nd</sup> order Butterworth LPF.....	36
2.7 Schematic diagram of an optical receiver showing the noise sources.....	40
2.8 Receiver sensitivity versus bit rate for a Si APD and a Ge APD bipolar receiver.....	50
2.9 Repeater spacing versus bit rate for System #1	51
2.10 Repeater spacing versus bit rate for System #2	52
2.11 Repeater spacing versus bit rate for System #3	53
3.1 The self-sustaining monostable multivibrator clock recovery circuit.....	56
3.2 Timing diagram of the self-sustaining monostable clock recovery circuit for an 10001 input sequence.....	58
3.3 Transition Detector output.....	62
3.4 Relationship between jitter and receiver noise	65

3.5	Pdf of output jitter when a primary pulse triggers the MM at the ideal time during the previous time slot.....	68
3.6	Pdf of output jitter when a feedback pulse triggers the MM at $\Delta$ seconds after the ideal time during the previous time slot.....	71
3.7	Pdf of the output jitter when the early primary pulses are also inhibited.....	73
3.8	Modified clock recovery circuit.....	75
4.1	Block diagram of the experimental Petrovic system.....	77
4.2	Schematic diagram of the Petrovic encoder.....	80
4.3	Schematic diagram of the monostables and the delay network.....	83
4.4	Schematic diagram of the preamplifier.....	89
4.5	Schematic diagram of the Petrovic decoder.....	94
4.6	Schematic diagram of the clock recovery circuit.....	98
5.1	Encoder output when the input is all zeroes....	105
5.2	Encoder output for an input 10 bit repeating sequence of 1001000000.....	105
5.3	Encoder output for an 101010.... NRZ input.....	106
5.4	Encoder output eye diagram.....	106
5.5	Main amplifier output eye diagram.....	107
5.6	Decoder output waveforms.....	109
5.7	Clock recovery circuit waveforms.....	112
5.8	Petrovic power spectrum.....	113
5.9	BER versus received power for the NRZ, CMI, and Petrovic line codes.....	116
5.10	Relationship between BER and receiver bandwidth for the NRZ and the Petrovic codes.....	119

5.11	Relationship between received optical power and receiver bandwidth, for $10^{-9}$ BER.....	120
5.12	Clock spectrum.....	124
5.13	Clock jitter spectrum of the original self-sustaining monostable multivibrator clock recovery circuit.....	127
5.14	Clock jitter spectrum of the modified self-sustaining monostable multivibrator clock recovery circuit.....	130
5.15	BER versus received optical power when the clock signal from the modified clock recovery circuit is used for the decoder clock.....	133

## CHAPTER 1

### INTRODUCTION

#### 1.1 Overview of Line Coding in Optical Fibre Communication Systems

The function of coding is to adapt a signal source to a transmission medium for the purpose of efficient and reliable communications. The subject of coding is divided into source coding and channel coding. Source coding is the conversion of the messages produced by a source into a string of binary digits. Channel coding, on the other hand, is the transformation of the binary digits generated by the source into a form suitable for a specific transmission medium. Line coding is a subset of channel coding that normally does not include error correction codes and is mainly concerned with matching the transmitted signal spectrum to the transfer function of the transmission channel while providing resistance to impairments such as timing jitter, ISI, baseline wander, etc. [1].

A line code that is attractive for optical fibre communications should possess the following characteristics [2-6]:

1. Frequent transitions.
2. Zero dc and small low frequency content.



3. Two level (binary).
4. Bit sequence independent.
5. Error detection capability.
6. Moderate redundancy.
7. Simple to implement.

A brief discussion of these characteristics is now given. The line code must have frequent transitions in order to easily extract a stable clock signal at the receiver (Clock recovery techniques will be discussed in Section 1.3). Furthermore, the longest interval between transitions must be restricted to a small value in order to prevent the clock recovery circuit from drifting to its free running frequency, and hence losing data synchronization. Ideally, the line code should provide a transition for every source bit.

The continuous spectrum of the line code should have zero dc content and a small low frequency component in order to minimize baseline wander, which is the shifting of the receiver output in the presence of a long string of ones or zeroes due to ac coupling in the receiver. Baseline wander is undesirable because it results in a reduction of the signal amplitude at the sampling instant, and hence in a reduced receiver sensitivity.

Multilevel transmission increases the information capacity of a fibre optic channel but it suffers from the following problems:

1. Due to signal dependent shot noise, the receiver threshold levels for multilevel systems need to be non-uniformly spaced, which complicates the receiver circuitry.

2. Lasers are non-linear devices, making the generation of multilevel signals more difficult than the generation of binary signals.

Theoretical considerations by Brooks and Jessop [5] reveal that multilevel codes show a small sensitivity penalty for single mode systems and show an advantage only in multimode systems where dispersion effects are significant. Since the majority of the fibre that is being installed today is single mode, the line code chosen for operation over these fibre should be binary (assuming intensity modulation).

A line code is bit sequence independent if the communication link can function properly regardless of what bit stream is emitted by the source. For example, if the message source were to emit all ones, the line code should provide sufficient transitions so that the system performance would not degrade due to baseline wander or drifting of the clock signal. In general, a line code is bit sequence independent if it contains only a small amount of low frequency energy, i.e., a long string of ones or zeroes is not possible.

The addition of redundancy into the source bit stream is essential for providing frequent transitions. However, the required system bandwidth is proportional to the amount of redundancy added. As the system bandwidth increases, the noise power at the receiver output increases, and the receiver sensitivity decreases. Thus, a compromise concerning redundancy is required.

In addition, the line code should provide a means of determining the bit error rate (BER) in real time and be simple to implement.

During the past decade, several line codes for fibre optic communications have been proposed [4,7-16] (see Fig. 1.1). These include simple 1B-2B (1 bit in, 2bits out) codes such as CMI, DMI, Manchester, Petrovic, Modified Miller, and more complex block codes like 3B-4B, 5B-6B, and 7B-8B, 10B-1C. However, the majority of the commercial fibre optic systems developed to date employ the NRZ code. This is because these systems are mainly intended for long haul applications where it is essential to maximize the receiver sensitivity and minimize the system bandwidth. Among the two level codes, the NRZ code requires the least amount of bandwidth (because it does not contain any redundancy)

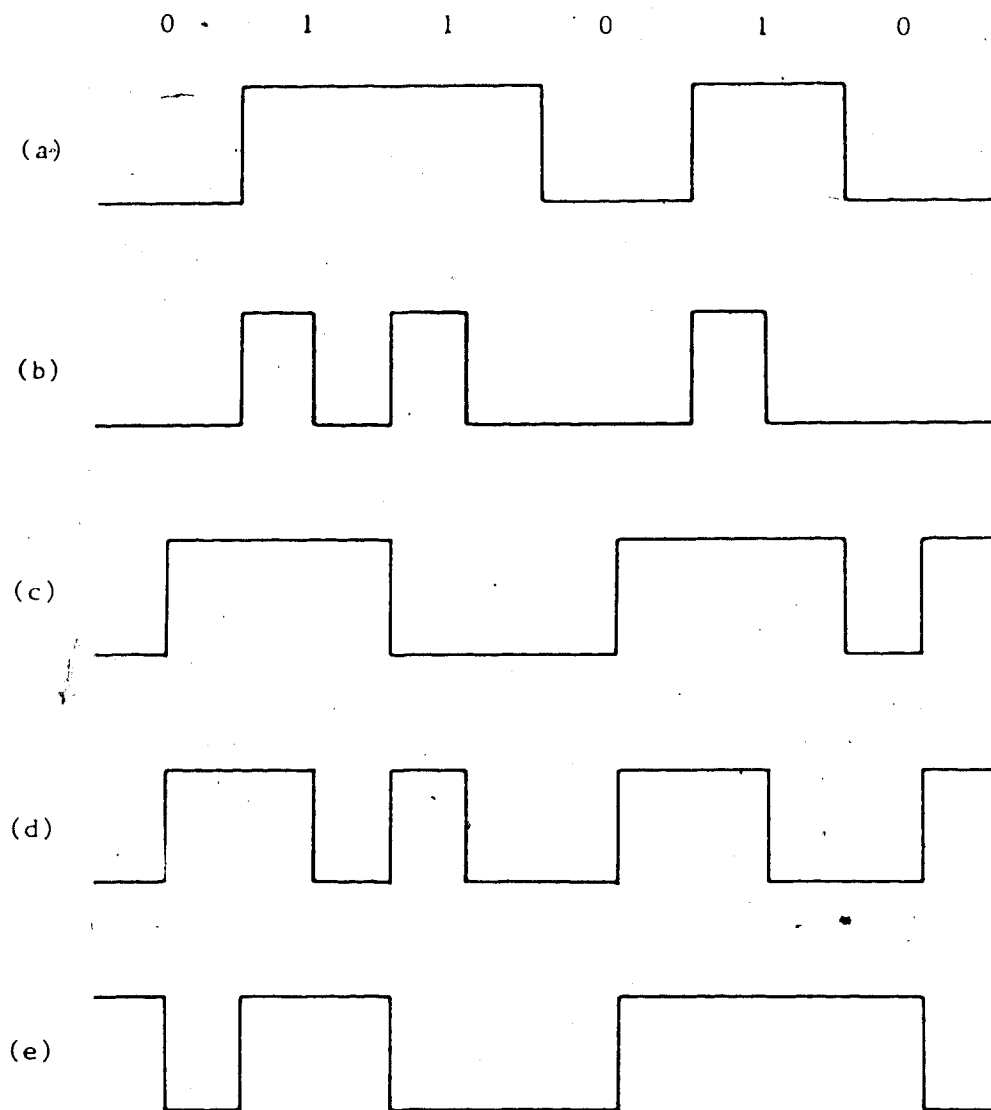


Fig. 1.1 Various Binary Line Codes

- (a) NRZ
- (b) RZ
- (c) CMI
- (d) Manchester
- (e) Petrovic

and provides the greatest sensitivity, for a given source bit rate, provided that it is scrambled. A data scrambler is required because the NRZ code is not bit sequence independent, i.e., a long string of ones or zeroes can result in loss of synchronization at the receiver.

In the future, it is anticipated that short haul fibre optic systems, e.g., local area networks (LANs) and subscriber feeder loops, will find widespread application. These systems have ample bandwidth and do not require the ultimate in receiver sensitivity. In these systems, simple 1B-2B codes such as the ones mentioned above can be utilized. Compared to the NRZ code, these codes provide ease of timing recovery, error detection capability, large dynamic range, and do not require a scrambler.

### 1.2 The Petrovic Code

The Petrovic code is a simple 1B-2B code with the following desirable features [7]:

- a) zero dc content
- b) small low-frequency and high-frequency content
- c) good timing content
- d) bandwidth which seems to be slightly greater than the NRZ format
- e) error detection capability

f) simple to implement

The Petrovic code has the following coding rule: 1 is encoded by 11 and 00 alternately; 0 is coded by 10 after 11 and 01, and by 01 after 00 and 10. The Petrovic code waveform for an arbitrary binary signal are shown in Fig. 1.1. The maximum encoded pulse duration is  $2T$  and the minimum is  $T/2$ . However, the majority of the pulses are  $T$  seconds long. The restriction of the maximum time interval without a transition to  $2T$  seconds gives this code excellent timing content.

Compared to the other simple codes, the Petrovic code is superior. This is obvious when the power spectral density (psd) curves for the various codes, shown in Fig. 1.2, are examined. The NRZ and Miller (or delay modulation) [17] code formats require a narrower bandwidth but they both contain a dc component. The Manchester code, on the other hand, has a zero dc component and small low frequency energy but it contains larger high frequency components.

Incidentally, the Petrovic code is identical to the first of a group of three coding schemes proposed by W.R. Hedeman for digital magnetic recording [18]. Both Hedeman and Petrovic reported the same code just a month apart. The first Hedeman code, also known as the H-1 code, has been further investigated by Lo Cicero,

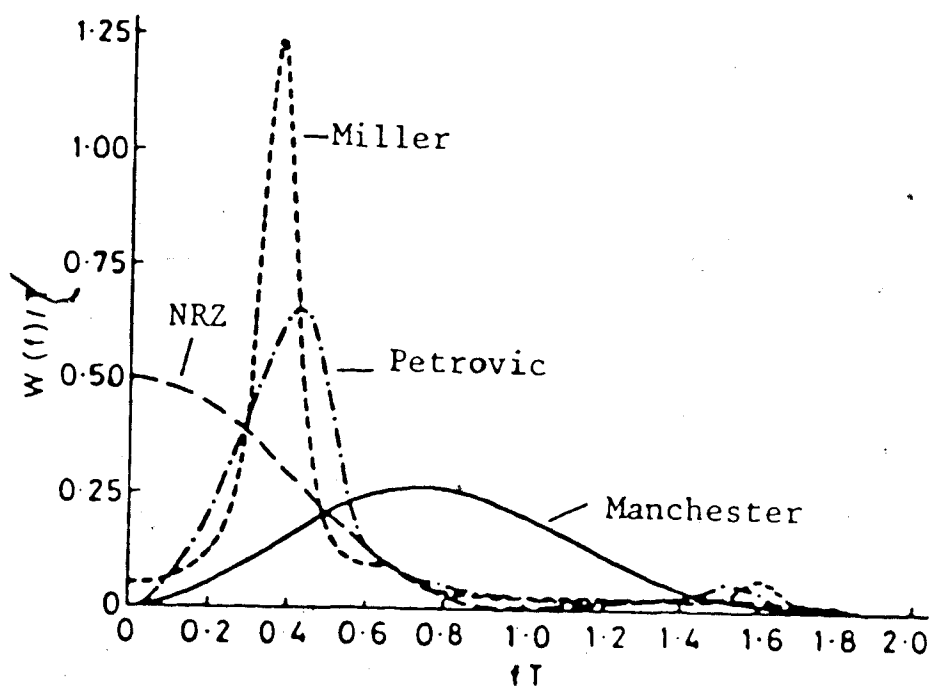


Fig. 1.2 Power Spectral Density of Various Binary Line Codes

Costello, and Peach [19], and R. Woods [20]. Lo Cicero et al. point out that the H-1 code has features that also make it attractive for data communications and they obtain its autocorrelation function and power spectral density function (which is identical to Petrovic's). They also comment on the synchronization properties of this code. R. Woods describes the H-1 code as a rate one-half, convolutional code and proposes a soft decision decoding structure.

To date, implementation of the Petrovic, or the H-1, code in a fibre optic system has not been reported. Since this code has properties that make it attractive for optical fibre communications, it is worthwhile to examine the performance of this code in a fibre optic system.

### **1.3 Clock Recovery**

In digital communication receivers, the received baseband signal must be sampled at precise instants in order to recover the original transmitted signal. This sampling procedure requires a clock signal that is synchronized (frequency and phase) with the transmitter clock signal. The most popular method of obtaining the clock signal is to extract it from the incoming message signal. The alternatives to this self-synchronization scheme include having the transmitter and receiver



slaved to a common timing standard or transmitting the clock signal along with the data. These methods, however, are costly and seldom used.

A block diagram of the self synchronization scheme is shown in Fig. 1.3 [21]. In this method, the received data signal is first applied to a non-linear circuit and then to a clock recovery circuit. The output of the clock recovery circuit is used to sample the received signal.

The non-linear element generates a spectral line at the clock rate. If a spectral line already exists in the line code, e.g., RZ and CMI codes, then the non-linear element is omitted. A non-linear element is capable of generating a clock spectral line because the input data signal is not truly random; it contains regular transitions at multiples of the bit interval.

The non-linear element essentially converts the negative transitions in the input signal into positive ones, and ensures that a positive transition occurs, on the average, every  $T$  seconds. Some common non-linear elements include: a differentiator followed by a full wave rectifier [21], squarer [23], and an exclusive OR gate with one input delayed with respect to the other [24,25].

The spectrum of the signal produced by the non-linear circuit consists of discrete spectral lines, at

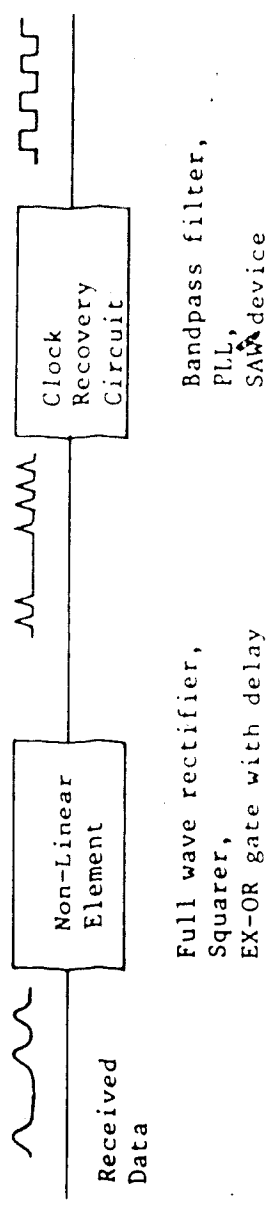


Fig. 1.3 Block Diagram of the Clock Recovery Circuit Using the Self-synchronization Scheme

multiples of the bit rate, superimposed on a continuous spectrum. The continuous spectrum arises since the output of the non-linear circuit is not periodic, i.e., it does not contain a positive going pulse every  $T$  seconds. This occurs because a line code, usually, does not contain a transition every  $T$  seconds.

Practical and useful clock recovery circuits have a narrow bandwidth centered at the clock frequency. Thus the output of the clock recovery circuit will not only contain the clock spectral line but also some of the surrounding continuous spectrum. This continuous spectrum gives rise to jitter [26], i.e., phase modulation in the clock signal. A useful figure of merit is the ratio between the power contained in the clock spectral line to the power contained in the continuous spectrum that falls within the passband of the clock recovery circuit. This ratio is proportional to the frequency of transitions in the input signal. Thus, in order to minimize jitter and extract a stable clock signal, the input signal must have a high transition density, which is obtained by coding the source data.

The clock recovery circuit is generally an LC bandpass filter, a surface acoustic wave (SAW) resonator, or a phase locked loop (PLL) tuned to the pulse repetition frequency. It is reported that a high

gain, second-order PLL is superior to an LC filter for timing extraction [27,28]. The main reason for the PLL's superiority is due to its constant output amplitude. The output amplitude of a bandpass filter is a function of its input bit sequence. If the incoming pulses occur at regular intervals, then the output amplitude of the filter will be fairly constant. In the absence of pulses, however, the output decays exponentially at a rate that is inversely proportional to the  $Q$  of the filter. Since the line code that is used may not have a pulse occurring in every bit interval, the output of the filter will contain amplitude modulation.

The amplitude modulated sinusoid from the bandpass filter is usually applied to a threshold detector, which drives a pulse generator. The threshold is set to zero but, in practice, it is offset from zero by a small amount. The presence of this offset results in phase modulation or jitter of the clock pulses due to the sinusoid crossing the threshold at irregular intervals.

Since the output of a PLL has a constant output amplitude, the amplitude-to-phase conversion problem will not be present. The PLL has many other advantages [29]. For example, its static phase error and noise bandwidth can both be made small at the same time. In a bandpass filter, a small static phase error is possible

- only if the noise bandwidth is decreased, i.e, its  $Q$  is decreased.

The SAW device suffers from the same problems as the LC filter, but not to as large an extent because it has a much higher  $Q$  (values of 1000 are possible) [30]. A further disadvantage of the SAW filter is that it suffers from a large insertion loss, typically 10db to 15dB. A PLL is superior to the SAW resonator, but at high bit rates (300 Mb/s and higher), it is difficult to construct a PLL circuit and hence SAW filters are often employed.

#### **1.4 Thesis Objectives and Organization**

##### **1.4.1 Objectives**

Although the Petrovic code has several attractive features, its implementation in a fibre optic system has not yet been reported. The purpose of this thesis is to implement the Petrovic code in a fibre optic system and determine its performance both theoretically and experimentally. Since ease of timing recovery is one of the main reasons for using a line code, clock recovery for the Petrovic code will also be studied. The self-sustaining monostable multivibrator clock recovery circuit [31] was used to recover the clock signal from the received Petrovič signal.

The main objectives of this thesis are as follows:

1. Compare the bandwidth and sensitivity requirements of the Petrovic code with those of the NRZ code.

2. Compare the repeater spacing for the Petrovic code with the NRZ code for some representative fibre optic systems.

3. Analyze the jitter produced by the self-sustaining monostable clock recovery circuit. During this analysis, it will be discovered that a simple modification to this circuit will result in significant jitter reduction.

4. Design and construct the Petrovic encoder and decoder, and the clock recovery circuit. The operating bit rate will be 44.736 Mb/s (the DS-3 rate). A fibre optic system employing these components will then be set up.

5. Experimentally compare the bandwidth and sensitivity requirements between the Petrovic and NRZ code.

6. Verify that the experimental power spectrum agrees with the theoretical spectrum derived by Petrovic and Lo Cicero.

7. Experimentally verify that the proposed modification to the clock recovery circuit does result in jitter reduction.

8. Determine, the sensitivity penalty, if any, when the recovered clock is used to sample the received waveform instead of the delayed transmitter clock.

#### 1.4.2 Organization

Chapter 1 has presented the characteristics that a line code should possess for optimal fibre optic transmission, showed that the Petrovic code satisfies these requirements, and has introduced the topic of clock recovery.

Chapter 2 will try to answer the following questions:

1. How much additional bandwidth does the Petrovic code require over the NRZ code?
2. What is the optical power penalty incurred when the Petrovic code is employed instead of the NRZ code?
3. Given the bandwidth and sensitivity requirements, what kind of repeater spacings can one expect?

Chapter 3 will describe the self-sustaining monostable clock recovery circuit and analyze its clock jitter. A simple modification to reduce this clock jitter will be proposed. The experimental Petrovic system will be described in Chapter 4. Chapter 5 will present the experimental results that were obtained. It will give the experimental bandwidth and sensitivity requirements and show that the modification to the

monostable clock recovery circuit does result in jitter reduction. Finally, a summary of the major results obtained in this thesis and recommendations for further research will be given in Chapter 6.

---



## CHAPTER 2

### SYSTEM PERFORMANCE COMPARISON BETWEEN THE PETROVIC AND THE NRZ CODE

As pointed out in the previous chapter, the Petrovic code has many advantages over the NRZ code, e.g., zero dc content, small low frequency content, frequent transitions, and error detection capability. However, the power spectrum of the Petrovic code contains larger higher frequency components than the NRZ code, due to the occurrence of half width ( $T/2$  seconds long) pulses. The Petrovic code therefore requires a larger transmission bandwidth than the NRZ code, at a given binary bit rate. Since thermal noise power is proportional to the receiver bandwidth, the noise level at the decoder is higher for the Petrovic code. In order to achieve the same signal-to-noise-ratio (SNR) and hence error performance, the signal power for the Petrovic code must be raised. Thus the receiver sensitivity, i.e., the signal power required to achieve a certain bit error rate (BER), is poorer for the Petrovic code than for the NRZ code. The increased bandwidth and the reduced sensitivity result in a decreased repeater spacing if the source is power limited.

The purpose of this chapter is to compare the NRZ code with the Petrovic code in terms of bandwidth requirements, receiver sensitivity, and repeater spacing. The results obtained from this comparison will allow the accurate design of a fibre optic system employing the Petrovic code.

### 2.1 BANDWIDTH REQUIREMENTS

The bandwidth required in a baseband digital communication system depends on several parameters, e.g., the line code, the desired BER, the channel and receiver transfer function, the noise characteristics, the sampling instant, the jitter in the sampling clock, etc. In this thesis, the term "bandwidth" will refer to the frequency at which the combined channel and receiver transfer function is down by 3dB from its mid-band value. Among the two-level codes, the NRZ code requires the least amount of bandwidth. (In practical systems, a general rule of thumb is that the NRZ code requires a bandwidth of approximately 0.8 times the bit rate). Thus, NRZ signalling is a popular choice among fibre optic system designers. However, a scrambler must be used in conjunction with the NRZ code to ensure bit sequence independence. Scrambling does not offer the possibility of error detection and can result in significant error multiplication. An alternative to

scrambling is to employ coding techniques, which do offer error detection capability. Since coding the data requires an increased system bandwidth, one question that needs to be answered when evaluating a particular line code is how much additional bandwidth the code will require, as compared to the NRZ code.

There are conflicting views in the literature regarding the bandwidth requirements of line codes. Several authors feel that the code's power spectral density (PSD) gives a valid indication of its bandwidth requirements [7,19,32,33]. The bandwidth required is that which contains a certain fraction of the total power. Other authors state that the required bandwidth is inversely proportional to the mean time between transitions [7,34]. Still others claim that the bandwidth is inversely proportional to the code's efficiency [5,35]. (The efficiency of a code is defined as the reciprocal of the average number of bits needed to represent a single source bit.)

Let us compare the bandwidth requirements of the NRZ, Manchester, and Petrovic codes using the above criteria. If we examine the bandwidth that contains 90% of the total power, then we find that the NRZ code requires a bandwidth of  $0.8/T$  Hz, where  $T$  is the incoming binary bit interval, the Petrovic code requires  $1.6/T$  Hz, and the Manchester code needs approximately

3.2/T Hz of bandwidth [2.4]. From these values one would conclude that the Petrovic code requires twice the bandwidth of the NRZ code and the Manchester code requires 4 times the bandwidth of the NRZ code.

If we consider the mean time between transitions,  $T_M$ , then we find that  $T_{M_{NRZ}} = 2T$ ,  $T_{M_{Petrovic}} = 18/15 T$ ,  $T_{M_{Manchester}} = 2/3 T$ . If the required bandwidth is assumed to be inversely proportional to  $T_M$ , then one would conclude that the Petrovic code requires 1.7 times the bandwidth of the NRZ code and the Manchester code requires 3 times the bandwidth of the NRZ code.

Since the Manchester and Petrovic codes belong to the 1B-2B class of block codes, they have an efficiency of 0.5. If one assumes that the bandwidth is inversely proportional to the efficiency, then one would conclude that both the Petrovic code and the Manchester code require twice the bandwidth of the NRZ code.

Note that all the three bandwidth comparison methods yield different results. Which one is correct? How much additional bandwidth does the Petrovic code require over the NRZ code for a given BER and under similar channel and receiver conditions? In order to answer these questions, a computer simulation study was performed to determine the BER versus receiver bandwidth for a simple additive white gaussian noise channel. The

system model used in the simulation is presented in the next section.

### 2.1.1 System Model

To compare the bandwidth requirements between the NRZ code and the Petrovic code, the simplified baseband communication model shown in Fig. 2.1 will be assumed. In this model, the input to the encoder consists of independent, equiprobable, binary symbols  $a_{2n}$  [ $a_{2n} \in \{0,1\}$ ], at a bit rate of  $1/T$ . The encoder will be of the 1B-2B type, i.e., each incoming bit  $a_{2n}$  will be converted into two outgoing bits  $b_n$  and  $b_{n+1}$ . The output bits  $b_n$  will have a bit interval of  $T/2$  and will not be independent since adjacent bits are correlated. For the NRZ code, both the encoder output bits are equal to the incoming bit, i.e.,  $b_n = b_{n+1} = a_{2n}$ . For the 1B-2B codes, e.g., Petrovic, Manchester, CMI, the encoder output bits are determined by applying the appropriate encoding rules.

The transmitter is assumed to generate rectangular pulses. Its output,  $p(t)$ , can be represented as follows:

$$p(t) = b_n h_p(t - nT) \quad (2.1)$$

$$\begin{aligned} \text{where } h_p(t) &= 1, & 0 < t < T/2 & \quad (2.2) \\ &= 0, & \text{elsewhere} & \end{aligned}$$

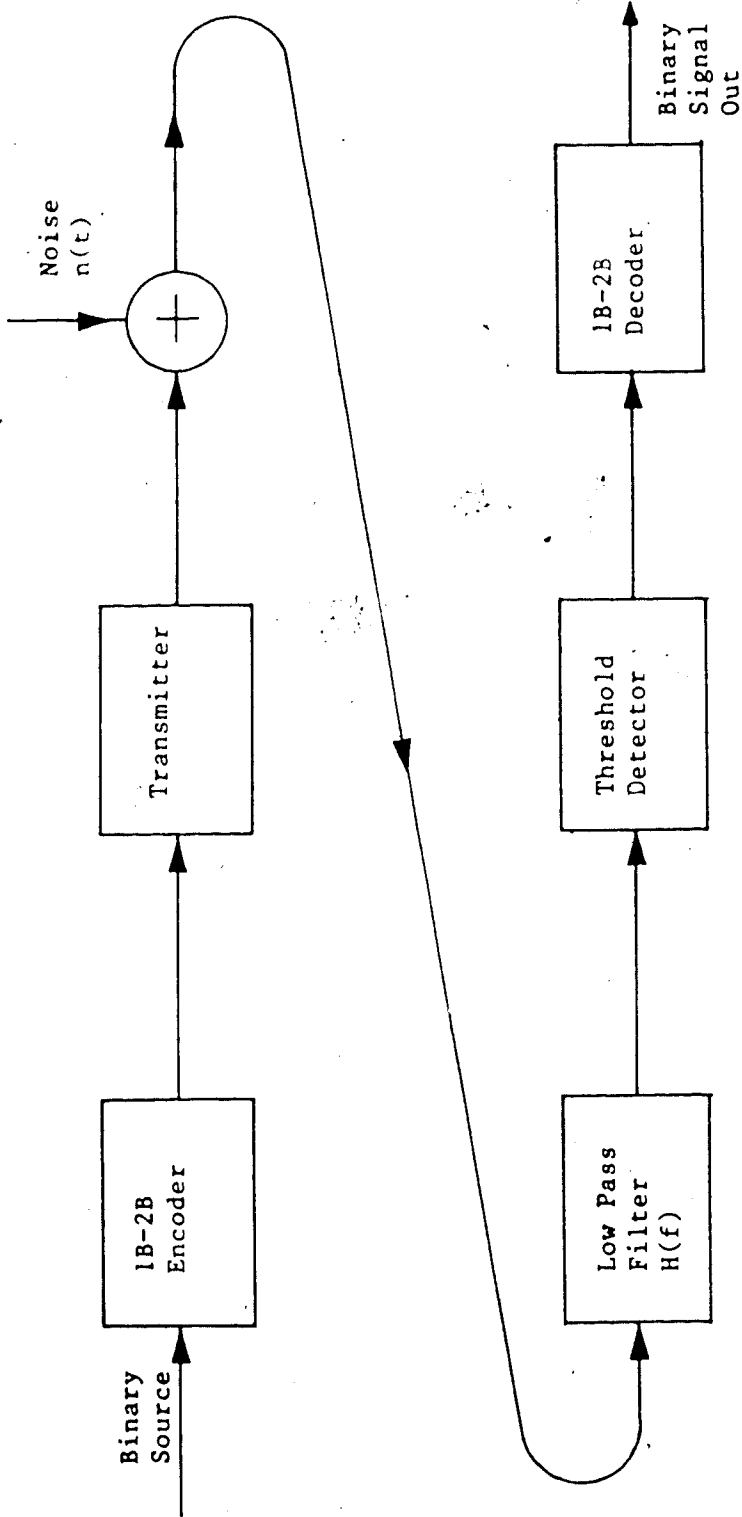


Fig. 2.1 Block Diagram of the System Used to Determine the Bandwidth Requirements

The received signal will be corrupted by additive white gaussian noise (AWGN)  $n(t)$ , which is assumed to have a zero mean and variance  $\sigma_n^2$ . The transmission channel will be assumed to have an infinite bandwidth. The received signal and the noise are applied to the receiver, which consists of a low pass filter, a threshold detector, and a decoder. The filtered signal and noise are applied to a threshold detector, which has a threshold set to 0.5 volts. The output of the threshold detector will be a 1 whenever its input is greater than 0.5 volts and a 0 whenever its input is less than 0.5 volts. The rectangular pulses from the threshold detector are then applied to a 1B-2B decoder. The decoder configuration for the Petrovic and the CMI codes is shown in Fig 2.2a while the decoder configuration for the Manchester code is shown in Fig. 2.2b. The NRZ decoder is shown in Fig 2.2c.

### 2.1.2 Calculation of BER

In order to compare the bandwidth requirements of the 1B-2B codes with that of the NRZ code, the BER of the system described in the previous section (see Fig. 2.1) will be calculated for several bandwidths of a given filter type. The noise variance, signal amplitude, and sampling instant will be held constant. The filter bandwidth that gives the lowest BER will be

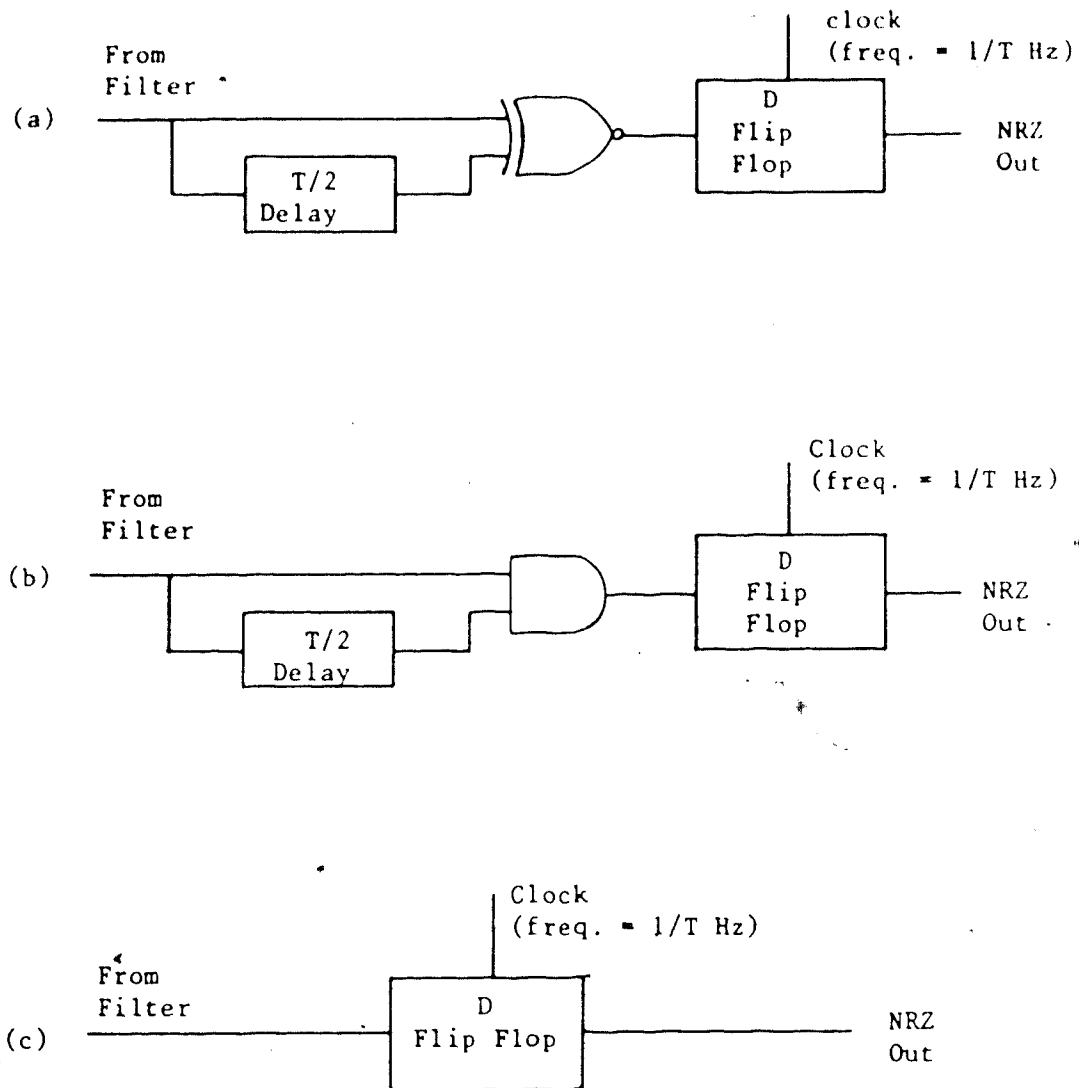


Fig. 2.2 Various Decoder Configurations

- (a) Petrovic and CMI codes
- (b) Manchester Code
- (c) NRZ Code



taken to be the bandwidth that is necessary for that particular line code .

To illustrate the calculation of BER, consider the system response to a source output of 001. The Petrovic encoder output will be 10 01 00. (see Fig. 2.3a). The high frequency components of the transmitter output will be attenuated by the filter and hence the filter output will contain rounded pulses. The amount of high frequency attenuation (or filtering) will depend on the filter type and its 3dB bandwidth. The filtered transmitter output for a first order Butterworth filter with a bandwidth of approximately  $0.5/T$  is shown in Fig. 2.3b. Figure 2.3c shows the output of the threshold detector. This signal is applied to the Petrovic decoder. In the decoding process, the threshold detector output and a delayed version of it (delay =  $T/4$ ) are applied to an exclusive-NOR (EX-NOR) gate. The output of the EX-NOR gate, shown in Fig. 2.3e, is sampled every  $T$  seconds (at the end of each bit interval) to recover the original source NRZ bit sequence. The first bit will be decoded incorrectly if the voltage at point A ( $V_A$ ) in Fig. 2.3e, due to noise, is greater than 0.5 volts in amplitude. This will occur if either point B is less than 0.5V or point C is greater than 0.5V. In the filter output, this situation corresponds to point D being less than 0.5V, due to

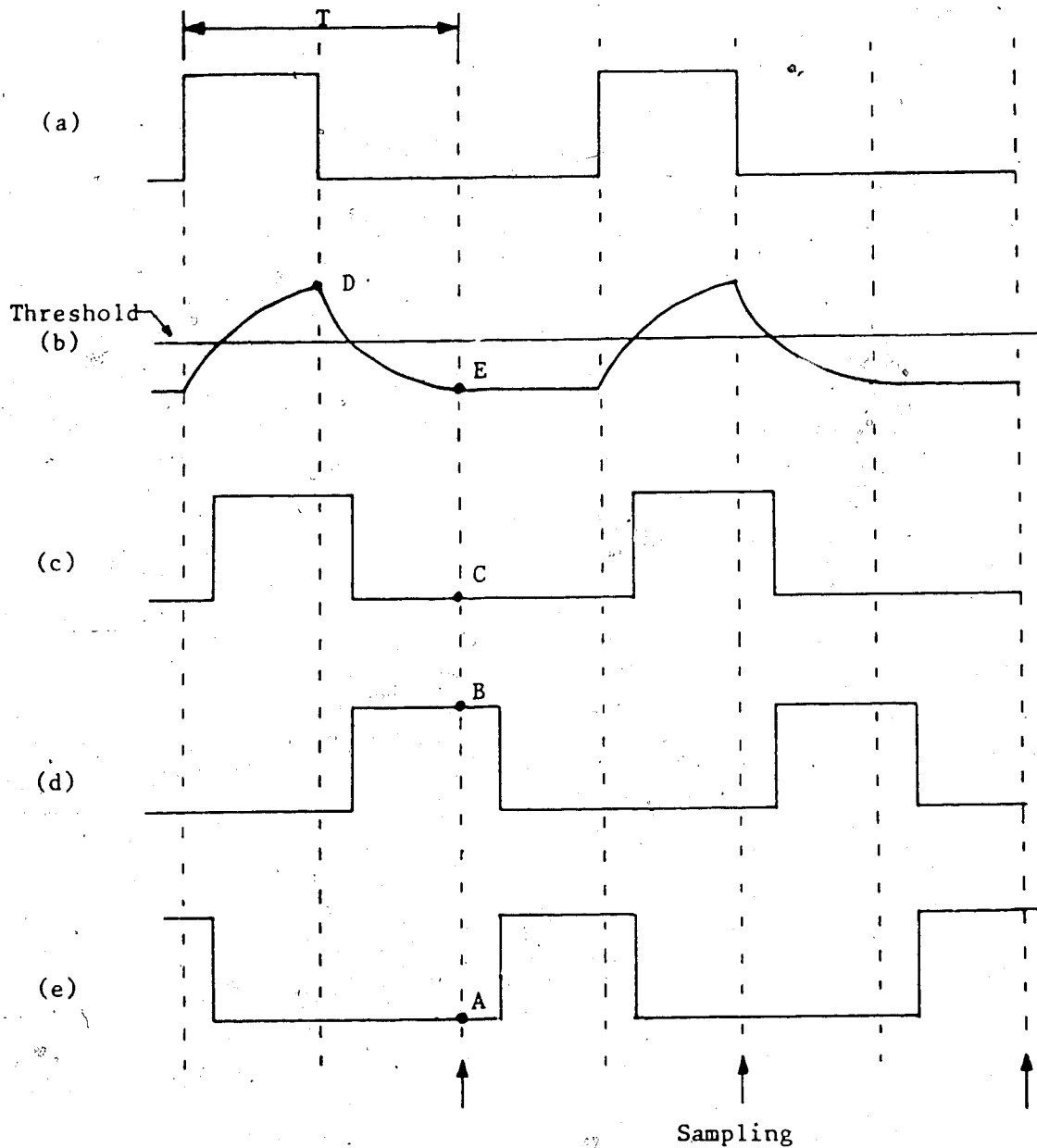


Fig. 2.3 System Waveforms

- (a) Petrovic Encoder output for an 001.. NRZ input
- (b) Filter Output (first order Butterworth)
- (c) Threshold Detector Output
- (d) Waveform (c) delayed by  $T/2$  seconds
- (e) EX-NOR Output

noise, or point E becoming greater than 0.5V. The probability of such an event occurring is given by [36]

$$P_e = Q[(0.5 - V_E)/\sigma_n] + Q[(V_D - 0.5)/\sigma_n] \quad (2.3)$$

$$\text{where } Q(x) = 0.5 \operatorname{erfc}(x/\sqrt{2}) \quad (2.4)$$

$$= \frac{1}{\sqrt{2\pi}} \int_x^{\infty} e^{-t^2/2} dt \quad (2.5)$$

If we let  $m_1$  and  $m_2$  represent the noise margin for the first and second bit interval respectively, i.e.,  $m_1 = 0.5 - V_E$  and  $m_2 = V_D - 0.5$ , then

$$P_e = Q(m_1/\sigma_n) + Q(m_2/\sigma_n) \quad (2.6)$$

Using similar reasoning it can be shown that the average probability of a bit error for an N bit Petrovic encoded sequence is

$$P_e = 1/N \sum_{n=1}^N Q(m_n/\sigma_n) \quad (2.7)$$

where  $m_n$  is the noise margin of the  $n^{\text{th}}$  bit interval.

For the NRZ code,  $n$  in the above equation has to be replaced by  $2n$ . Since the CMI decoder is the same as the Petrovic decoder, the same equation will apply for the BER of an N bit CMI sequence. Even though the Manchester decoder is slightly different (see Fig. 2.2), it can be shown that the above equation will apply for it as well.

If the bandwidth of the low pass filter is very high and sampling is assumed to take place at the end of the bit interval, then the filtered waveform will have risen to 1V or fallen to 0V by the time sampling occurs, i.e., the rise and fall times of the filtered signal will be small, when compared to the bit interval, and thus  $m_n = 0.5V$ . If we substitute  $m_n = 0.5$  in the above equation we get:

$$P_e = Q(0.5/\sigma_n) \quad (2.8)$$

$$\text{But } \sigma_n = \sqrt{\text{noise power}} = \sqrt{\eta BK} \quad (2.9)$$

where  $\eta$  = noise spectral density

$B$  = 3 dB bandwidth of the low pass filter

$K$  = noise equivalent bandwidth constant

= 1.57 for a first order Butterworth LPF

= 1.11 for a second " " "

As the filter bandwidth is reduced from a very large value,  $\sigma_n$  will decrease but initially the noise margin  $m_n$  will not decrease significantly because the rise and fall time of the signal will be much less than the bit interval. Thus the argument of the Q function will increase and the BER will decrease. As the bandwidth is further decreased, however, a point will be reached where the rise and fall times become comparable to the bit interval. Decreasing the bandwidth further from this point will result in the noise margin  $m_n$  reducing significantly. The decrease in the noise

margin will be greater than the decrease in the noise power and the BER will increase. Thus there is an optimum bandwidth for a given filter type and noise characteristics which will yield the lowest BER.

The noise margin will be constant from one bit interval to the next for only very large bandwidths. For small bandwidths,  $m_n$  will vary between adjacent bit intervals due to ISI and pattern variations. This point can be explained with the aid of Fig. 2.4. Fig. 2.4a shows a encoder output of 0110100; Fig. 2.4b is the corresponding filter output when the bandwidth is very large. Notice that due to the small rise and fall time of the filter output, the noise margin is approximately 0.5 for every bit interval (sampling is assumed to take place at the end of the bit interval). In this case the BER will be given by equation 2.8. However, if the bandwidth is small, i.e., less than  $1/T$ , then  $m_n$  will vary from one bit interval to the next due to pattern variations and ISI from neighboring pulses as shown in Fig. 2.4c. In this case, a closed form expression for BER cannot be obtained and the general expression given by equation 2.7 has to be used. One solution to this problem is to determine all the possible values of  $m_n$  if ISI from only the neighboring pulses is taken into account [37]. Then the average BER can be determined by the following equation:

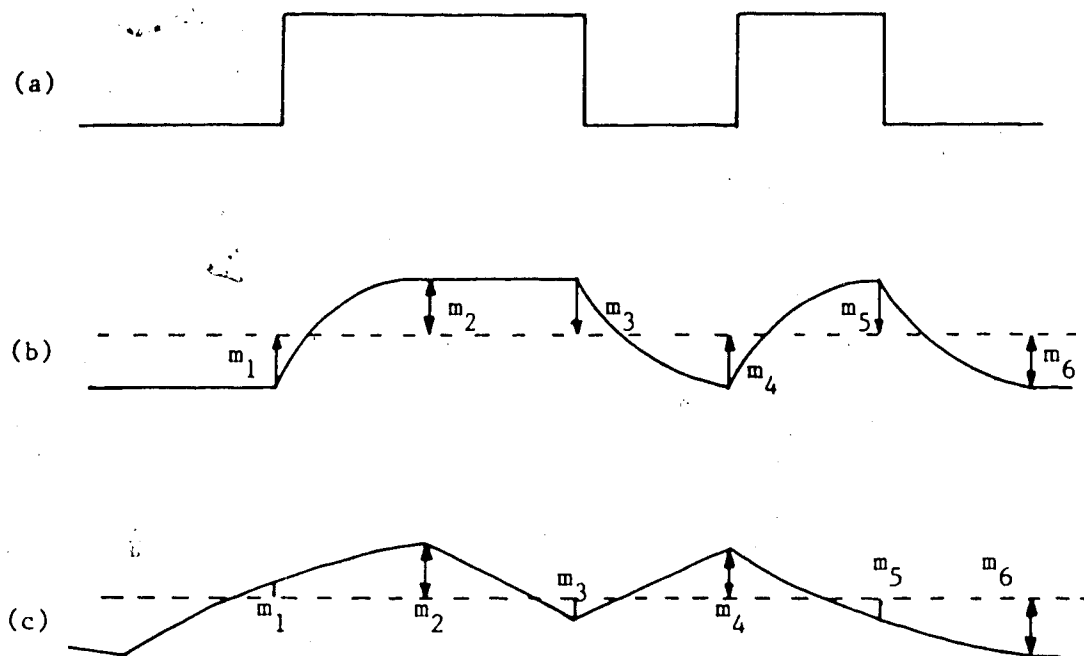


Fig. 2.4 Dependence of the noise margin ( $m_n$ ) on the bit pattern for large and small filter bandwidths.  
 ( The dotted line indicates the threshold, which is 0.5 V. )

- (a) Encoder output
- (b) Filter output when bandwidth is large, e.g.,  $2/T$ . Note that the noise margin is constant from one bit interval to the next.
- (c) Filter output when the bandwidth is small. Note that the noise margin is not constant from one bit interval to the next.

$$\text{BER} = 1/L \sum_{k=1}^L P_k Q(m_k / \sigma_n) \quad (2.10)$$

where, L = number of different noise margins

$m_k$  =  $k^{\text{th}}$  noise margin

$P_k$  = probability of  $m_k$

The problem with this approach is that determining the values of  $P_k$  and  $m_k$  is very difficult unless one is dealing with a simple line code and a simple receiver transfer function. Another approach is to determine the noise margin for each bit in a representative, finite data sequence by simulating the filtering operation on a computer and then using equation 2.7 to determine the average BER. This approach is attractive because, once the software is written, the BER for any encoded bit sequence can be determined for various filter transfer functions, noise power, sampling instant, etc. In the following analysis, this method was chosen.

### 2.1.3 Computer Simulation to determine the BER

Several computer programs were written to numerically determine the system BER as various parameters were changed. The program listings, which contain ample documentation, are given in Appendix A. A description of the BER calculation is as follows: Program Random generates 128 random binary digits.

These bits are encoded by the appropriate encoding scheme by programs Petrovic, Manchester, CMI, NRZ. Then, each bit is spread out to 16 points and the spectrum is determined by invoking the fast fourier transform (FFT) in Program Spectra. An incoming bit rate of 44.736 MHz (DS 3 rate) is assumed. The spectral resolution is 710 KHz ( $1/256T$ , where  $T$  = bit interval) and the spectrum repeats every 1.43 Ghz ( $16 \times 2/T$ ) [38]. The spectral components are weighted by the filter transfer function and the time domain signal is obtained by determining the inverse FFT (program Filter). First- and second order low pass Butterworth filters are used for the filter transfer function. The filtered time domain signal is sampled every  $T$  seconds at the end of each bit interval to determine the noise margin  $m_n$ . The BER is determined by evaluating equation 2.7. The  $Q$  function is approximated by the relation

$$Q(x) \approx (1/\sqrt{2\pi}) \int_x^\infty \exp(-t^2/2) dt$$

This approximation is valid for  $x > 4$ , i.e., small values of BER.

#### 2.1.4 Results

The relationship between the BER and filter bandwidth for the first- and second order Butterworth low pass filters are shown in Fig. 2.5 and Fig. 2.6 respectively for the following line codes: NRZ,



Petrovic, CMI, and Manchester. These results are obtained for an incoming bit rate of 44.736 Mb/s, a signal amplitude of 1V, a noise spectral density of  $10^{-10}$  W/Hz, and with sampling occurring at the end of each bit interval.

### 2.1.5 Discussion of Results

As the filter bandwidth is reduced from a large value, the BER for both the first-and second order filter decreases until a certain optimum bandwidth is reached. Any further reduction in bandwidth from this value results in the BER increasing, as predicted in Section 2.1.3. For each filter type the relationship between BER and filter bandwidth is almost identical for the 1B-2B codes. For the first order Butterworth the optimum bandwidth for the 1B-2B codes is 36 MHz ( $0.8/T$ ), while for the second order case, it is 48 MHz ( $1.07/T$ ). For the NRZ code, however, the optimum bandwidth for the first and second order case is 18 Mhz and 24 Mhz respectively.

These results indicate that the Petrovic, CMI, and Manchester codes require double the bandwidth of the NRZ code. Referring to Section 2.1, this result agrees with the value obtained by assuming that the required bandwidth is inversely proportional to the efficiency, i.e., since the 1B-2B codes have an efficiency of 0.5,

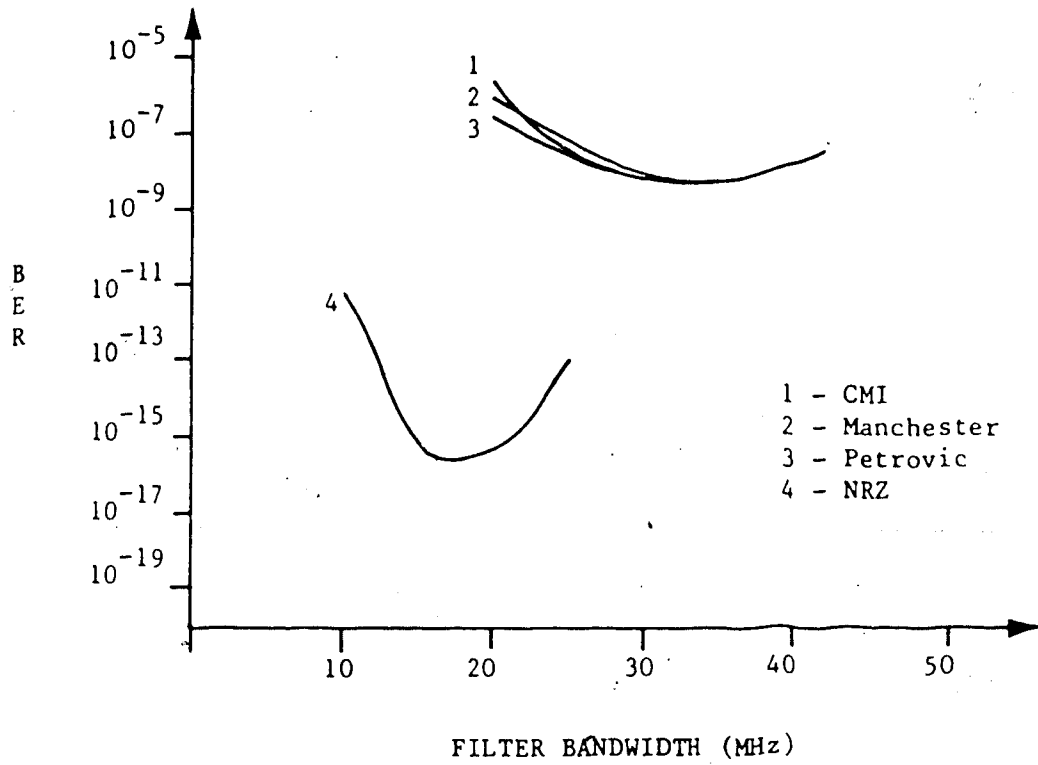


Fig. 2.5 BER versus Bandwidth for 1<sup>st</sup> order Butterworth LFF

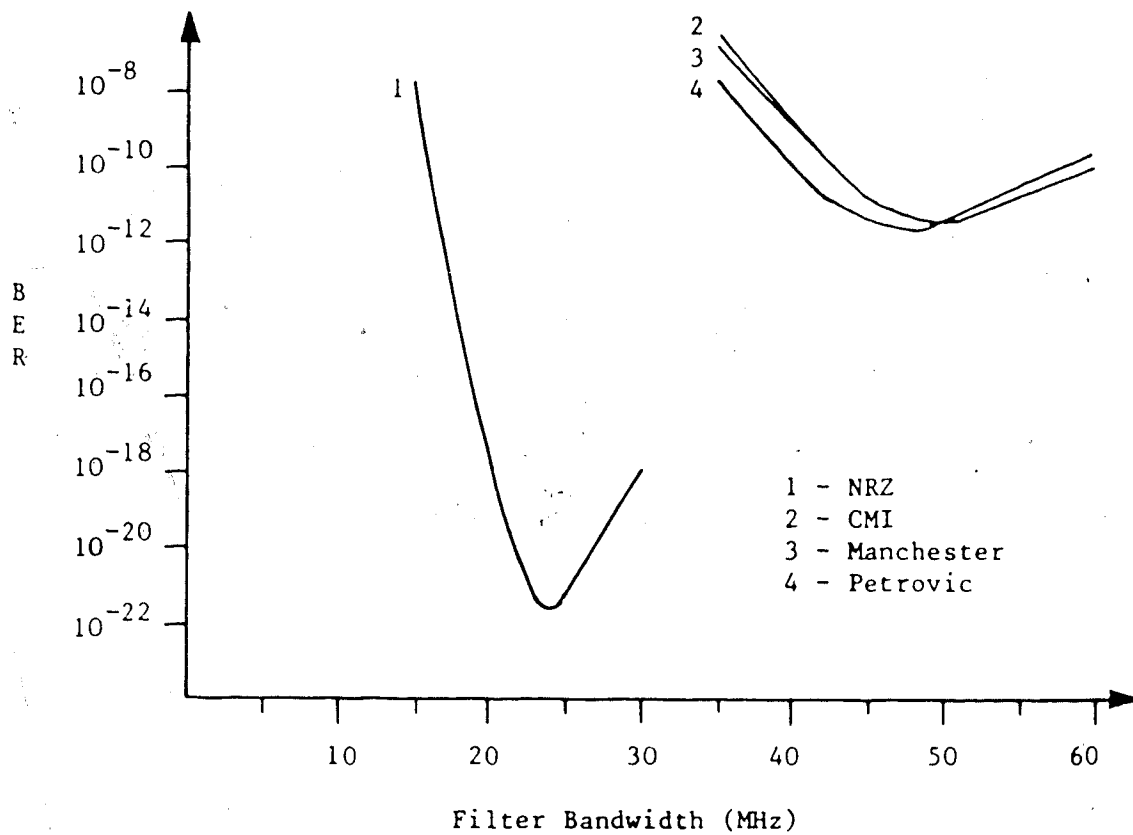


Fig. 2.6 BER versus Bandwidth for 2<sup>nd</sup> order Butterworth LPF

they require twice the bandwidth of the NRZ code. Since the 1B-2B codes contain half width pulses, intuitively, one would expect them to require twice the bandwidth of the NRZ code.

It is surprising to note that, although the power spectral density (PSD) of the Manchester code contains significantly larger high frequency components than the Petrovic code, they both require the same bandwidth. An intuitive explanation of this phenomenon is as follows. The PSD of a line code is simply an average spectrum for all the possible encoded bit sequences. The probability of occurrence of a short pulse ( $T/2$  seconds long) is higher for the Manchester code than for the Petrovic code. Thus the PSD for the Manchester code contains larger high frequency components. However, in order to obtain a reasonable BER, the receiver must have a large enough bandwidth to faithfully reproduce the short pulse. Since a short pulse can be found in both these codes, these codes will require a similar bandwidth.

The optimum bandwidth for the second order Butterworth LPF is found to be higher than for the first order Butterworth. The reason for this is that the second order filter attenuates the high frequency components more than the first order case, due to the steeper rolloff. Thus in order to ensure that the

signal has a sufficient rise time, the bandwidth for the second order filter must be increased.

Also notice that the lowest BER for the NRZ code is a few orders of magnitude better than the 1B-2B codes for both the first and second order filter. This is because we have assumed equal signal amplitudes (and hence signal power) for all these codes. Since the NRZ code requires half the bandwidth, the noise power entering the NRZ decoder will be a factor of 2 smaller than the noise power entering the decoder for the 1B-2B codes. Thus the argument of the Q function will be higher by a factor of  $\sqrt{2}$  for the NRZ code (see eqn. 2.7). A factor of  $\sqrt{2}$  difference in the argument of the Q function results in a significant difference in the BER due to the exponential nature of the Q function. To obtain the same BER performance, the signal power of the 1B-2B codes must be increased by a factor of 2. Thus the Petrovic code requires double the signal power to achieve the same BER as the NRZ code; i.e., it suffers from a 3dB receiver power penalty.

## 2.2 OPTICAL POWER PENALTY

The optical power penalty incurred when the Petrovic code is employed instead of the NRZ code is equal to the difference between the receiver sensitivity for the NRZ code and the receiver sensitivity for the Petrovic code. In the previous section it has been shown that, for an AWGN channel, this power penalty is 3dB, since the Petrovic code requires twice the bandwidth and the noise power is linearly proportional to the bandwidth. Extension of the results obtained in the previous section to a fibre optic system is not straight forward since the noise present in a fibre optic receiver is signal-dependent, non-gaussian, and is not white, i.e., constant with frequency.

Brooks and Jessop [5] have determined the power penalty for mB-nB block codes for several optical receiver configurations. In their calculations they assume that the 1B-2B codes require double the bandwidth of the NRZ code. In view of the results obtained in the previous section and the fact that the 1B-2B codes contain halfwidth pulses, this is a reasonable assumption. Before their results are presented, it is instructive to briefly examine the noise sources present in a fibre optic system.

A block diagram of a fibre optic receiver showing the major noise sources is shown in Fig. 2.7 [39].

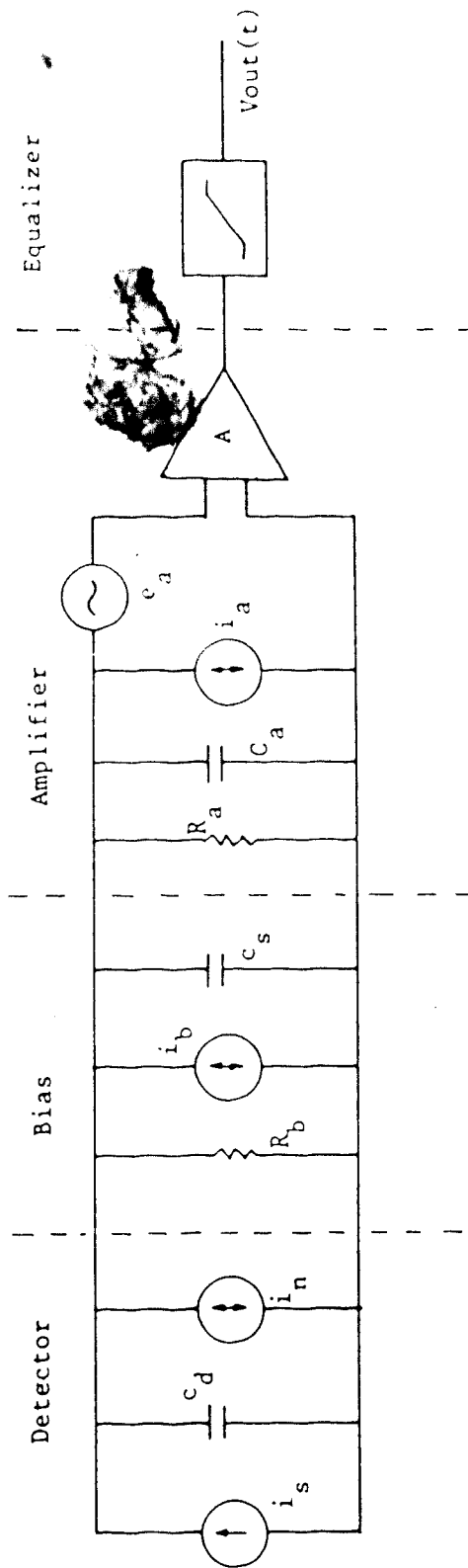


Fig. 2.7 Schematic Diagram of an Optical Receiver Showing the Noise Sources

In this diagram, the detector, which is normally a PIN diode or an APD, is modelled as a current source,  $i_s(t)$ , in parallel with a capacitance  $C_d$ . The noise generated by the detector is represented by  $i_n$ . The bias circuitry of the detector and amplifier is represented by an equivalent resistor  $R_b$ . The thermal noise generated by this resistor is denoted by  $i_b$ , which is white and has a spectral density given by  $4kT/R_b$ , where  $k$  = Boltzman's constant and  $T$  = absolute temperature. The amplifier has an input resistance  $R_a$ , input capacitance  $C_a$ , and a gain  $A$ . The noise generated by the amplifier is represented by a series voltage source  $e_a(t)$  and a shunt current source  $i_a(t)$ . The strength of these noise sources will depend on the active device used for the first stage and its dc bias point. A quantitative assessment of  $e_a(t)$  and  $i_a(t)$  for a bipolar transistor and a field effect transistor can be found in reference 40. The output of the preamplifier is equalized to obtain a flat frequency response over the desired pass band. Since the equalizer follows a high gain stage, its contribution to the overall noise will be negligible.

The input equivalent current noise power  $\langle i_n^2 \rangle$  can be shown to be equal to [39,40]:

$$\langle i_n^2 \rangle = (h\nu/n)^2 [(g^x/e) \langle i_o \rangle_T B I^2 + Z/g^2] \quad (2.11)$$

where,  $h\nu$  = photon energy



$\eta$  = quantum efficiency of the detector

$g$  = mean gain of the detector ( $g=1$  for a PIN diode)

$x$  = excess noise factor of the APD

$e$  = electron charge

$\langle i_0 \rangle_T$  = mean unity gain photocurrent over the bit time

$B$  = bit rate

$$I_2 = \int_{-\infty}^{\infty} \left| H_{out}(y)/H_p(y) \right|^2 dy \quad (2.12)$$

where,  $y = f/B$

$Z$  = dimensionless parameter representing the signal independent noise terms

$$= \left[ (B/e^2) (S_I + 2kT_0/R_b + S_E/R_T^2) I_2 + (2\pi C_t)^2 S_E I_3 B^3/e^2 \right] \quad (2.13)$$

where,  $R_T$  = total input resistance =  $R_b/R_a$

$C_T$  = total input capacitance =  $C_a + C_d + C_{stray}$

$$I_3 = \int_{-\infty}^{\infty} \left| H_{out}(y)/H_p(y) \right|^2 y^2 dy \quad (2.14)$$

The above equation is essentially a sum of signal-level dependent noise, represented by  $\langle i_0 \rangle_T$ , plus signal-level independent noise, which is represented by the parameter  $Z$ . The signal-level dependent noise at

the decision point is determined not only by the signal power and pulse shape during the present bit interval but also by the ISI that occurs from neighboring pulses. Since the sequence of pulses that is received depends on the line code used,  $\langle i_o \rangle_T$  will be a function of the line code. In the literature, a worst case value of  $\langle i_o \rangle_T$  is often used. This is calculated by assuming all the neighboring pulses are on. In this case the dependence of  $\langle i_o \rangle_T$  on the line code is removed. In the present analysis, this assumption will also be employed. The mean unity gain photocurrent over the bit time for an on pulse is

$$\langle i_o \rangle_{T, \text{on}} = \eta e/h\nu \cdot b_{\text{on}}/T \quad (2.15)$$

where,  $b_{\text{on}}$  = energy in the pulse

and similarly

$$\langle i_o \rangle_{T, \text{off}} = \eta e/h\nu \cdot b_{\text{on}}/T (1 - \gamma) \quad (2.16)$$

where  $\gamma$  = fraction of the energy of a single pulse which is contained within the bit interval.

The signal independent noise parameter  $Z$  arises due to the noise in the bias resistor and amplifier. It is interesting to note that the thermal noise of the resistor and the amplifier current noise generator have a noise contribution that varies as the bit rate while the noise due to the series voltage generator varies as the bit rate cubed. Thus, the noise spectrum at the

output of an optical receiver is not flat, as in the AWGN model described in the previous section.

In the power penalty analysis by Brooks and Jessop, they calculate the power penalty associated with block codes when an APD or PIN diode is used as the detector and when the input stage is a FET or a bipolar transistor. For the FET case, they examine the following two limiting cases:

a) when  $Z$  is dominated by the  $I_2$  term (noise that varies linearly with the bit rate, e.g, thermal noise) and

b) when  $Z$  is dominated by the  $I_3$  term (noise that varies as the bit rate cubed, e.g, FET channel noise).

For the bipolar front-end, they examine the optimized case which occurs when the series and shunt amplifier noise sources are made equal by judiciously selecting the collector bias current. The six cases that result from their simplification are:

- (i) APD,  $I_2$  dominates  $Z$ ; denoted as APD- $I_2$
- (ii) APD,  $I_3$  dominates  $Z$ ; denoted as APD- $I_3$
- (iii) APD, optimized bipolar; denoted as APD-OB
- (iv) PIN,  $I_2$  dominates  $Z$ ; denoted as PIN- $I_2$
- (v) PIN,  $I_3$  dominates  $Z$ ; denoted as PIN- $I_3$
- (vi) PIN, optimized bipolar; denoted as PIN-OB

The approach that Brooks and Jessop have taken is to determine expressions for the receiver sensitivity

for the NRZ code and the mB-nB code for the above six cases. The power penalty is then obtained by subtracting the two receiver sensitivities. Their results for 1B-2B codes when fibre dispersion is negligible is shown in Table 2.1. For the optimized bipolar case, the power penalty is 3 dB for both the APD and PIN detector. For an APD-FET receiver, the power penalty varies from 2.3 db to 3.8 dB. In the case of a PIN-FET receiver, the power penalty varies from 1.5 dB to 4.5 dB. It should be noted that in a practical PIN-FET or APD-FET receiver the power penalty will be somewhere between these limits because neither the I<sub>2</sub> or the I<sub>3</sub> term would dominate. Thus in a practical system employing a FET front end or a bipolar front end, the receiver penalty is around 3dB.

### 2.3 REPEATER SPACING

The distance between repeaters is an important parameter for the design of fibre optic systems. The maximum spacing of repeaters in an optical fibre communication system is determined by the following two transmission parameters: attenuation and dispersion. Dispersion reduces the bandwidth available while attenuation reduces the power available at the receiver. The distance between repeaters is then determined as the smaller of the distance limitation due to dispersion and

Table 2.1 Optical Power Penalty for the 1B-2B Codes,  
as calculated by Brooks and Jessop [5].

For the APD case, the excess noise factor  
is assumed to be 1.

Case	Optical Penalty (dB)
APD-I2	2.3
APD-I3	3.8
APD-OB	3.0
PIN-I2	1.5
PIN-I3	4.5
PIN-OB	3.0

that due to attenuation. In general, repeater spacing is limited by attenuation at lower bit rates and limited by dispersion at higher data rates.

Since the Petrovic code requires approximately double the bandwidth and power as compared to the NRZ code, the repeater spacing for the Petrovic code will vary considerably from that of the NRZ code. The repeater spacing of the NRZ code and the Petrovic code will be compared for three representative systems:

1. a 0.83  $\mu\text{m}$  LD with multimode fibre and a Si APD-bipolar receiver
2. a 1.3  $\mu\text{m}$  LED with single mode fibre and a Ge APD-bipolar receiver
3. a 1.3  $\mu\text{m}$  LD with single mode fibre and a Ge APD-bipolar receiver.

Important specifications for the above system are given in Table 2.2.

If the system is attenuation limited, then the repeater spacing,  $L$ , is given by the following equation:

$$L = (P_{\text{in}} - P_{\text{rx}} - P_{\text{sys}}) / \alpha \quad \text{km} \quad (2.17)$$

where  $P_{\text{in}}$  = power coupled into fibre (dB)

$P_{\text{rx}}$  = receiver sensitivity (dBm)

$P_{\text{sys}}$  = system degradation margin (dB)

$\alpha$  = fibre attenuation (dB/km)

If the system is dispersion limited, then the repeater spacing is given by:

$$L = \text{BDP}/B \quad (2.18)$$

where B = bit rate

$$\begin{aligned} \text{BDP} &= \text{bandwidth distance product of fibre (optical)} \\ &= 440/D \cdot \text{MHz km} \end{aligned} \quad (2.19)$$

where D = pulse dispersion in ns/km (FWHM)

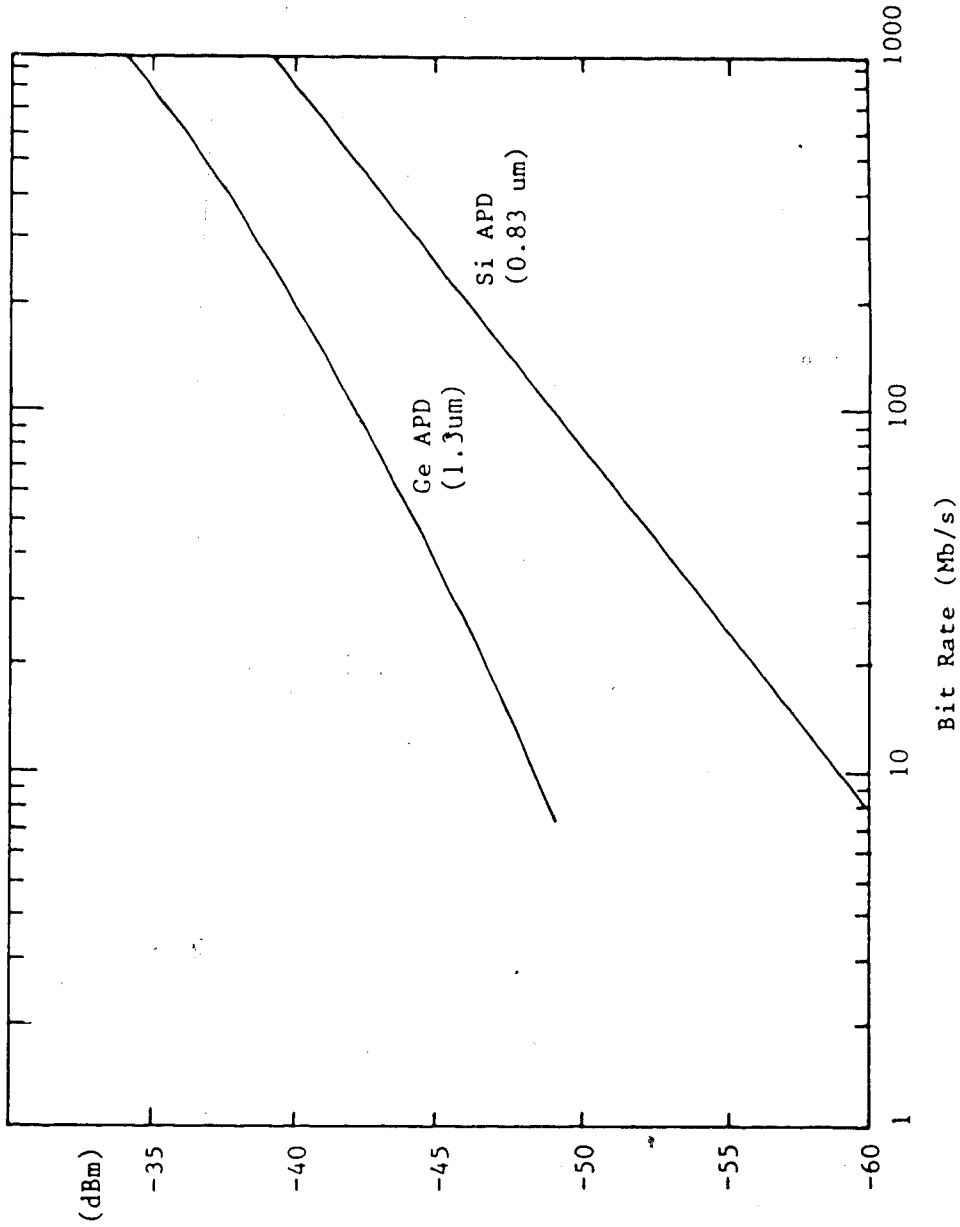
The sensitivity versus bit rate curves for a Si APD-bipolar receiver and a Ge APD-bipolar receiver are given in Fig. 2.8 for the NRZ code (BER =  $10^{-9}$ ) [44]. The receiver sensitivity of the Petrovic code was obtained by assuming a 3dB power penalty. The repeater spacing for the three systems under consideration were calculated; the results are shown in Figures 2.9 to 2.11.

From these curves we see that the repeater spacing for the Petrovic code is always less than that of the NRZ code. Under attenuation limited conditions, the repeater spacing is smaller by  $3/\alpha$  km, where  $\alpha$  is the fibre attenuation in dB/km. Under dispersion limited situations, the repeater spacing is smaller by a factor of 2. Usually, the difference in repeater spacing between the NRZ and the Petrovic code is smallest when the system is attenuation limited. For example, in System 3, the repeater spacing is smaller by 6 km when the system is attenuation limited and smaller by 25 km when the system is dispersion limited (bit rate of 1 Gb/s). Thus, in order to achieve the smallest

Table 2.2 System Specifications

Parameter	System #1	System #2	System #3
Wavelength	0.83 $\mu\text{m}$	1.3 $\mu\text{m}$	1.3 $\mu\text{m}$
Fibre Type	Multimode	Single mode	Single mode
Fibre Attenuation	3 dB/km	0.5 dB/km [43]	0.5 dB/km
Fibre Dispersion	1.5 ns/nm km	3 ps/nm km [41]	3 ps/nm km
Source Type	Laser Diode (LD)	Edge Emitting LED	LD
Source Spectral Width	2 nm	60 nm	2 nm
Bandwidth Dist. Product (BDP)	300 MHz km	2.4 GHz km	73.3 GHz km
Power Coupled into Fibre	0 dBm	-20 dBm [42]	-3 dBm
Detector	Si APD	Ge APD	Ge APD
System Margin	6 dB	6 dB	6 dB





R X S E N S I T I V I T Y

Fig. 2.8 Receiver Sensitivity versus Bit Rate for a Si APD and a Ge APD Bipolar Receiver [44].

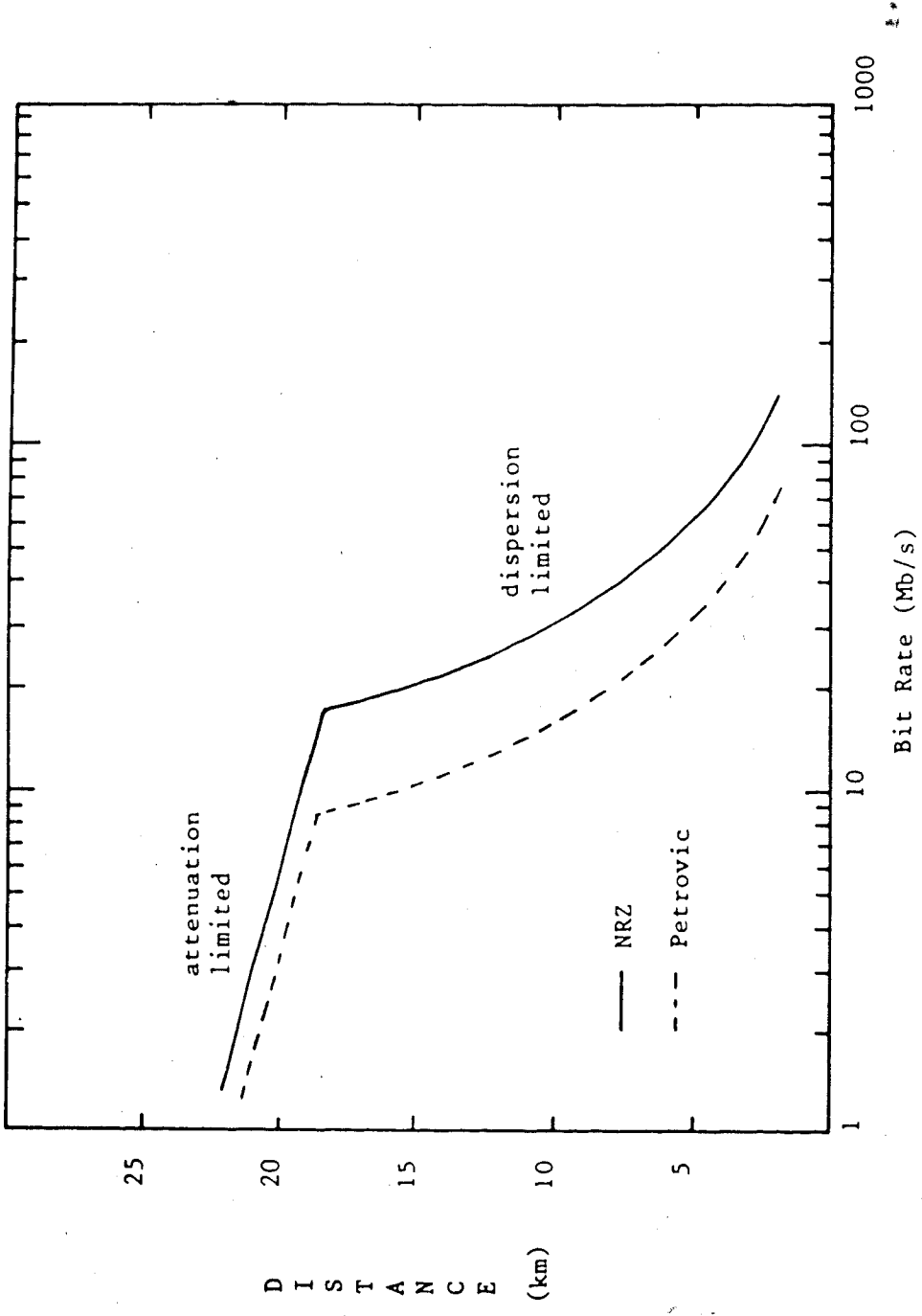


Fig. 2.9 Repeater Spacing versus Bit Rate for System #1

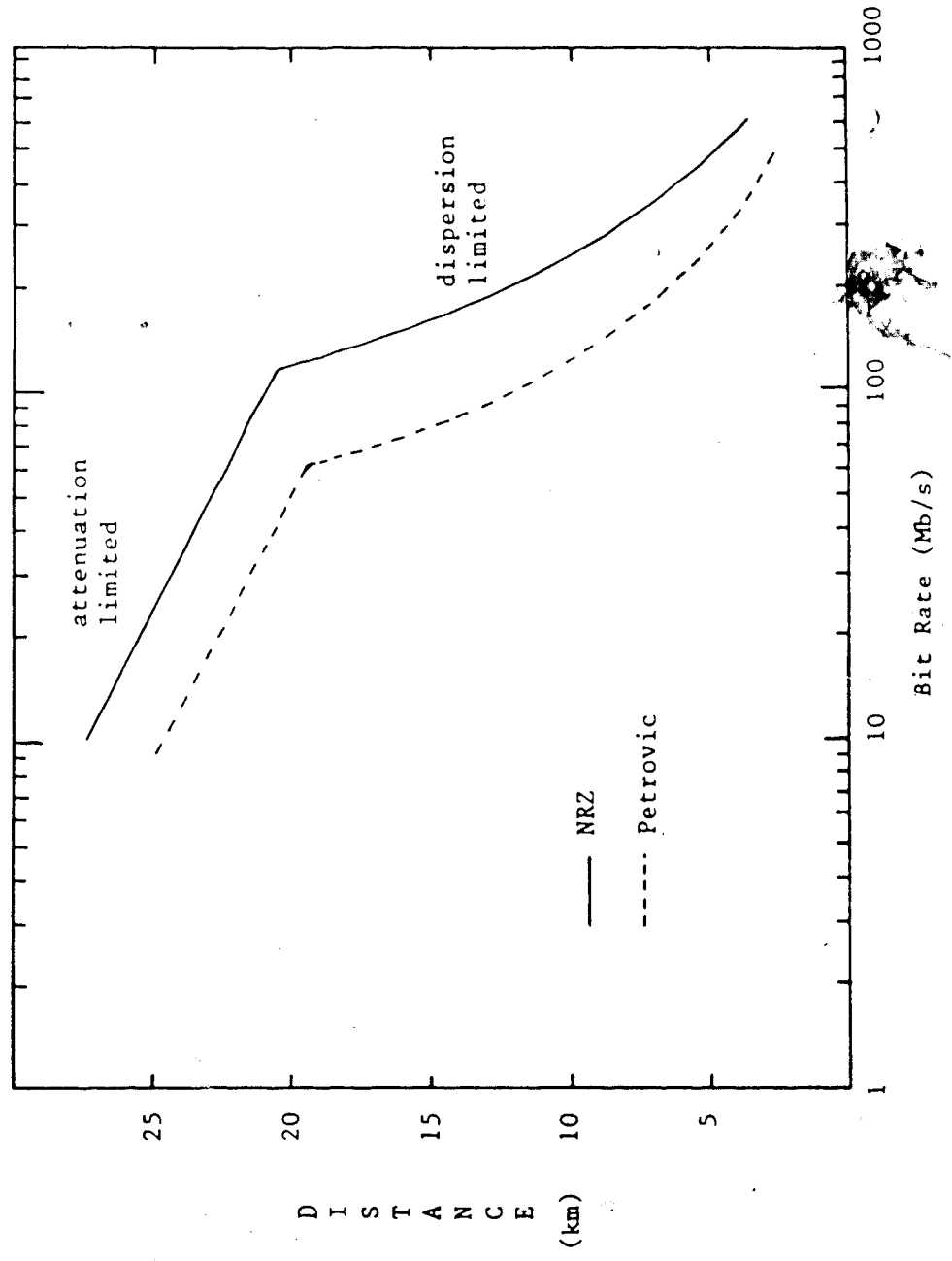


Fig. 2.10 Repeater Spacing versus Bit Rate for System #2

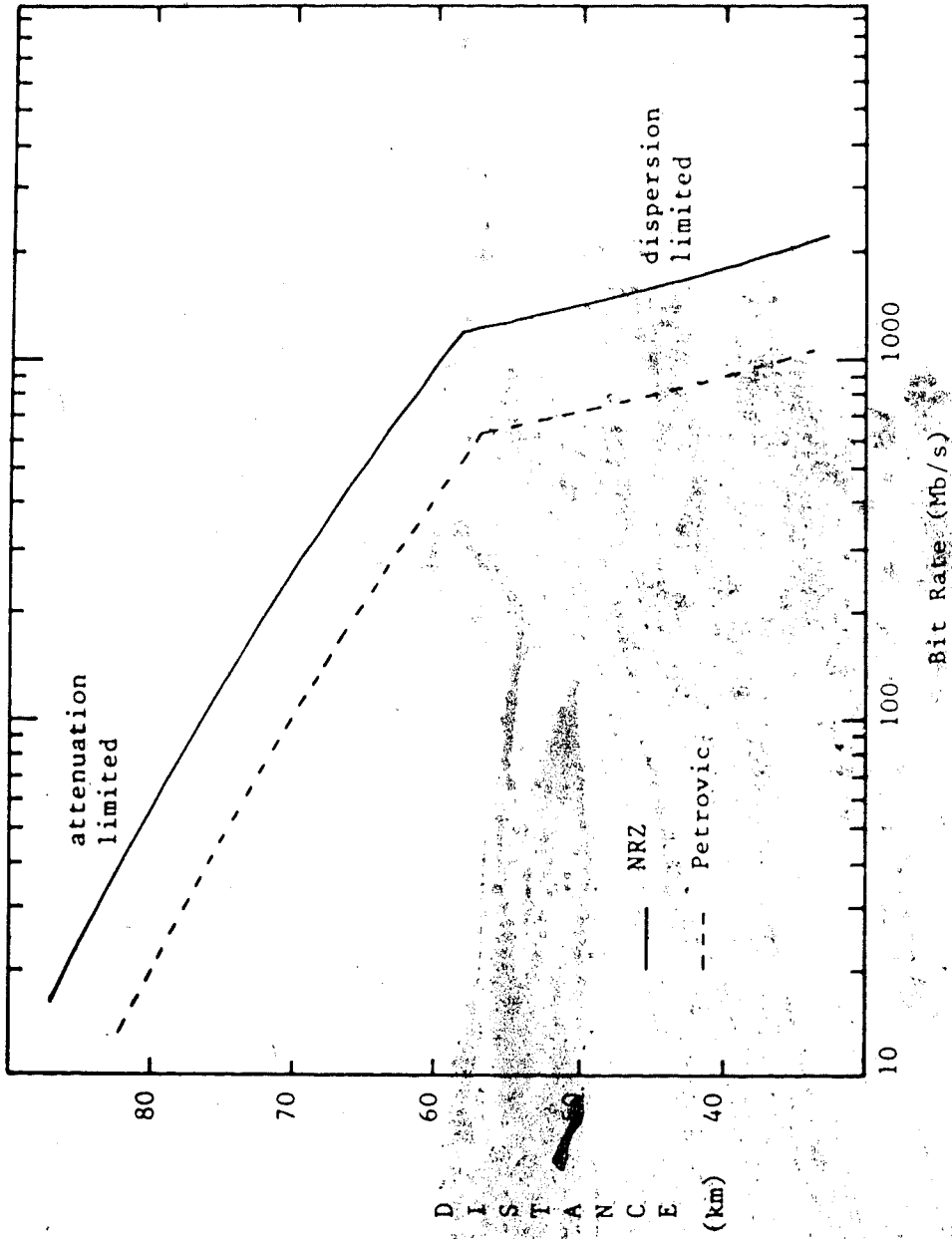


Fig. 2.11 Repeater Spacing versus Bit Rate for System 3

reduction in repeater spacing, the Petrovic code and other bandwidth expansion codes should be seriously considered only under attenuation limited conditions. Under dispersion limited conditions, multilevel signalling methods are attractive [5]. One group of systems which are virtually always attenuation limited are local area networks. (Dispersion and attenuation is not significant in LANs because of the short path length between terminals, which is usually under a few kilometres).

Although this section has emphasized that, with the Petrovic code, a shorter distance between repeaters is realized, the positive aspects of this code must not be forgotten, i.e., it is bit sequence independent and it provides ease of clock recovery.

A novel clock recovery circuit that can be used to recover the sampling signal from the Petrovic code will be described in the next chapter.

## CHAPTER 3

### THE SELF-SUSTAINING MONOSTABLE MULTIVIBRATOR CLOCK RECOVERY CIRCUIT

Recently, a novel clock recovery circuit consisting of a self-sustaining monostable multivibrator, shown in Figure 3.1, was reported by Witte and Moustakas [31]. This timing extraction device is very attractive because it is simple to implement, inexpensive and, since it is digital, it can be constructed using logic gate array technology. Furthermore, this clock recovery circuit is not restricted to only the NRZ code with a scrambler (the application reported in [31]), it can be used with any line code that has a reasonable restriction placed on the number of consecutive ones and zeroes allowed, e.g., simple 1B-2B codes, such as the Petrovic, CMI, DMI and Miller. Even though the self-sustaining monostable multivibrator clock recovery circuit has many attractive features, it has received very little attention in the literature. The original and only paper on this clock recovery circuit, which was by Witte and Moustakas in October 1983 [31], concentrates on the circuit operation and gives an equation for determining the maximum number of consecutive 1s or 0s allowed in the input signal for proper operation. It also gives experimental

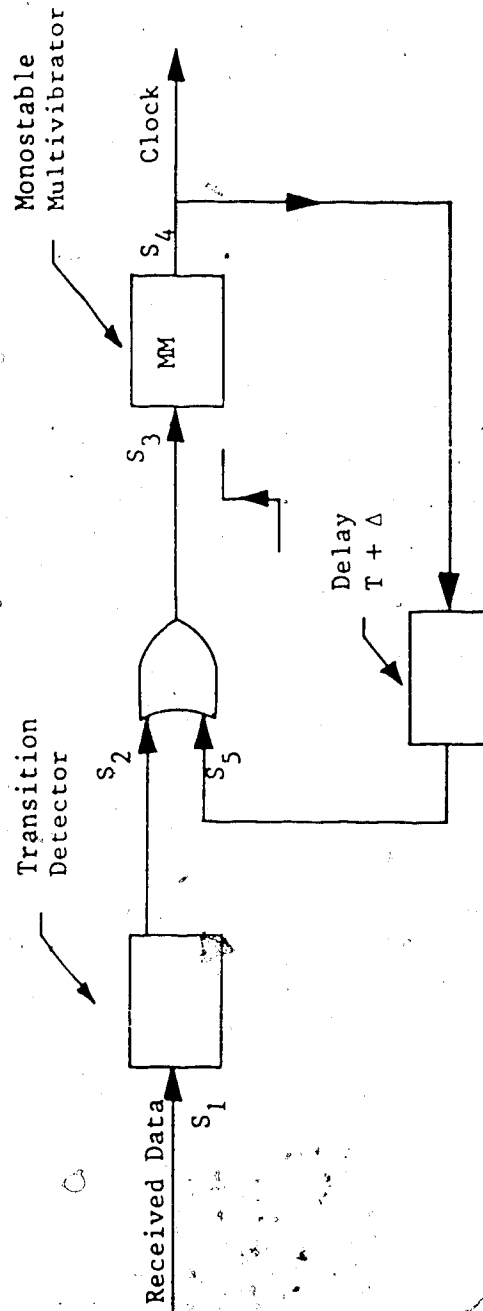


Fig. 3.1 The Self-Sustaining Monostable Multivibrator Clock Recovery Circuit [31]

verification of the circuit operation for a 16 Mb/s fibre optic local area network (LAN) employing NRZ signalling with a scrambler. The jitter performance and the application of this clock recovery circuit to other line codes have not yet been reported, to the author's knowledge. Thus in this project, it was felt that it would be worthwhile to implement the self-sustaining monostable circuit in an experimental Petrovic system and examine its jitter performance.

### 3.1 Circuit Operation \*

A timing diagram of the self-sustaining monostable multivibrator clock recovery circuit is shown in Figure 3.2 (from [31]). For convenience, the propagation delay of the gates and the monostable multivibrator (MM) are assumed to be zero. In order to understand the operation of this circuit, consider the circuit response, after being turned on, to the input bit sequence 10001, waveform S1 in Figure 3.2. (S1 is obtained directly from the receiver output). The transition detector generates a pulse on every rising and falling edge of the input signal, as shown by S2 in Figure 3.2. (Referring to Section 1.3, the transition detector forms the non-linear element which is required to generate the clock spectral line). The width of these pulses is equal to the delay  $T_p$  and is not critical as



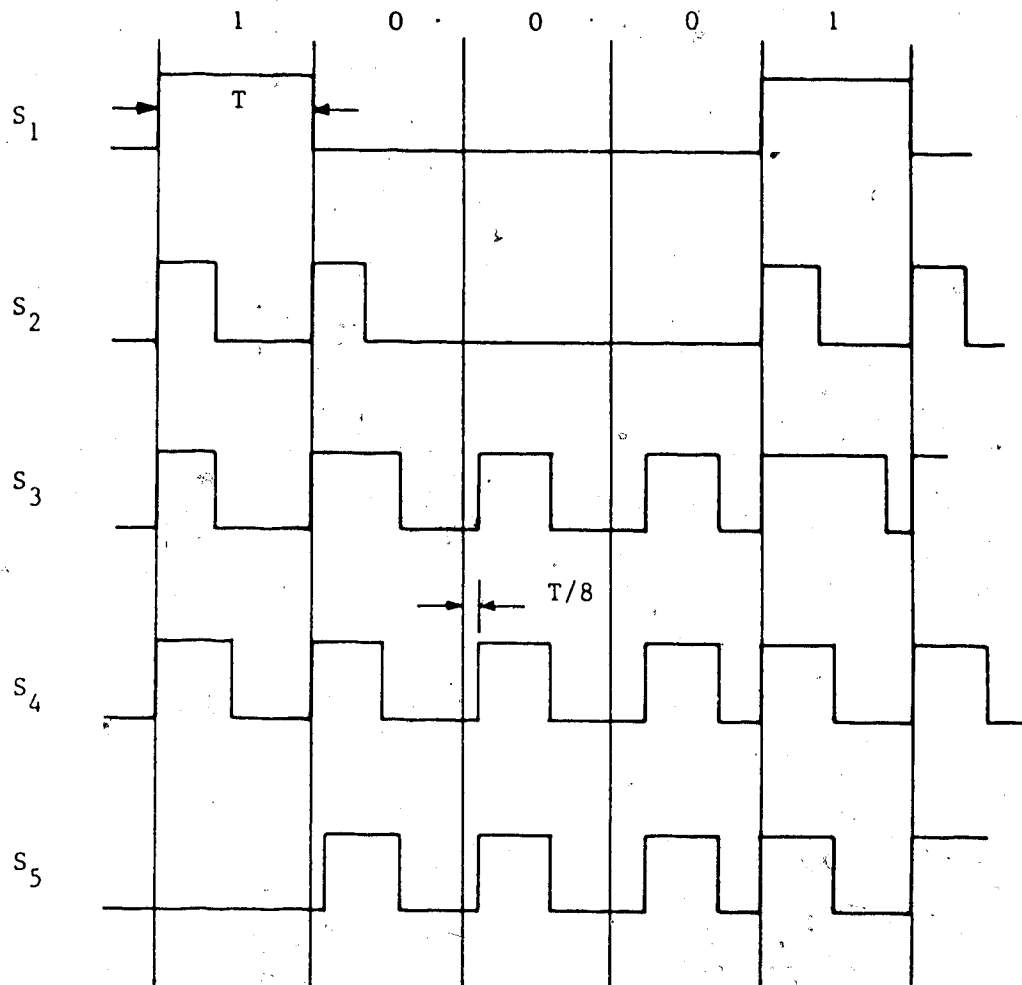


Fig. 3.2 Timing Diagram of the Self-Sustaining Monostable Clock Recovery Circuit for an 10001 Input Bit Sequence

long as it is of sufficient duration to trigger the MM. In Figure 3.2,  $T_p$  is arbitrary chosen to be  $3T/8$ , where  $T$  is the bit interval. A monostable multivibrator with a feedback path around it follows the transition detector. The MM produces a pulse on every rising edge of its input (S4). It can be triggered by the pulses generated by the transition detector, here referred to as the primary pulses, or by the feedback pulses (S5 in Figure 3.2). The feedback delay  $T_1$  is chosen to be slightly greater than  $T$ , i.e.  $T_1 = T + \Delta$  where  $\Delta$  is a small positive quantity. Thus, the feedback pulse triggers the MM only when the primary pulse is missing (or late). In practice,  $\Delta$  is chosen to be as small as possible, in Figure 3.2 it is chosen to be  $T/8$  for ease of illustration. The third and fourth bit interval of the input signal shown in Figure 3.2 do not contain transitions. Hence, the transition detector does not produce a pulse during these intervals. In this situation the feedback pulse triggers the MM to produce the clock pulse  $\Delta$  seconds after the ideal time for the third bit interval and  $2\Delta$  seconds after the ideal time for the fourth bit interval. In the fifth bit interval, a transition from a 0 to a 1 occurs in the input bit stream and hence a primary pulse triggers the MM at the ideal time. Thus, we see that when a long sequence of 0s or 1s occur in the input, the clock signal advances

in time by  $\Delta$  seconds during each bit interval until a transition occurs. This is a simplified description of the circuit operation and is valid only when jitter is negligible; the effect of jitter will be considered in the next section.

The feedback delay must be greater than the bit interval  $T$ . If this is not so, the positive edges of  $S_4$  will not coincide with the input bit transitions, independent of  $S_3$ , and the clock will drift out of phase and synchronization will never be attained. The maximum number of consecutive 1s or 0s that can occur in the input with synchronization still being maintained is determined by how small  $\Delta$  can be made, i.e. how closely  $T_1$  approximates  $T$ , but with the restriction  $T_1 > T$ . This depends on the variation of propagation delays of the logic gates and the delay network with temperature.

In addition, the recovery time of the MM,  $T_r$ , affects the maximum interval between transitions by limiting the maximum possible phase shift. (In this context, the recovery time of the MM is defined as the time required by the MM, after its output has returned to the stable state, before it can be triggered again). The maximum possible phase shift that is allowed is  $T - T_m - T_r$ , where  $T_m$  is the MM output pulse width. Thus, the maximum length of consecutive 1s or 0s allowed in the input bit stream,  $N$  is [31]:

$$N = 1 + (T - T_m - T_r) / \Delta \quad (3.1)$$

The "1" in the above equation accounts for the fact that the first bit in the input has already been received before the MM output begins to drift out of phase. From this equation, we see that for high bit rate operation (i.e., small values of  $T$ )  $T_m$  and  $T_r$  should be made as small as possible. Also, notice that for fixed values of  $T$ ,  $T_m$ , and  $T_r$ , the value of  $\Delta$  increases as the number of consecutive 1 or 0s in the input signal,  $N$ , decreases. It is advantageous to make  $N$  small since it is easier to construct a delay network that provides a delay of  $T + \Delta$  seconds for large values of  $\Delta$  than for small values of  $\Delta$ . Since the Petrovic code has a small value of  $N$ , this type of clock recovery circuit is easier to implement for the Petrovic code than for the NRZ code.

### 3.2 Clock Recovery in a Petrovic System

The self-sustaining monostable multivibrator clock recovery circuit described in the previous section can easily be used to recover the clock from the Petrovic code. However, due to the mid-bit transitions present in the Petrovic code, the recovered clock will operate at twice the bit rate. Thus, the MM output has to be divided by two before it can be applied to the decoder. Figure 3.3 shows the transition detector output for an

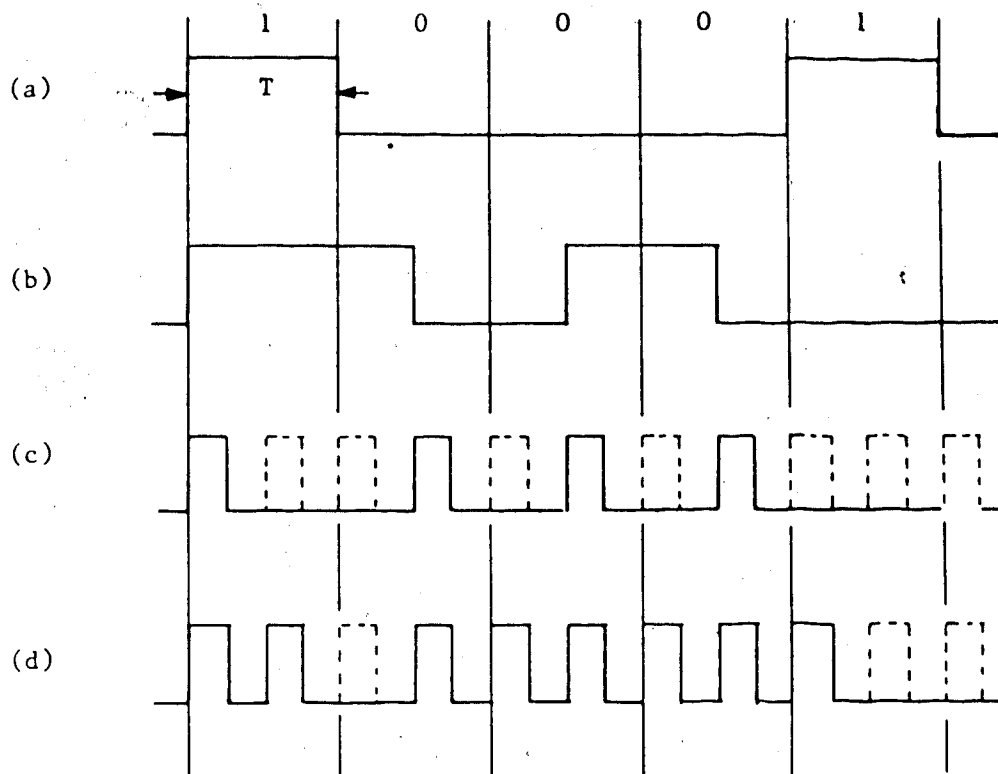


Fig. 3.3 Transition Detector Output

- (a) 100010 NRZ bit sequence
- (b) Output of the transition detector when waveform (b) is its input. The missing primary pulses are shown in dotted lines.
- (c) Output of transition detector when the EX-NOR output of the decoder (for the Petrović bit stream shown in (b)) forms the input. Note that this waveform contains a greater number of primary pulses than waveform (c).

arbitrary Petrovic encoded bit stream. The delay in the transition detector is chosen to be  $T/4$ . Notice that the output of the transition detector contains pulses occurring at multiples of  $T/2$  seconds. The pulses in dotted lines represent the pulses that will be inserted by the self-sustaining MM circuit. Also, since the maximum interval between transitions in the input is  $2T$ , a maximum of 3 consecutive pulses can be missing from the transition detector output. This is one of the advantages of the Petrovic code. With the NRZ code, there is no such restriction, unless a scrambler is used.

In the Petrovic decoding process, the incoming Petrovic bit stream and a delayed version of it are applied to an exclusive NOR (EX-NOR). The resulting output signal still has transitions at multiples of  $T/2$  seconds but the maximum interval between transitions is reduced from  $2T$  to  $3T/2$ . When this signal is applied to the clock recovery circuit, the maximum number of consecutive pulses that can be missing ( $N$ ) from the transition detector output is now 2. From jitter considerations (see Section 3.3) it will be seen that one would like to make  $N$  as small as possible. Thus it is advantageous to use the EX-NOR output of the decoder instead of the received Petrovic signal as the input to the clock recovery circuit. The resulting transition

detector output when the EX-NOR output is applied to the input is shown in Fig. 3.3d.

### 3.3 Jitter Analysis

In the ideal case, when jitter is absent, the pulses generated by the transition detector (the primary pulses) will trigger the MM at integral multiples of the bit interval  $T$  for the NRZ code and  $T/2$  for the Petrovic code. In practice, the arrival times of the primary pulses will fluctuate or "jitter" around the ideal arrival times. Jitter in the primary pulses will be assumed to have a gaussian probability distribution function (pdf) with a zero mean and a variance  $\sigma_i^2$ . This is a reasonable assumption and its justification is as follows. If the fibre-receiver bandwidth is large enough so that intersymbol interference will be negligible, then pattern jitter (or systematic jitter) will be negligible and the jitter will be mainly due to the receiver noise [45]. The relationship between input jitter  $j_i(t)$  and receiver noise  $n(t)$  can be obtained with the aid of Figure 3.4. When the received signal is first applied to a logic gate, it will cross the gate threshold every  $T/2$  seconds. However, due to noise contained in the input signal, the threshold crossings will deviate from the ideal times. In Figure 3.4, the received signal will ideally cross the threshold at time

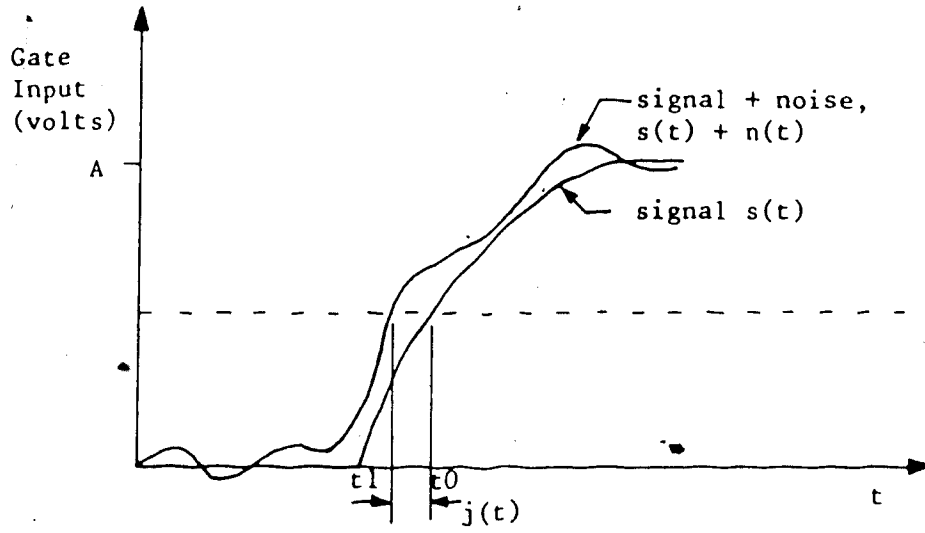


Fig. 3.4 Relationship between jitter,  $j(t)$ , and receiver noise,  $n(t)$ , when the received signal is first applied to a logic gate.



$t_0$ . Due to noise, the signal actually crosses at  $t_1$ . The difference  $t_0 - t_1$  is the jitter  $j_i(t)$ . If the rising edge of the received signal is assumed to be linear, then [46]

$$n(t_i)/j(t_i) = A/t_r \quad (3.2)$$

$$\text{or } j(t_i) = t_r n(t_i)/A \quad (3.3)$$

Thus, the jitter is a function of the receiver noise characteristics and is proportional to the rise time of the input signal. Noise in fibre optic systems is non-gaussian due to the poisson statistics of the incoming photons and the complex statistics of the APD gain (if an APD is used). However, in most cases, the thermal noise of the preamplifier dominates the total noise and thus the receive noise can be assumed to be gaussian. If the noise is assumed to be a zero mean, gaussian process with a variance  $\sigma_n^2$ , then the jitter will also be gaussian, have a zero mean and its variance  $\sigma_i^2$  can be obtained from equation 3.3 to be

$$\sigma_i^2 = t_r^2 \sigma_n^2 / A^2 \quad (3.4)$$

Let us next calculate the output jitter pdf of the self-sustaining monostable multivibrator clock recovery circuit for a gaussian input jitter pdf. For convenience, the delay of the gates and of the MM will be assumed to be zero. Assume that initially a primary pulse triggers the MM at the ideal time (i.e.  $j_i(t) = 0$ ), causing the delayed output pulse to arrive at the OR

gate (see Figure 3.1)  $T + j_i(t)$  seconds later. If  $j_i(t) < \Delta$ , then the primary pulse will trigger the MM because it will arrive at the OR gate before the delayed output pulse. In this case, the output pulse will occur  $j_i(t)$  seconds away from the ideal time and hence the output jitter  $j_o(t)$  will be equal to  $j_i(t)$ . If  $j_i(t) > \Delta$ , then the delayed output pulse will trigger the MM and  $j_o(t)$  will be equal to  $\Delta$ , irrespective of the actual value of  $j_i(t)$ . Note that the feedback has inhibited any primary pulse arriving  $\Delta$  seconds or more after the ideal time from triggering the MM. The output jitter pdf for this case is shown in Figure 3.5. This is an example of a half-wave rectifier transformation; an impulse exists at  $t = \Delta$  to ensure that the area under the pdf curve is unity [47]. The amplitude of this impulse,  $A$ , is equal to the area under the gaussian curve from  $\Delta$  to  $\infty$ , i.e.,

$$A = \frac{1}{\sqrt{2\pi} \sigma_i} \int_{\Delta}^{\infty} e^{-t^2/2\sigma_i^2} dt \quad (3.5)$$

The calculation of the output jitter variance,  $\sigma_o^2$  is as follows:

$$\sigma_o^2 = E[j_o^2(t)] - E^2[j_o(t)] \quad (3.6)$$

where  $E(\cdot)$  denotes the expectation.

Although the input jitter has a zero mean, the output jitter pdf will have a non-zero mean.

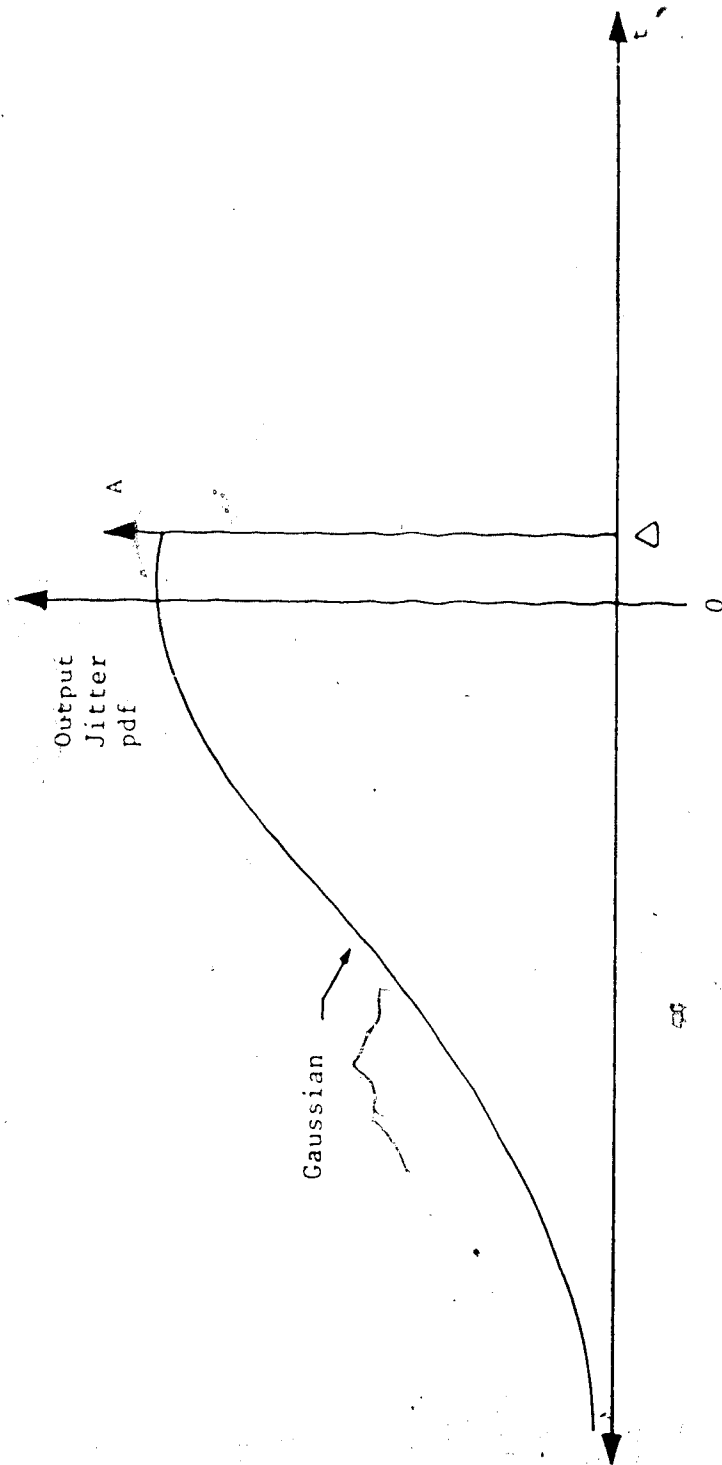


Fig. 3.5 Pdf of output jitter when a primary pulse triggers the MM at the ideal time during the previous time slot.

$$E(j_o(t)) = \frac{1}{\sqrt{2\pi}\sigma_i} \int_{-\infty}^{\Delta} t e^{-t^2/2\sigma_i^2} dt + A\Delta \quad (3.7)$$

$$= \frac{-\sigma_i}{\sqrt{2\pi}} + \frac{1}{\sqrt{2\pi}\sigma_i} \int_0^{\Delta} t e^{-t^2/2\sigma_i^2} dt + A\Delta \quad (3.8)$$

$$= \frac{-\sigma_i}{\sqrt{2\pi}} + \frac{\Delta^2}{2\sqrt{2\pi}\sigma_i} + A\Delta \quad (\text{when } \Delta < \sigma_i/10) \quad (3.9)$$

Similarly,

$$E(j_o^2(t)) = \frac{1}{\sqrt{2\pi}\sigma_i} \int_{-\infty}^{\Delta} t^2 e^{-t^2/2\sigma_i^2} dt + A\Delta^2 \quad (3.10)$$

$$\text{but } \frac{1}{\sqrt{2\pi}\sigma_i} \int_{-\infty}^{\Delta} t^2 e^{-t^2/2\sigma_i^2} dt = 0.5\sigma_i^2 \quad (3.11)$$

$$\therefore E(j_o^2(t)) = 0.5\sigma_i^2 + \underbrace{\frac{1}{\sqrt{2\pi}\sigma_i} \int_0^{\Delta} t^2 e^{-t^2/2\sigma_i^2} dt}_C + A\Delta^2 \quad (3.12)$$

For small values of  $\Delta$ , (e.g.,  $\Delta < \sigma_i/10$ ), then the integral denoted by  $C$  becomes

$$\frac{1}{\sqrt{2\pi}\sigma_i} \int_0^{\Delta} t^2 dt = \frac{1}{\sqrt{2\pi}\sigma_i} \frac{\Delta^3}{3} \quad (3.13)$$

$$\therefore E(j_o^2(t)) = \frac{\sigma_i^2}{2} + \frac{1}{\sqrt{2\pi}\sigma_i} \frac{\Delta^3}{3} + A\Delta^2 \quad (3.14)$$

Substituting (3.14) and (3.9) into (3.6) we get:

$$\sigma_o^2 = 0.5\sigma_i^2 + \frac{1}{\sqrt{2\pi}} \frac{\Delta^3}{\sigma_i^3} + A\Delta^2 - \left( \frac{-\sigma_i}{\sqrt{2\pi}} + \frac{\Delta^2}{2\sqrt{2\pi}\sigma_i} + A\Delta \right)^2 \quad (3.15)$$

If  $\Delta = 0$  (the ideal case), then  $A = 0.5$  and

$$\sigma_o^2 = 0.5\sigma_i^2 - \sigma_i^2/2\pi \quad (3.16)$$

$$= 0.341 \sigma_i^2 \quad (3.17)$$

The ratio of the output jitter variance to the input jitter variance,  $\sigma_o^2/\sigma_i^2$ , is 0.341.

If  $\Delta = \sigma_i/10$ , then  $A = 0.5$  and from (3.15) we get:

$$\sigma_o^2 = 0.384 \sigma_i^2 \quad (3.18)$$

The ratio  $\sigma_o^2/\sigma_i^2$  is now 0.384 (as compared to 0.341 for  $\Delta = 0$ ). Notice that as the value of  $\Delta$  increases, the ratio between the output jitter variance to the input jitter variance increases.

The output jitter pdf is not time independent. When primary pulses are missing or late, the MM is triggered by the feedback signal. This extends the pdf to the right by  $\Delta$  seconds for each such event. For example, if a primary pulse is missing and the delayed output pulse triggers the MM  $\Delta$  seconds after the ideal arrival time, then the output jitter pdf for the next bit interval will be as shown in Figure 3.6. The ratio  $\sigma_o^2/\sigma_i^2$  for this case with  $\Delta = \sigma_i/10$  (using equation 3.15) is approximately 0.432. An exact value of  $\sigma_o^2/\sigma_i^2$  is difficult to obtain. However, if  $\Delta \ll \sigma_i$ , it can be

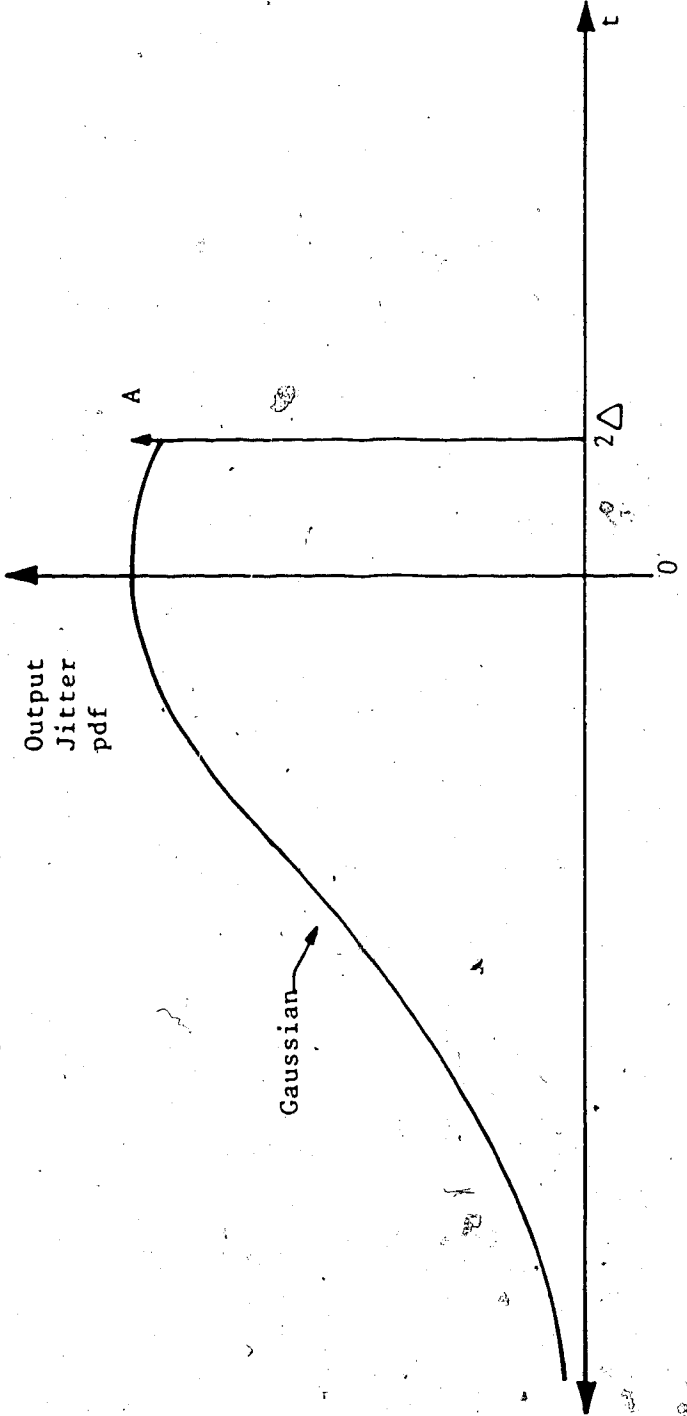


Fig. 3.6 Pdf of output jitter when a feedback pulse triggers the MM at  $\Delta$  seconds after the ideal time during the previous time slot.

intuitively seen that the average value of  $\sigma_o^2/\sigma_i^2$  will be approximately 0.34, i.e., the value obtained with  $\Delta = 0$  (see equation 3.17).

### 3.4 Circuit Modification

If early arriving primary pulses were inhibited from triggering the MM as well as the late arriving ones, then a substantial further reduction in the output jitter variance would occur. If all the primary pulses that arrive earlier than  $\Delta'$  seconds before the ideal time were made to trigger the MM only  $\Delta'$  seconds early and the late pulses are inhibited as before, then the output jitter pdf will take the form shown in Figure 3.7 (for the case when a primary pulse triggers the MM in the previous time slot with  $j_i(t) = 0$ ). If  $\Delta = \Delta' = \sigma_i/10$ , then  $E(j_o(t)) = 0$  and

$$\sigma_o^2 \cong \frac{1}{\sqrt{2\pi} \sigma_i} \int_{-\Delta}^{\Delta} t^2 e^{-t^2/2\sigma_i^2} dt + 2A \frac{\sigma_i^2}{100} \quad (3.19)$$

$$\cong \left[ \frac{2}{\sqrt{2\pi} \sigma_i} \frac{\sigma_i^3}{3000} \right] + \frac{\sigma_i^2}{100} \quad (3.20)$$

$$\cong 2\sigma_i^2 / (3000 \sqrt{2\pi}) \quad (3.21)$$

$$\text{and } \sigma_o^2/\sigma_i^2 = 0.01207.$$

The ratio  $\sigma_o^2/\sigma_i^2$  is approximately 37 times less than when the early pulses are not inhibited. Thus,

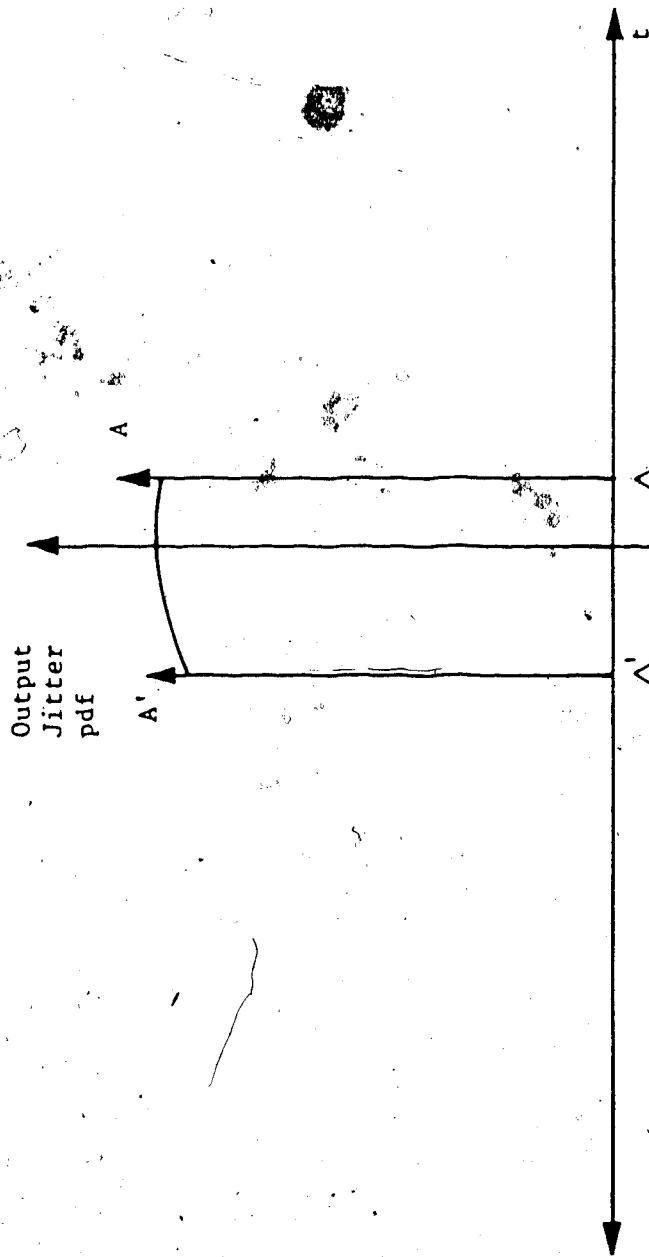


Fig. 3.7 Pdf of the output jitter when the early primary pulses are also inhibited.



inhibiting the early arriving pulses from triggering the MM as well as the late arriving ones, does result in jitter reduction.

In the actual circuit, primary pulses that arrive too early can be prevented from triggering the MM by simply delaying the transition detector output with a delay equal to the output clock signal, as shown in Figure 5.3. The outer feedback path pulls the AND gate low until  $\Delta'$  seconds before the ideal time. The inverter in the feedback path is essential for proper operation. Initially, the MM output is low. If the inverter were not included, then the input to the AND gate would be low and the primary pulses would never be able to trigger the MM. The delay  $T_2 = T - T_q - \Delta'$ , where  $T_q$  is equal to the monostable pulse width. The time interval  $\Delta'$  should be made as close to zero as practicable.

Experimental verification that the simple modification described in this section results in jitter reduction will be given in Section 5.4. The experimental Petrovic system will be described in the next section.

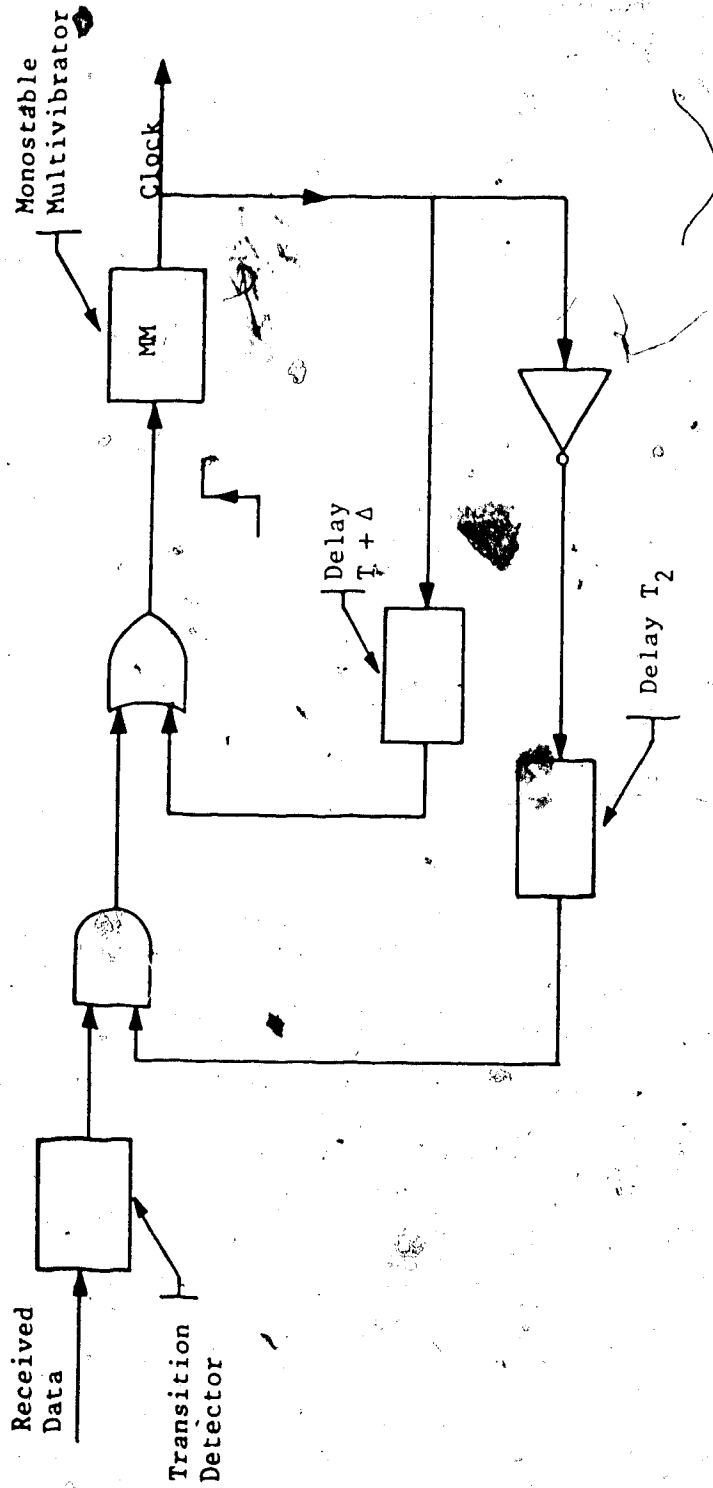


Fig. 3.8. Modified Clock Recovery Circuit

## CHAPTER 4

### THE EXPERIMENTAL PETROVIC SYSTEM

An experimental optical fibre communication system employing the Petrovic code was designed and constructed. The main objectives for setting up this experimental system were the following:

1. Compare the bandwidth and power requirements for the Petrovic code with that of the NRZ code, for a BER of  $10^{-9}$ .

2. Verify that the circuit modification to the self-sustaining monostable clock recovery circuit, described in Chapter 3, results in jitter reduction.

3. Determine the power penalty (if any) when the recovered clock is used to sample the received signal instead of the transmitter clock.

A block diagram of the experimental system is shown in Figure 4.1. The experimental system consists of a Petrovic encoder, laser transmitter, multimode optical fibre, APD-preamplifier, main amplifier, clock recovery circuit, and a Petrovic decoder. The encoder accepts binary NRZ data at 44.736 Mb/s (DS-3 rate) and generates a Petrovic encoded data stream which modulates the laser transmitter. The optical signal from the laser diode, which operates at a wavelength of  $0.83 \mu\text{m}$ , is fed to a

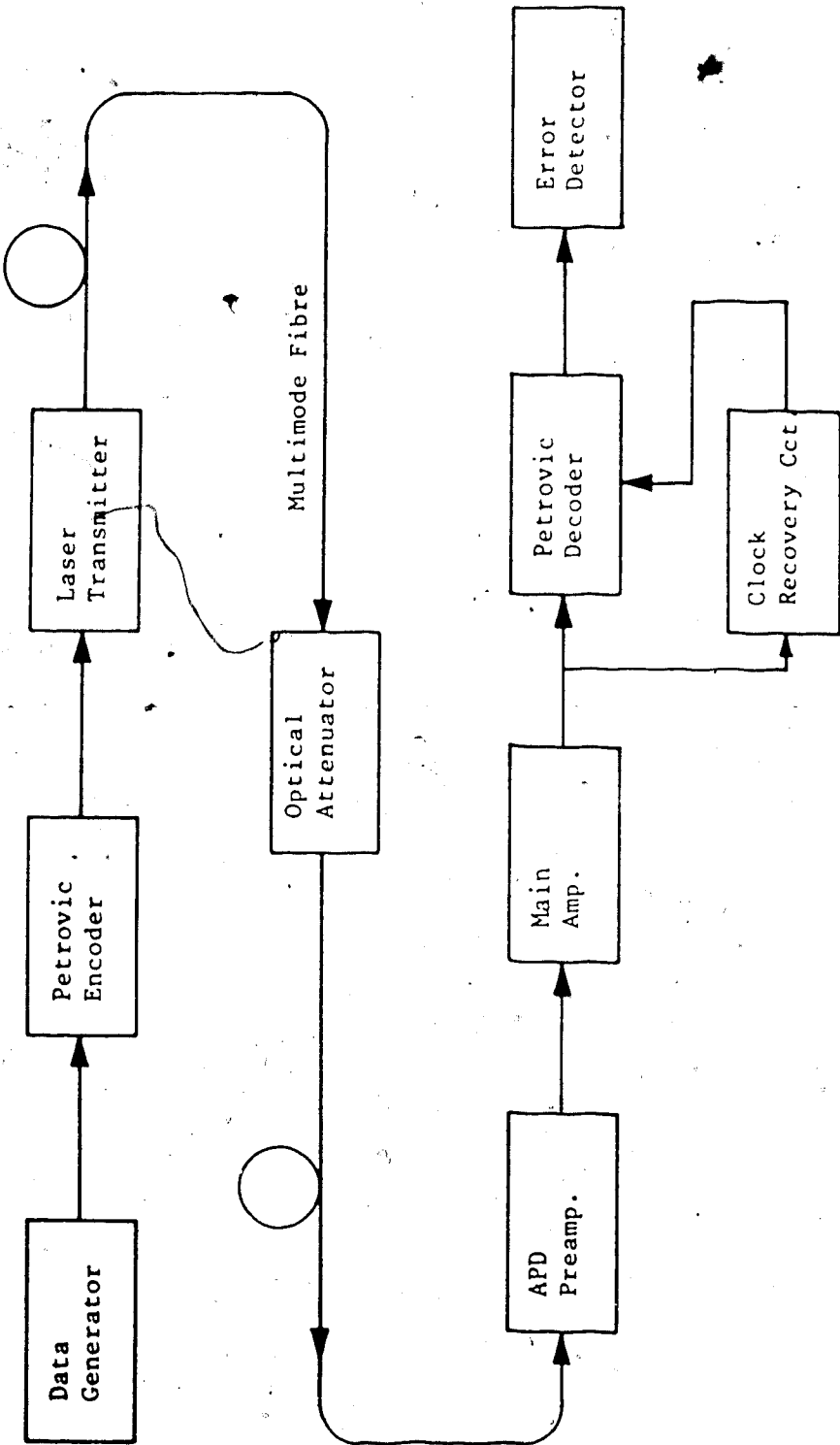


Fig. 4.1 Block Diagram of the Experimental Petrovic System

multimode optical fibre. At the receiving end, the weak optical signal is converted to an electrical signal by an avalanche photodiode (APD). The signal current produced by the APD is amplified to a useful level with a low noise preamplifier followed by a main amplifier. The output of the main amplifier is applied to the decoder, which performs the inverse operation of the encoder, resulting in the original binary NRZ data. The sampling clock required in the decision circuitry of the decoder is derived from the received signal by a novel self-sustaining monostable clock recovery circuit. In this chapter, the design and operation of each of the experimental components is described in detail.

#### 4.1 Petrovic Encoder

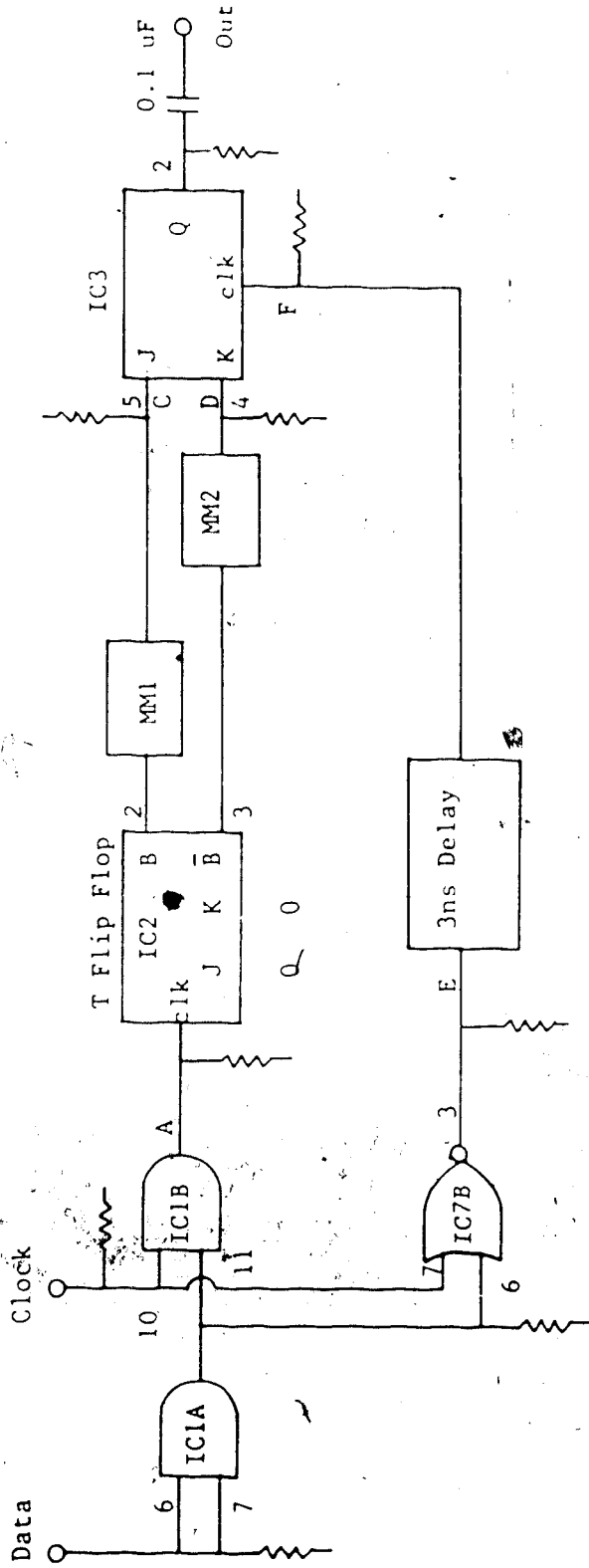
The Petrovic encoder converts a binary NRZ input data stream at 44.736 Mb/s into a Petrovic encoded data stream at a bit rate of 89.472 Mb/s. Each outgoing bit is  $T/2$  seconds in duration, where  $T$  is the bit interval of the incoming NRZ bit stream. The encoding rules for the Petrovic code are the following: an incoming 1 is encoded by 11 and 00 alternately; an incoming 0 is coded by 01 if the previous two encoded bits were 00 or 10, and by 10 if the previous two encoded bits were 11 or 01. Due to the simplicity of the encoding rules, the

encoder is not very complex. A schematic diagram of the encoder is shown in Figure 4.2.

The data and clock inputs to the encoder are obtained from an HP 3762A Data Generator. This unit produces pseudo-random binary bit sequences ( $10^{23}-1$ ,  $10^{15}-1$ ,  $10^{10}-1$ ) as well as periodic 16 bit and 10 bit word sequences in the frequency range 1 KHz to 150 MHz. The output data can be in the NRZ, RZ, or CMI code format. The bit rate of the data stream can be determined by an external clock source or by two internal crystal oscillators, which are set at 44.736 MHz and at 137.088 MHz.

For proper operation of the encoder, the clock and data signals must have coincident rising and falling edges. However, it was observed that the clock signal from the data generator lagged the data signal by approximately 1 ns. In order to make the transitions coincide, the data signal is delayed by the AND gate IC 1A (see Figure 4.2), which has propagation delay of approximately 1 ns.

Even though the Petrovic code is a 1B-2B code, a clock at double the incoming bit rate is not required in the encoding process. In the encoder, mid-bit transitions, which are characteristic of 1B-2B codes, are triggered by the falling edge of the clock signal. Thus, in order to have transitions occurring at exactly



- IC1 - MC10H104 AND Gate
- IC2, IC3 - MC10135 JK Flip-Flop
- IC7 - MC10H102 NOR Gate

Note - All resistors are 51 ohms terminated to -2V.

Fig. 4.2 Schematic Diagram of the Petrovic Encoder

in the middle of the bit interval, it is imperative that the clock signal have a 50% duty cycle.

When a 1 is to be transmitted, the encoder must determine what was sent for the previous 1 and output its complement. For example, if the last 1 was encoded by 00, then the next 1 should be encoded by 11. IC 1B, IC2 and monostable multivibrators MM1 and MM2 are responsible for encoding a 1 in the input data stream. When the input data is a 1 and the clock undergoes a positive transition, i.e. from low to high, then point A in Figure 4.2 goes high. This causes outputs B and B' of the Toggle flip flop to change state. (The Toggle flip flop is implemented by a JK flip flop with inputs  $J=K=0$ ). The Toggle flip flop serves as a memory device for encoding the ones. When its output (point B in Fig. 4.2) is low, a 00 was sent for the last 1; when it is high a 11 was sent. Monostable multivibrators MM1 and MM2 are designed to trigger on the rising edge of their input signal. The pulses generated by MM1 set the output flip flop IC3; while pulses from MM2 reset this flip flop. Thus, when the signal at point B becomes high, indicating that a 1 is received and it should be encoded by 11, MM1 is triggered. The pulse generated by MM1 sets flip flop IC3, causing the output to go high. The length of time the output will remain a 1 is dependent upon the value of the next incoming bit. If



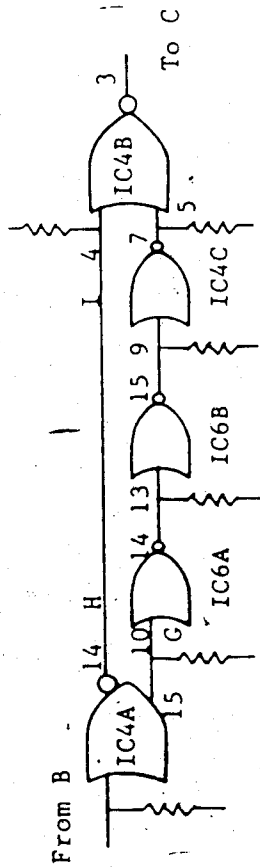
the next incoming bit is a 1, the output will remain high for  $T$  seconds (IC3 will be reset by a pulse generated by MM2,  $T$  seconds later). If the next incoming bit is a zero, the output will remain a 1 for  $3T/2$  seconds.

The monostable multivibrators MM1 and MM2 are realized by logic gates [48]. A schematic diagram of their circuitry is shown in Figure 4.3. The monostables trigger only on the rising edge of their input signal.

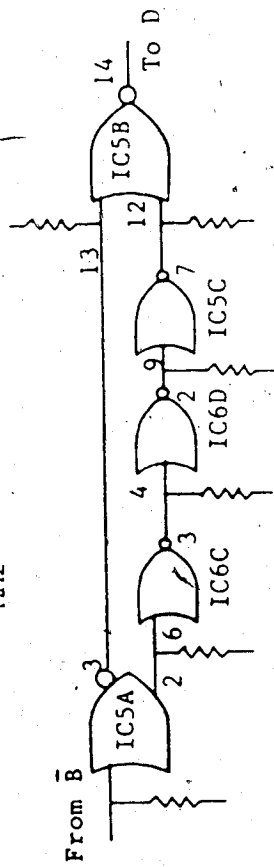
When a 0 is received, the output of the encoder must toggle states after  $T/2$  seconds. This is accomplished by gating the clock signal and the data signal by IC7, a NOR gate. When the input is a 0, the output of IC7, point E in Figure 4.2, becomes high on the falling edge of the clock signal. Since the clock signal has a 50% duty cycle, point E goes high  $T/2$  seconds after a 0 is received. This signal is then delayed by an additional 3ns by a delay network consisting of 3 OR gates (see Figure 4.4) and applied to the clock input of the output flip flop (IC3). The 3 nsec delay compensates for the delay introduced by the monostables in the encoding process for a 1. When the clock input to IC3 goes high, the output will toggle states, as required, because both the J and K inputs to the output flip flop are low.

In order to encode the 0s successfully, both the

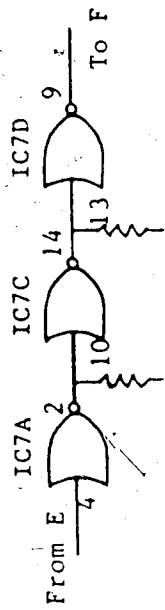
MM1



MM2



Delay



- IC4 - MC10H105 NOR Gate
- IC5 - " " " "
- IC6 - MC10H102 NOR Gate

Note - All resistors are 51 ohms  
and are terminated to -2V.

Fig. 4.3 Schematic Diagram of the Monostables and Delay Network

J and K inputs to IC3 must be low when its clock input becomes high. This is the reason why the monostables are included. If they were not included, then either the J or K input would be high, and the output will not toggle states for an incoming 0. Simple RC differentiators can be used instead of the monostable multivibrators at low speeds. However, at speeds at which the encoder operates, it was found that due to stray capacitances, RC differentiators did not produce pulses with fast enough rise times.

The encoder was constructed on a 7cm by 14cm printed circuit (pc) board and placed in a die cast metal chassis (for shielding). Since high speed operation was desired, emitter coupled logic (ECL) gates were used. Power supply lines coming into the chassis were shielded by feed through capacitors (Filter-cons) and ferrite beads. Coaxial BNC connectors (50 ohm) were used at the inputs and output. Circuit interconnections were kept as short as possible. In order to avoid problems due to reflections, fifty ohm microstrip transmission lines were used whenever the interconnection length exceeded 5 cm. ECL outputs were terminated with a 51 ohm resistor to -2V at the destination point. Power supply lines on the pc board were decoupled to ground by high quality RF (mylar) capacitors (0.1  $\mu$ F and 47 pf) at several points.

#### 4.2 Laser Transmitter

A General Optronics short wavelength ( $0.83 \mu\text{m}$ ) single longitudinal mode laser diode was used for the optical source. This laser diode has the drive circuitry, which incorporates automatic power and temperature control and performance warning alarm, built into the same package (model GO-ANA). The laser can be modulated over a frequency range of 20 Hz to 1.25 GHz, has an average output power of 1 mW, and has a fairly linear output power versus current characteristic. The electrical input to the laser transmitter is capacitively coupled and has an impedance of approximately 50 ohms. The laser is biased at the centre of its linear operating region. An input peak to peak voltage swing of 0.8 volts is sufficient to turn off the laser for the zero level.

#### 4.3 Fibre

The experimental system utilizes graded index, multimode fibre manufactured by Northern Telecom. This fibre has a numerical aperture of 0.2, an average attenuation of 2.75 dB/km, and a dispersion of 1.5 ns/km (FWHM) at a wavelength of  $0.83 \mu\text{m}$ . The experimental system was tested with 5 km of fibre in place. A variable optical attenuator was placed in series with

the fibre link to control the amount of optical power falling upon the APD.

Multimode fibre was used in this project because it was readily available in the laboratory. Single mode fibre and a long wavelength source (1.3  $\mu\text{m}$  or 1.55  $\mu\text{m}$ ) could also have been used. In this case, a considerably longer length of fibre would have been required because of the lower dispersion of the single mode fibre and the lower fibre attenuation at longer wavelengths.

The 3 dB electrical bandwidth of the fibre ( $F_{3\text{dB}}$ ) can be easily determined from the well known equation [49]:

$$F_{3\text{dB}} = 311/D \quad \text{MHz.km}, \quad (4.1)$$

where  $D$  = pulse dispersion in ns/km (measured at FWHM)

For the experimental fibre,  $F_{3\text{dB}} = 311/(1.5 \times 5) = 207 \text{ MHz.km}$ . Since 5 km of fibre was used, the bandwidth for the total section is approximately  $207/5 = 41.5 \text{ MHz}$ . This is a conservative figure because the total dispersion should be smaller than 7.5 ns (5 km  $\times$  1.5 ns/km) because of mode mixing, which is caused by microbending and splices [49].

The bandwidth of the fibre should be sufficiently large or else a power penalty is incurred at the receiver. According to Personic and Smith [40], less than 1.5 dB power penalty occurs if

$$\sigma/T < 0.3, \quad (4.2)$$

where  $T$  = bit interval

$$\begin{aligned} \sigma &= 0.5 \times \text{rms pulse width of impulse response} \\ &\quad \text{of the fibre} \\ &= 2.355 D \\ &= 3.18 \text{ ns for the experimental fibre.} \end{aligned}$$

Therefore,  $\sigma/T = 3.18/11.18 = 0.28$ . Since  $\sigma/D < 0.3$ , the bandwidth of the fibre should be sufficient to transmit the 89.4716 Mb/s Petrovic encoded bit stream.

#### 4.4 Optical Preamplifier

The optical receiver consists of a detector, preamplifier, and a main amplifier. The sensitivity of the receiver is determined mainly by the noise sources in the preamplifier stage. The noise generated by the optical detector (APD or PIN diode) and by the front-end electronics usually dominate the noise entering the decoder. In order to achieve a low BER, it is necessary to minimize the contributions from these noise sources while maintaining signal integrity. Thus, a proper design of the preamplifier stage is essential for good system performance.

The experimental optical receiver employs a silicon APD followed by a low gain bipolar transimpedance preamplifier. An APD was chosen instead of a PIN diode because an APD-receiver is more sensitive than a PIN-

receiver at a wavelength of 850 nm [40]. The particular detector used is an RCA C30908E APD. Important characteristics of this device are as follows: operating voltage and breakdown voltage of 228V and 241V respectively; dark current of 18 nA; responsivity of 65 A/W; and a noise current of  $2E-13$  A/ Hz. Although the high-impedance preamplifier design offers the best sensitivity, a transimpedance design was employed in the experimental system because it offers a wide dynamic range and does not need equalization [50,51].

A schematic diagram of the preamplifier is given in Figure 4.4. The preamplifier consists of 3 stages. The first stage is a low gain common emitter amplifier. This is followed by a differential pair and finally a common collector stage. Bipolar transistors, each with an  $f_T$  of 4 GHz (BFR 90) were used for the active devices.

The first stage of the preamplifier, i.e. the stage immediately following the photodetector, should have a low input capacitance ( $C_i$ ) since the bandwidth is inversely proportional to  $C_i$ . The first stage should also have sufficient gain, so that noise generated by succeeding stages will be small when referred to the input of the first stage [52]. A cascode stage is often used for the first stage [53] because it has a low input capacitance and a reasonable gain. In the experimental

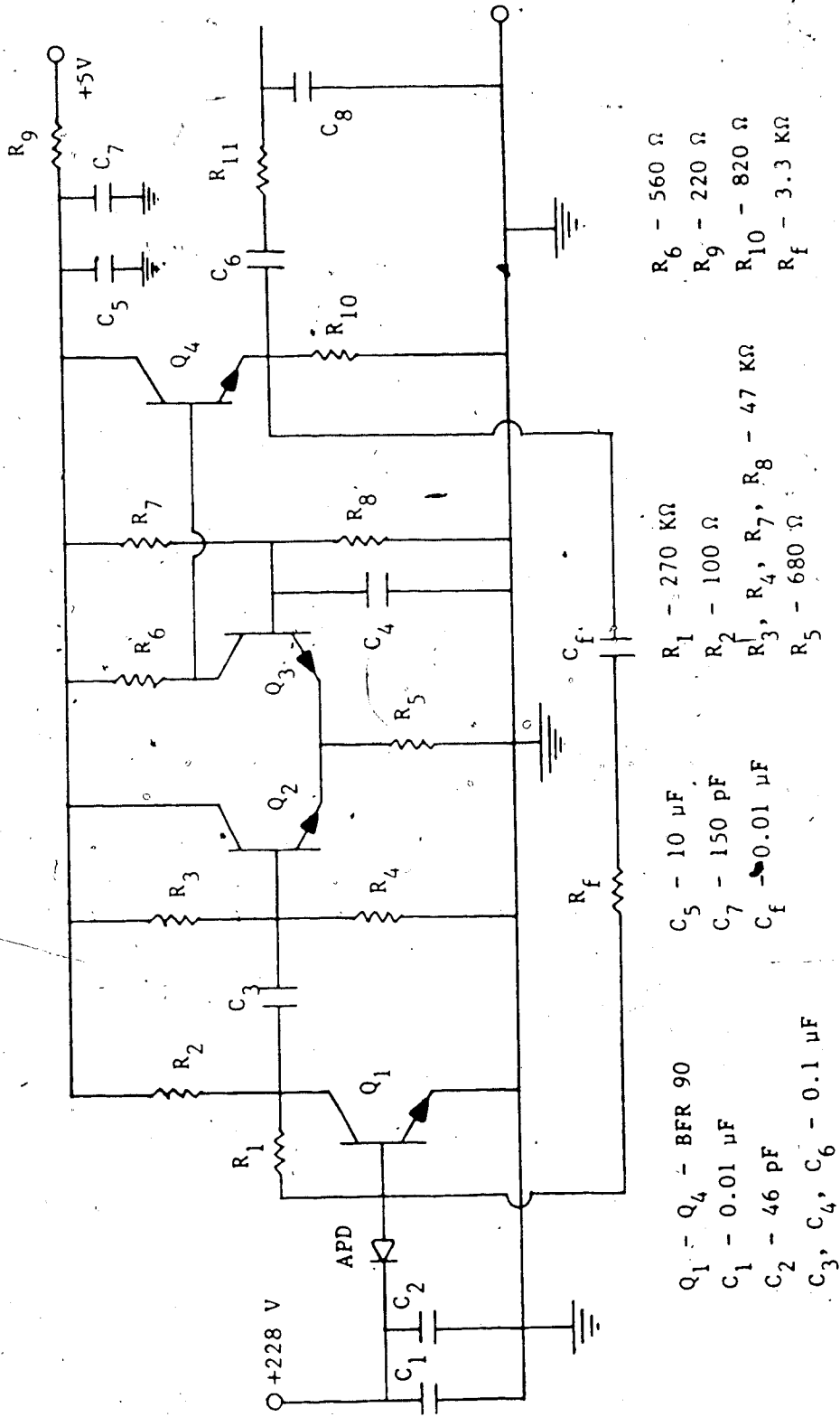


Fig. 4.4 Schematic Diagram of the Preamplifier



preamplifier, a common emitter stage was used for the first stage. The drawback of this configuration is that the Miller capacitance is large when the gain is large. Thus, the gain of the first stage was kept low.

In the experimental preamplifier, the shunt capacitance of the APD,  $C_d$ , is approximately 0.3 pF, the base-collector junction capacitance is 0.5 pF, the base-emitter diffusion capacitance is approximately 10pF, and the stray capacitance due to finite lead lengths, pc board trace for the base, etc., is estimated to be 2 pF. The mid-band gain of the first stage is approximately

$$\begin{aligned} R_C/h_{ib} &= - (R_C I_C) / 26 \text{ mV} && (4.3) \\ &= 100/43 = -2.3. \end{aligned}$$

The effective input capacitance due to the base-collector junction capacitance, invoking Miller's theorem, is approximately  $[1 - (-2.3)]0.5 = 1.65\text{pF}$ . Thus, the base-emitter capacitance dominates the total capacitance at the input and the use of a low gain, common emitter first stage does not increase the input capacitance significantly.

A differential pair was used for the second stage. This stage was capacitively coupled to the first stage in order to simplify biasing. Since the spectrum for the Petrovic code contains a null at dc and has small low frequency components, the low frequency pole (approximately 20 KHz) due to the coupling capacitor

should not cause any problems. The differential pair provides adequate gain, and has a good high frequency response. The collector of the first transistor (Q2) was tied directly to the power supply, which is an ac ground, thereby reducing the Miller capacitance. The output signal is taken from the collector of Q3 because signal inversion is not required (Q1 provides the signal inversion necessary for negative feedback).

A common collector configuration is used for the third stage. This stage provides a low output impedance, which is necessary to drive the main amplifier, and exhibits good high frequency response. The output of this stage is filtered by a first-order low pass filter (R11 and C8). A low pass filter was required for some of the experiments that were carried out (see Chapter 5). Resistor R11 was chosen to be 24 ohms so that the output impedance of the preamplifier would be approximately 50 ohms (to minimize reflections between the preamplifier and the main amplifier).

In order to reduce the effective resistance seen by the input capacitance, voltage-shunt feedback is employed. The signal from the emitter of Q4 is fed back to the base of Q1 via  $R_f$  and  $C_f$ . Capacitor  $C_f$  serves to block dc. The value of  $R_f$  determines the bandwidth and transimpedance of this circuit. The transimpedance is

directly proportional to the value of  $R_f$  but the bandwidth is inversely proportional to it.

Since the preamplifier was required to have a large bandwidth (about 100 MHz), certain precautions were taken in its construction. The preamplifier was constructed on a 4 cm x 5 cm printed circuit board with the components surface mounted on the top surface of the board; the bottom surface was a ground plane. Care was taken to ensure that the copper traces were short, especially for the feedback path and the forward path (i.e. between Q1 and Q2). High quality RF capacitors were used for decoupling the  $V_{GC}$  and APD bias voltage lines. The pc board was enclosed in a die cast metal chassis with the APD mounted to one of its sides. Care was also taken to block stray RF energy from entering the preamplifier. Short, twisted pair wires with ferrite beads placed in series were used between the power supply and the preamp chassis. Power lines enter the interior of the chassis through feedthrough capacitors (Filter-con connectors), which helped to further suppress any stray RF energy.

#### 4.4 Main Amplifier

The output of the preamplifier is applied to a Keithley Instruments Pulse Amplifier (model 105). This amplifier provides a voltage gain of 100 (40 dB), has a

bandwidth of 500 MHz, and an input impedance of 50 ohms. At low power levels (around -48 dBm), the output of this amplifier was approximately 0.2 V<sup>p-p</sup>. Since this is too low to trigger ECL gates, it was amplified further by a HP 461A amplifier, which has a voltage gain of 10 (20 dB) and a bandwidth of 150 MHz.

#### 4.6 Petrovic Decoder

The Petrovic Decoder converts the received Petrovic encoded data to the corresponding NRZ data. A schematic diagram of the decoder is shown in Figure 4.5. In the Petrovic encoder, each incoming NRZ bit is encoded into a block of two outgoing bits. Adjacent bits in each block are identical if the incoming bit is a 1 and are different if the incoming bit is a 0. Thus, the Petrovic encoded bit stream can be easily decoded by simply comparing the first and second bit in each block. In the experimental decoder, this comparison is performed by an exclusive NOR (EX-NOR) gate.

Circuit operation of the decoder is as follows. Since the optical receiver is ac coupled, the signal entering the decoder is symmetrical about the 0 volt level, i.e. it has zero dc content. In order to trigger ECL gates, however, the received signal must be level shifted. The level shifting is accomplished by capacitor C1, diode D1, and resistors R3, R4. These

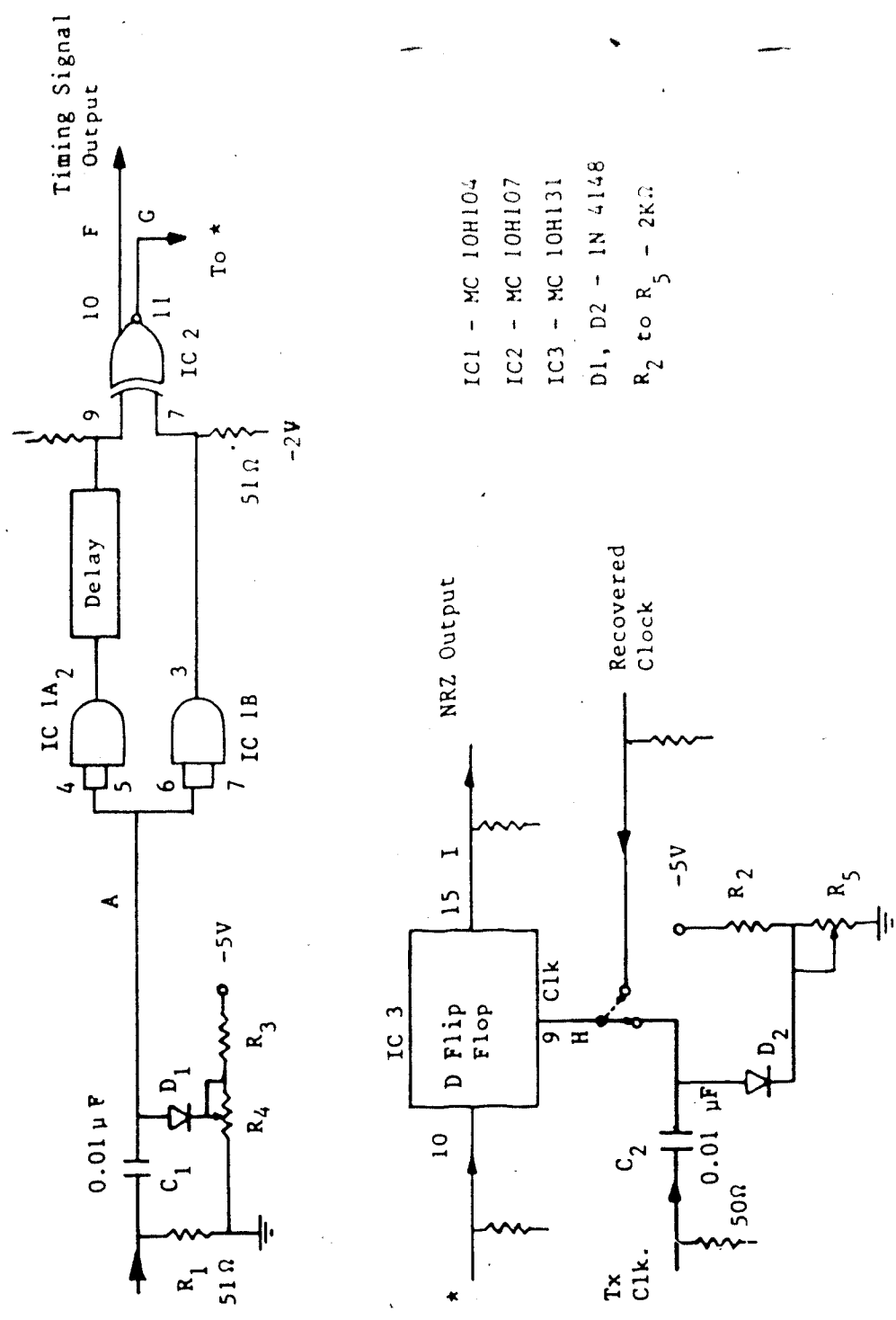


Fig. 4.5 Schematic Diagram of the Decoder

elements form a clamp circuit . By adjusting the value of potentiometer R4, the dc level of the signal at point A (see Figure 4.5) can be controlled. Potentiometer R4 was adjusted until the peaks of the incoming signal were clamped to -0.8 volts, the high level for ECL gates.

The incoming level-shifted signal is applied to the inputs of the AND gates IC 1A and IC 1B. The outputs of these gates are identical. The output of IC 1B is applied directly to the input of the EX-NOR gate (IC 2) while the output of IC 1A is first delayed by  $T/2$  seconds with a coaxial line and then applied to the second input of the EX-NOR gate. The output of IC 2 can be sampled to give the original transmitted signal. If the two inputs to IC 2 are identical, its output is high, indicating that a 1 is received. Similarly, the output of IC 2 will be low when its inputs differ, which indicates that a 0 is received. It is inevitable that in this decoding scheme, the first bit of a particular block and the last bit of the previous block will also be processed by the EX-NOR circuitry. In order to avoid errors, therefore, sampling must occur when the EX-NOR output contains the resulting signal when its inputs are the first and second bit of the same block. Furthermore, the received signal must be sampled at the centre of the eye pattern, i.e when the SNR is the

greatest. The optimum sampling instant is achieved by delaying the clock signal by a suitable amount.

The output of the EX-NOR gate is sampled via a D flip flop (IC 3). A clock signal at a frequency of 44.736 MHz is applied to the clock input of the D flip flop. The output of the D flip flop contains the decoded NRZ signal. This signal is then applied to the HP 3736A Error Detector to determine the BER.

One of the objectives for setting up this experimental system was to compare the system performance obtained when the delayed transmitter clock is used in the decoder with the system performance obtained with the recovered clock. When the transmitter clock was used, the clock output of the HP 3762A Data Generator was delayed by a suitable amount using an HP 1906A Delay Generator, which is adjustable from 0 to 100 ns in increments of 5 ns. This Delay Generator requires a TTL compatible input signal. Thus, the ECL clock signal from the Data Generator was first level shifted by an HP 1910A Rate Generator and then applied to the Delay Generator. The TTL output of the Delay Generator was level shifted in the decoder by clamp circuitry similar to that used for the main amplifier output (see Figure 4.5). When the recovered clock from the clock recovery circuit was used as the decoder clock, it was found that only a few nanoseconds of delay was required

for proper operation of the decoder. Thus, instead of the Delay Generator, a short coaxial transmission line was used to provide the necessary delay. Since the output of the clock recovery circuitry is already ECL compatible, the level shifting circuitry was not needed (see Figure 4.7).

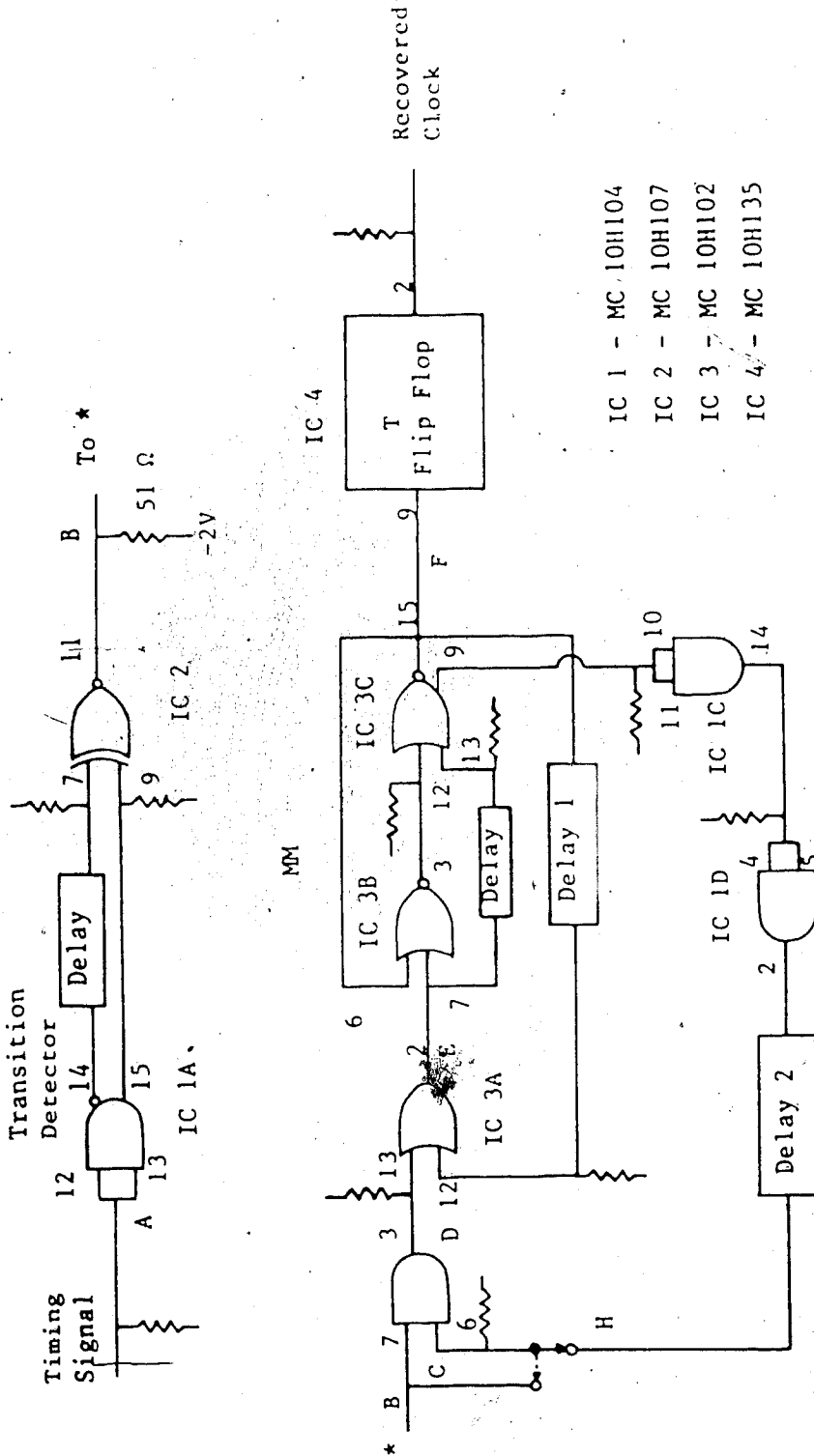
The decoder was constructed on a 10 cm by 8 cm pc board and enclosed in a die cast metal chassis. Construction practices incorporated for the encoder (see Section 4.1) were employed here as well. The performance of the decoder will be discussed in the next chapter.

#### 4.7 Clock Recovery Circuit

The self-sustaining monostable clock recovery circuit (see Chapter 3) was used to recover the clock signal from the incoming data. A schematic diagram of the experimental clock recovery circuit is shown in Figure 4.6. The original circuit developed by Witte and Moustakas [31] is obtained by connecting point C to point B and leaving point H open. The modified clock recovery circuit is obtained by joining point H to point C as shown in Figure 4.6.

The input to the clock recovery circuit is obtained from the timing output of the decoder (see Figure 4.5). This input signal is applied to the transition detector,





- IC 1 - MC 10H104
- IC 2 - MC 10H107
- IC 3 - MC 10H102
- IC 4 - MC 10H135

Fig. 4.6 Schematic Diagram of the Clock Recovery Circuit

which produces approximately a 4 ns wide pulse on each rising and falling edge. The EX-OR and the transition detector form the non-linear element required to generate a spectral line at twice the incoming NRZ bit rate. The transition detector is realized by a NOR gate, an EX-OR gate, and a coaxial delay line (see Figure 4.6). On every input transition, a pulse is generated at the output of the EX-OR gate because its two inputs have unequal propagation delays (due to the delay line). The duration of the pulse is equal to the length of the delay. In the experimental system, a 0.78m long coaxial line was used (RG 174/U). This corresponds to a pulse length of 3.9ns, which is of sufficient duration to trigger the monostable multivibrator (MM).

The pulses from the transition detector, which will be referred to here as the primary pulses, are fed to an AND gate (IC 1B). If the original clock recovery circuit is desired, both the inputs to this gate are tied together and hence its output will be equal to its input. However, for the modified circuit, the transition detector output is gated (by an AND gate) with the delayed clock output (delay  $< T/2$ ). This AND operation prevents primary pulses that arrive too early from triggering the MM, which results in clock jitter reduction. The output of the AND gate forms one of the

inputs to an OR gate (IC 3A). The other input to the OR gate is the output clock signal delayed by the inner feedback loop by  $T_1$  seconds ( $T_1 > T/2$ ). If the primary pulse is late or missing, this delayed clock signal will trigger the MM.

The monostable multivibrator is similar to those used in the encoder. It produces a 4.8 ns pulse on every rising edge of its input signal. The output of the MM is at twice the clock rate (i.e. 89.472 MHz). Since the decoder clock should be at half this rate, this clock signal is divided by two using a T flip-flop (IC 4).

When the input to the clock recovery circuit is left open, the circuit oscillates at a free running frequency of  $0.5/T_1$ . This oscillation is started by a transient pulse triggering the MM when the power is turned on. Due to the inner feedback, the MM is then repeatedly triggered every  $T_1$  seconds. Since the MM output is divided by 2, the oscillation frequency at the clock output terminal is  $0.5/T_1$ . By measuring the frequency of oscillation, which was accomplished by an HP 5326A Timer-Counter, the exact value of the delay  $T_1$  can be obtained. Also, when the -2V ECL power supply is adjusted slightly, the frequency of oscillation changes slightly (by a few hundreds of KHz). This occurs because the amplitude of the gate outputs are slightly

changed, resulting in changes in propagation delay due to amplitude-to-phase conversion that occurs because of non-zero gate thresholds. When the input to the clock recovery circuit is connected, the frequency of oscillation locks to the bit rate (44.736 MHz).

The clock recovery circuit was constructed on a 7 cm by 14 cm pc board and enclosed in a metal container for shielding. Delay 1 was realized by a 1.6 m coaxial line (RG 174/U), whose delay of approximately 8 ns together with the propagation delay of the gates makes  $T_1 = 11.21$  ns. Delay 2 was realized with two AND gates and a 20 cm coaxial line ( $T_2 \approx 11.0$  ns).

#### 4.8 Jitter Measurer

In order to determine the reduction in clock jitter power obtained by the simple circuit modification to the self-sustaining monostable clock recovery circuit a jitter power measuring device was constructed. This jitter measurer consists of an EX-OR gate followed by a low pass filter. The transmitter clock and the recovered clock form the two inputs to the EX-OR gate. The output of an EX-OR is high whenever its two inputs differ. Thus, the output contains pulses of width equal to the phase difference, or jitter, between the transmitter clock and the recovered clock. A blocking capacitor is used to remove the dc component of the

output signal. The dc component results from a constant phase difference between the two inputs. The low pass filter removes the clock frequency from the signal; its 3 dB cutoff frequency is approximately 23 MHz. The output of the jitter measurer is measured using an HP 8557A spectrum analyser. The area under the jitter spectral curve is proportional to the jitter power, which, neglecting the dc offset, is equal to the jitter variance. A similar scheme to measure the jitter power is reported in [45].

## CHAPTER 5

### EXPERIMENTAL RESULTS

The experimental Petrovic system described in the previous chapter was set up and various measurements were made. The relationship between BER, received power, and receiver bandwidth was obtained for the Petrovic and NRZ codes. These results will be used to compare the bandwidth and power requirements of the Petrovic code with that of the NRZ code. The clock jitter spectrum of the original self-sustaining monostable multivibrator clock recovery circuit and of the modified self-sustaining monostable circuit was obtained for various values of feedback delay and received power. An examination of these results will aid in understanding the jitter performance of the clock recovery circuits and in determining whether the proposed modification will result in jitter reduction.

The performance of the encoder, optical receiver, decoder, and clock recovery circuits are presented first. Then a comparison is made between the experimental and theoretical power spectral density of the Petrovic code. Next, the experimental relationship between BER and various parameters, i.e. received power, receiver bandwidth, bit sequence are given. Finally,

the jitter performance of both the clock recovery circuits is discussed.

## **5.1 System Operation and Waveforms**

### **5.1.1 Petrovic Encoder**

Figures 5.1 to 5.4 demonstrate the operation of the encoder for various incoming NRZ data sequences at a bit rate of 44.736 Mb/s. When the encoder input is all zeros, the output should alternate between 10 and 01 (i.e. 10011001 ...), as shown in Figure 5.1. Figure 5.2 illustrates the encoder output for an input ten bit repeating sequence of 1001000000. Note the occurrence of short pulses (of duration  $T/2$ , where  $T$  = incoming bit interval) for this input sequence. The Petrovic encoded bit stream for an NRZ input of 101010 ... is shown in Figure 5.3. This input sequence produces pulses of length  $2T$ , which are the longest that are possible for the Petrovic code. An examination of these encoder outputs reveals that the encoder is functioning properly. Finally, the eye diagram of the encoder output for an input  $10^{23} - 1$  pseudorandom binary sequence is shown in Figure 5.4.

### **5.1.2 Optical Preamplifier and Main Amplifier**

Figure 5.5 shows the eye diagram of the main amplifier output for a  $10^{23} - 1$  pseudorandom NRZ input to

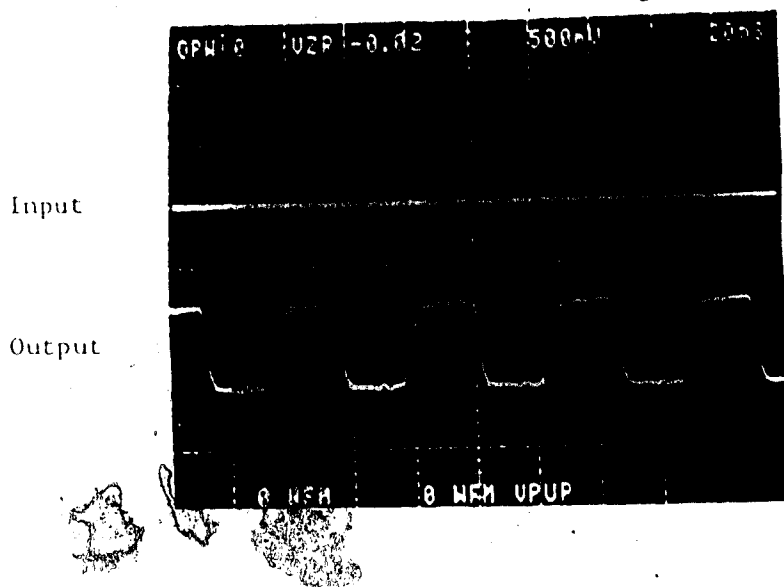


Fig. 5.1 Encoder Output when the Input is all Zeroes

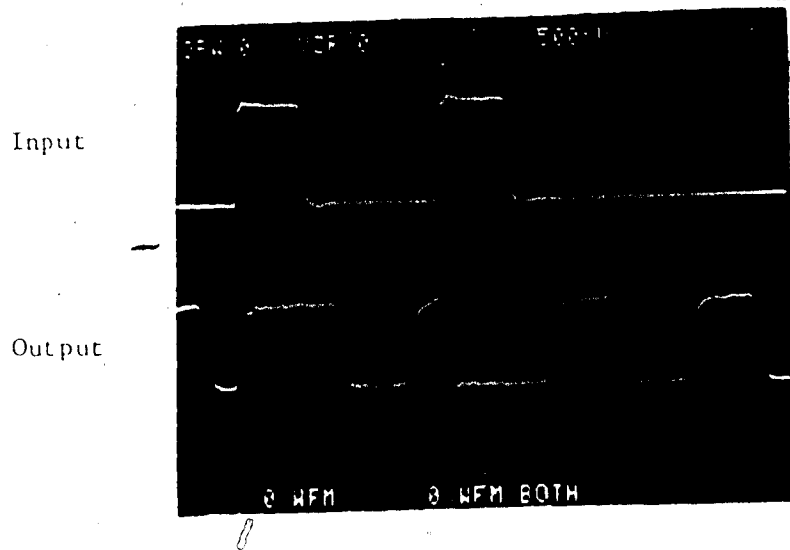


Fig. 5.2 Encoder Output for an Input 10 Bit Repeating Sequence of 1001000000...



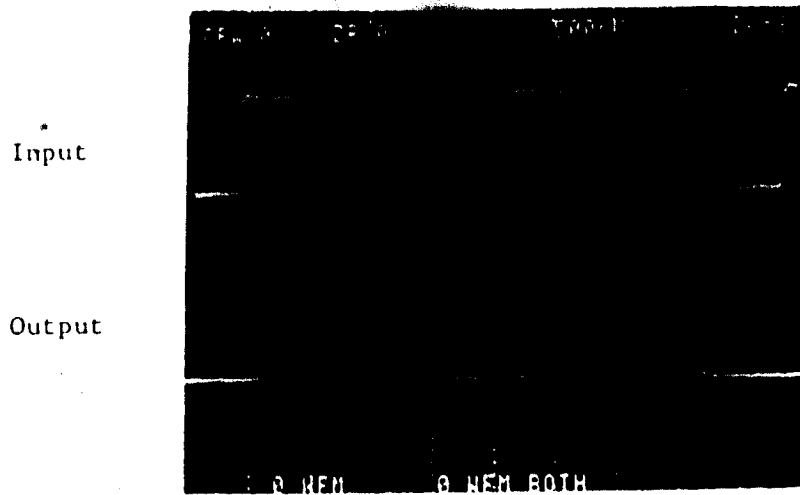


Fig. 5.3 Encoder Output for an 101010... NRZ Input

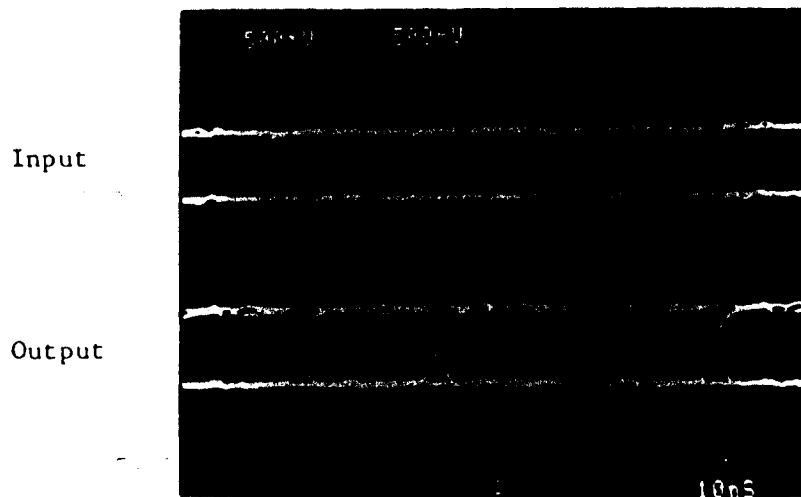


Fig. 5.4 Encoder Output Eye Diagram

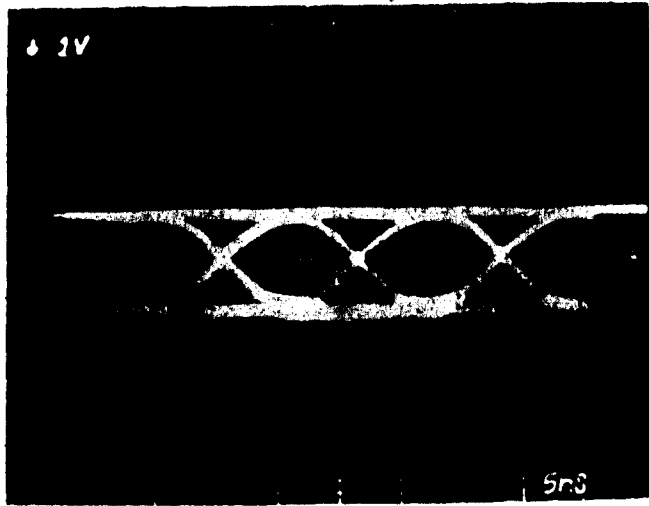


Fig. 5.5 Main Amplifier Output Eye Diagram  
(Received Power = -48.6 dBm, Preamplifier  
Bandwidth = 65 MHz)

the encoder, at a received power of  $-48.6$  dBm (which results in a BER of  $10^{-9}$ ) and without a low pass filter at the preamplifier output, i.e. C8 (Figure 4.4) is absent. Note that the eye is open, indicating that the fibre-receiver bandwidth is sufficient. The transimpedance of the preamplifier circuit was measured to be approximately 1980 ohms (into a 50 ohm load). The measured 3 dB bandwidth of the receiver, with C8 absent, is approximately 65 MHz.

### 5.1.3 Petrovic Decoder

The operation of the decoder is demonstrated in Figure 5.6. Figure 5.6a illustrates the decoder output eye diagram for a  $10^{23}-1$  pseudorandom Petrovic input (see Figure 5.5). Figure 5.6b shows the decoder output for the Petrovic encoded bit stream corresponding to the following repeating ten bit NRZ sequence :1001000000. These waveforms were obtained with the decoder clock taken from the modified self-sustaining monostable multivibrator clock recovery circuit. The decoder output was applied to the HP3763A Error Detector. The various BER curves that were obtained are given in Section 5.3.

During the course of the measurements, it was found that as the received power is varied, potentiometer R4 of the level shifting circuitry in the decoder (see

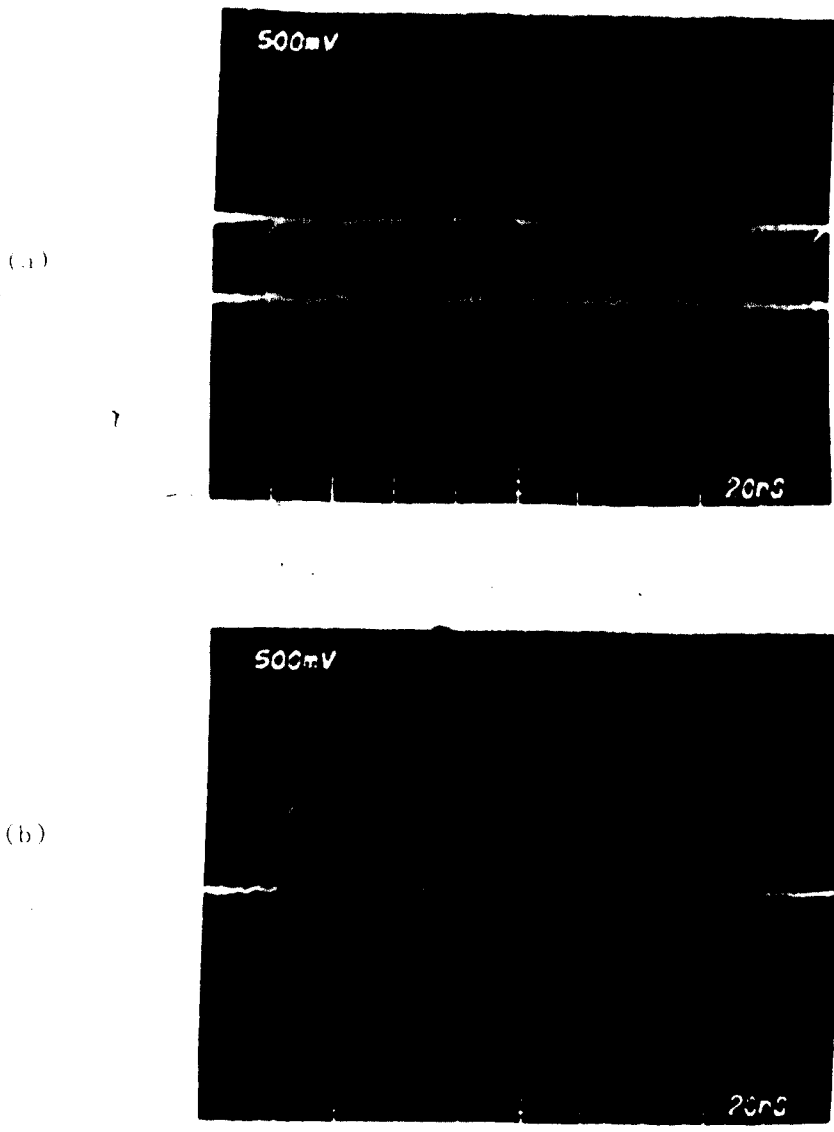


FIGURE 5.6 Decoder Output Waveforms.  
Received Optical Power = -48.5 dBm, Modified  
Clock Recovery Circuit Output was used for the  
Decoder Clock ( $A = 0.034\text{ns}$ ,  $A' = 0.17\text{ns}$ )  
(a)  $10^{23}-1$  Pseudorandom Input  
(b) 1001000000 Repeating 10 Bit Sequence

Figure 4.5) had to be adjusted to give minimum BER. This is because when the received optical power is changed, the amplitude of the main amplifier output changes because AGC (automatic gain control) is not incorporated in the optical receiver. This results in a slight phase shift in the output of the EX-NOR gate (IC2, see Figure 4.5) due to the incoming signal crossing the ECL gate threshold at a slightly different time. This phenomenon is known as amplitude-to-phase conversion. Since the sampling instant is fixed, a phase shift in the EX-NOR output will result in a deviation from the ideal sampling instant resulting in an increased BER. In order to compensate for the phase shift, and thus ensure that sampling occurs at the ideal time, i.e. when SNR is the highest, the input signal must be level shifted (up or down) until minimum BER is achieved. Shifting the incoming signal, which is accomplished by varying R4 (of Figure 4.5) until minimum BER is obtained was tedious and time consuming. To avoid this problem, an amplifier that provides a constant output amplitude and phase shift for a large input signal dynamic range would be required.

#### 5.1.4 Clock Recovery Circuit

The input signal to the self-sustaining monostable multivibrator clock recovery circuit, which is obtained

from the "timing" output of the decoder, is shown in Figure 5.7a for a  $10^{23}-1$  pseudorandom Petrovic bit stream input signal to the decoder (see Figure 5.5) and a received power of -48.5 dBm. The clock output from the modified clock recovery circuit, for the input shown in Figure 5.7a, is shown in Figure 5.7b. The clock signal from the original clock recovery circuit contains more jitter although it appears virtually the same on the oscilloscope. The clock jitter power of the original and of the modified self-sustaining monostable multivibrator clock recovery circuit will be discussed in Section 5.4.

## 5.2 Power Spectrum

The experimental Petrovic code spectrum is shown in Figure 5.8a. This spectrum was obtained by applying the encoder output, for a  $10^{23}-1$  pseudorandom NRZ input, to an HP8557A spectrum analyzer. The theoretical spectrum, which was derived by Petrovic [7] for rectangular output pulses, is shown in Figure 5.8b. Comparison between the theoretical and the experimental spectrum reveals that they are virtually identical. The experimental spectrum approaches zero at dc and near 89.5 MHz, has a main lobe centered at 20 MHz, and a secondary lobe at 68 MHz, as predicted by theory. The ratio between the height of the main lobe to the height of the secondary lobe, for the

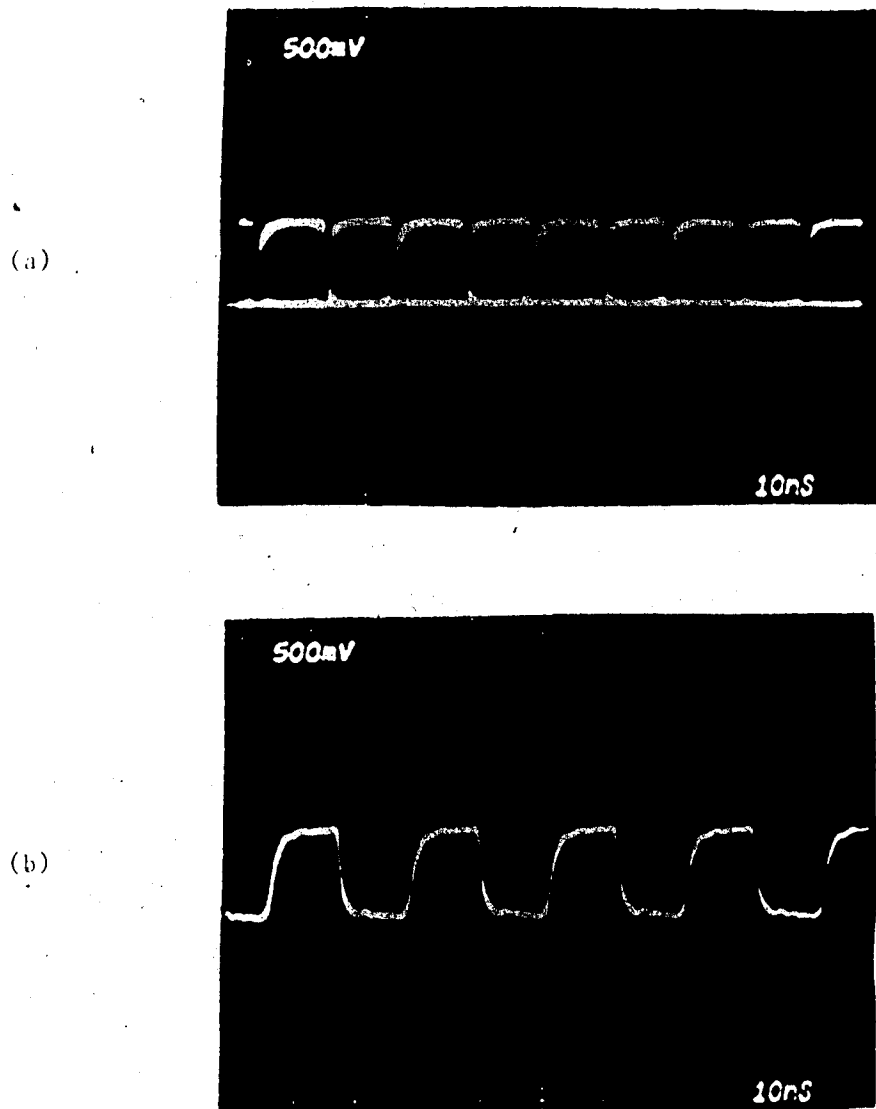


Fig. 5.7 Clock Recovery Circuit Waveforms

- (a) Input (Received Optical Power = -48.5 dBm,  
Encoder Input =  $10^{23}-1$  Pseudorandom NRZ)
- (b) Output, for the Modified Clock Recovery  
Circuit ( $A = 0.034\text{ns}$ ,  $A' = 0.12\text{ns}$ )

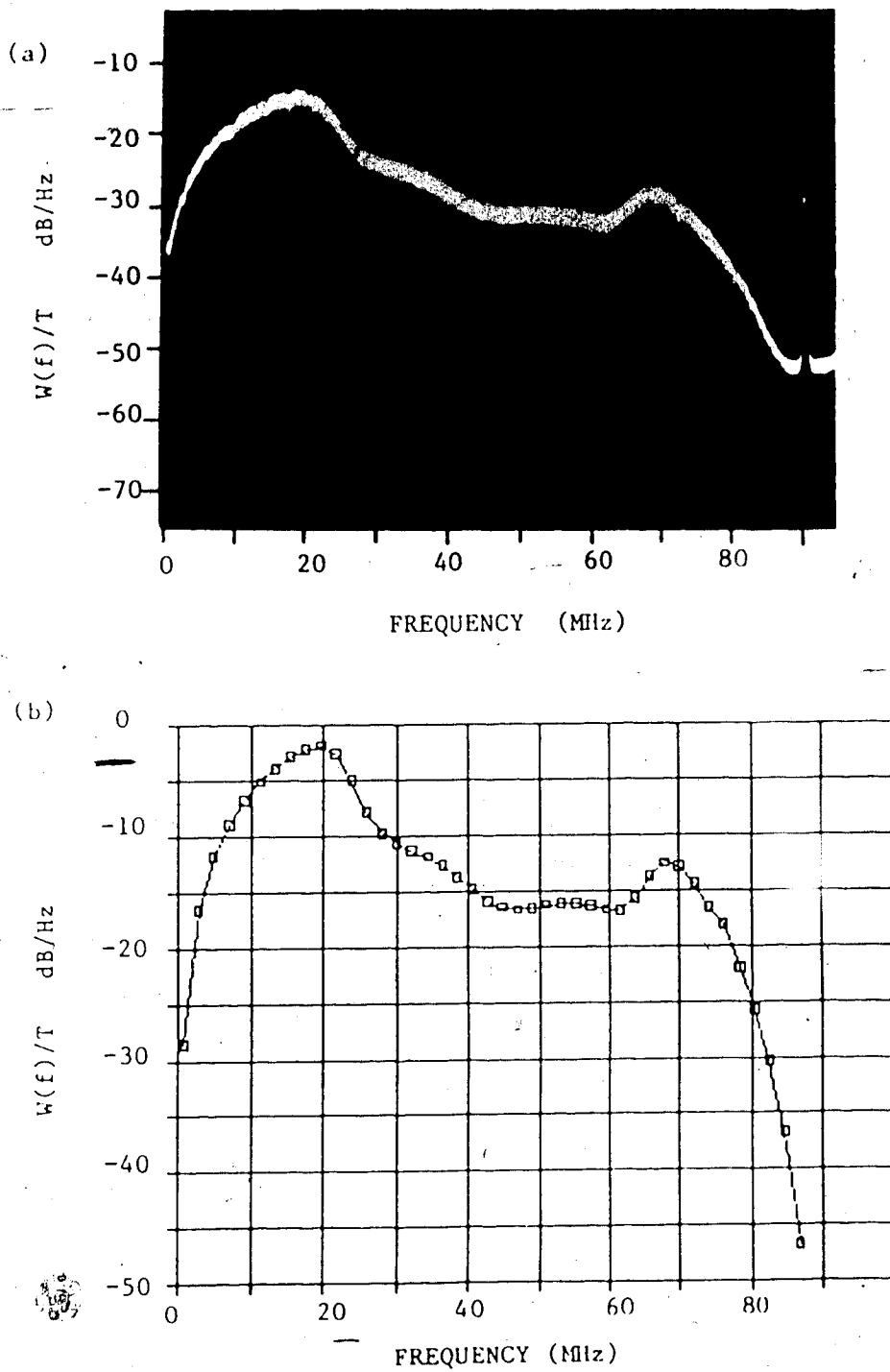


Fig. 5.8 Petrovic Power Spectrum

(a) Experimental

(b) Theoretical



experimental spectrum (see Figure 5.8) is approximately 12 dB. In the theoretical spectrum, this ratio is approximately 11.5 dB. This 0.5 dB discrepancy can be explained by the fact that the encoder output does not contain perfectly rectangular pulses, i.e. the encoder output pulses have finite rise and fall times. Since rounded pulses contain less higher frequency content than rectangular pulses, the ratio between the heights of the main lobe and the secondary lobe should be greater for the experimental spectrum.

### 5.3 BER Measurements

The bit error rate (BER) of a digital optical fibre communication system depends on several parameters, e.g., received power, receiver noise characteristics, fibre transfer function and bandwidth, receiver transfer function and bandwidth, received pulse shape, APD gain, sampling instant, jitter in sampling clock, decoder threshold, bit sequence, etc. In this section, the relationship between BER and the following parameters will be presented: received optical power, receiver bandwidth, and source bit sequence. A delayed version of the transmitter clock will be used to sample the received waveform in the decoder; BER results with the recovered clock will be given in Section 5.5. Where applicable, a comparison between results obtained with

the Petrovic code and with the NRZ code will be made. (The NRZ code results are obtained by bypassing the Petrovic encoder and decoder).

The BER measurements reported in this section were obtained with the experimental setup located inside a screened room. The laboratory environment contained significant stray RF energy from various sources, e.g., high power industrial lasers located on the same floor, switching circuits in elevators, soldering irons, campus FM radio station, etc. Inside the Faraday cage, this interference was reduced by approximately 40 dB and reliable and repeatable BER measurements were obtained.

### 5.3.1 BER Versus Received Power

A plot of BER versus received power is shown in Figure 5.9 for the NRZ, Petrovic, and CMI line codes, for a  $10^{23}-1$  pseudorandom sequence (the CMI code is available from the Data Generator and can be correctly decoded by the Petrovic decoder). The received power was varied using an optical attenuator and was measured by using a Photodyne model 22XLA optical power meter, which has an accuracy of  $\pm 0.1$  dB. The output of the preamplifier was not filtered by a LPF. The receiver bandwidth was 65 MHz, and all other parameters, e.g., sampling instant, power supply voltages, etc. were kept

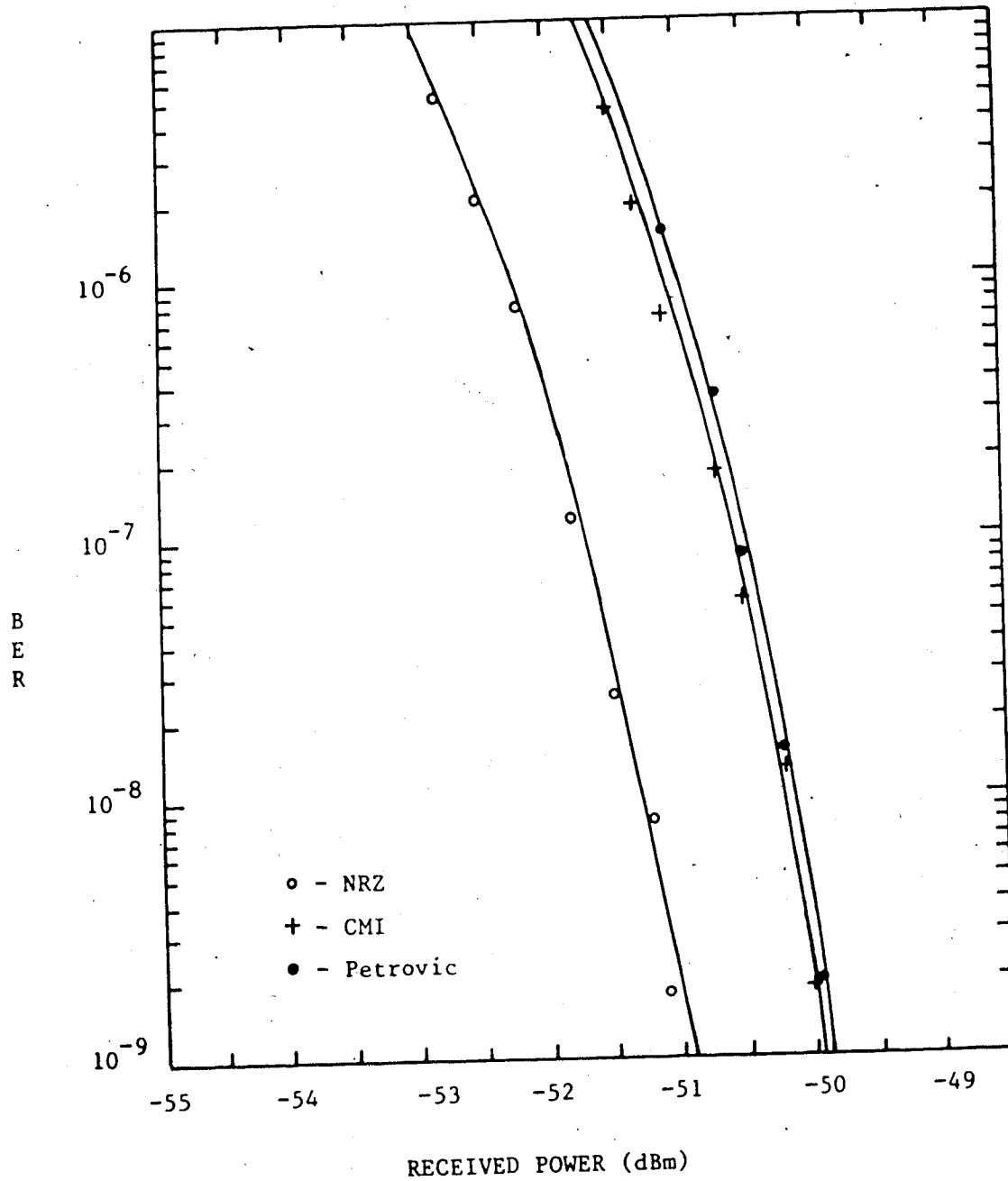


Fig. 5.9 BER versus Received Power for the NRZ, CMI and Petrovic Line Codes.  
 ( $10^{23}-1$  Pseudorandom sequence, Bandwidth = 65MHz)

constant. The following observations can be made from the BER versus received power curves shown in Figure 5.9:

1. The Petrovic code and the CMI code require virtually the same power for a given BER and receiver characteristics. This observation agrees with the computer simulation results obtained in Chapter 2, i.e. even though the Petrovic and CMI codes have different spectral distributions, they both have almost the same BER for a given receiver bandwidth, signal, and noise level.

2. The sensitivity of the NRZ code for a BER of  $10^{-9}$  is approximately 1 dB better than the Petrovic or the CMI code for this particular receiver bandwidth. (In the next section it will be seen that this sensitivity will vary with the bandwidth).

3. The shape of the BER curves closely approximates the Q function [ $Q(x) = 1/2 \operatorname{erfc}(x/\sqrt{2})$ ]. This indicates that the noise at the decoder is mainly gaussian.

### 5.3.2 BER Versus Receiver Bandwidth

In Chapter 2, computer simulation studies showed that, for a given receiver signal power, filter type, and noise power, an optimum bandwidth exists which will yield the lowest BER. Furthermore, for a BER of  $10^{-9}$ , the NRZ code will require approximately 3 dB less power and half the receiver bandwidth, when compared to the

Petrovic code. The receiver bandwidth in the experimental system was varied by changing the value of  $C_8$  (see Fig. 4.4). The bandwidth was determined from the noise spectrum of the optical receiver (with -48 dBm of optical power, without modulation, falling upon the APD). The noise spectrum of the receiver output takes the shape of the receiver's transfer function since the noise generated at the front-end of the preamplifier, which can be assumed to be white, is the dominant noise source. Figure 5.10 shows the relationship between BER and receiver bandwidth for the NRZ code at a received power of -54 dBm and for the Petrovic code at a received power of -51 dBm. Figure 5.11 shows the relationship between received power and receiver bandwidth for a BER of  $10^{-9}$ . From these curves we see that the minimum received power required for a  $10^{-9}$  BER is -50.2 dBm for the Petrovic code (bandwidth = 51 MHz) and -53.4 dBm for the NRZ code (bandwidth = 27 MHz). Thus the Petrovic code requires approximately 3.2 dB more power and approximately 1.9 times more bandwidth. This agrees quite well with the computer simulation results of Chapter 2.

It may also be noted that the best sensitivity yet obtained for a  $10^{-9}$  BER at a bit rate of 45 Mb/s and NRZ signalling is -56 dBm (using direct detection) [40].

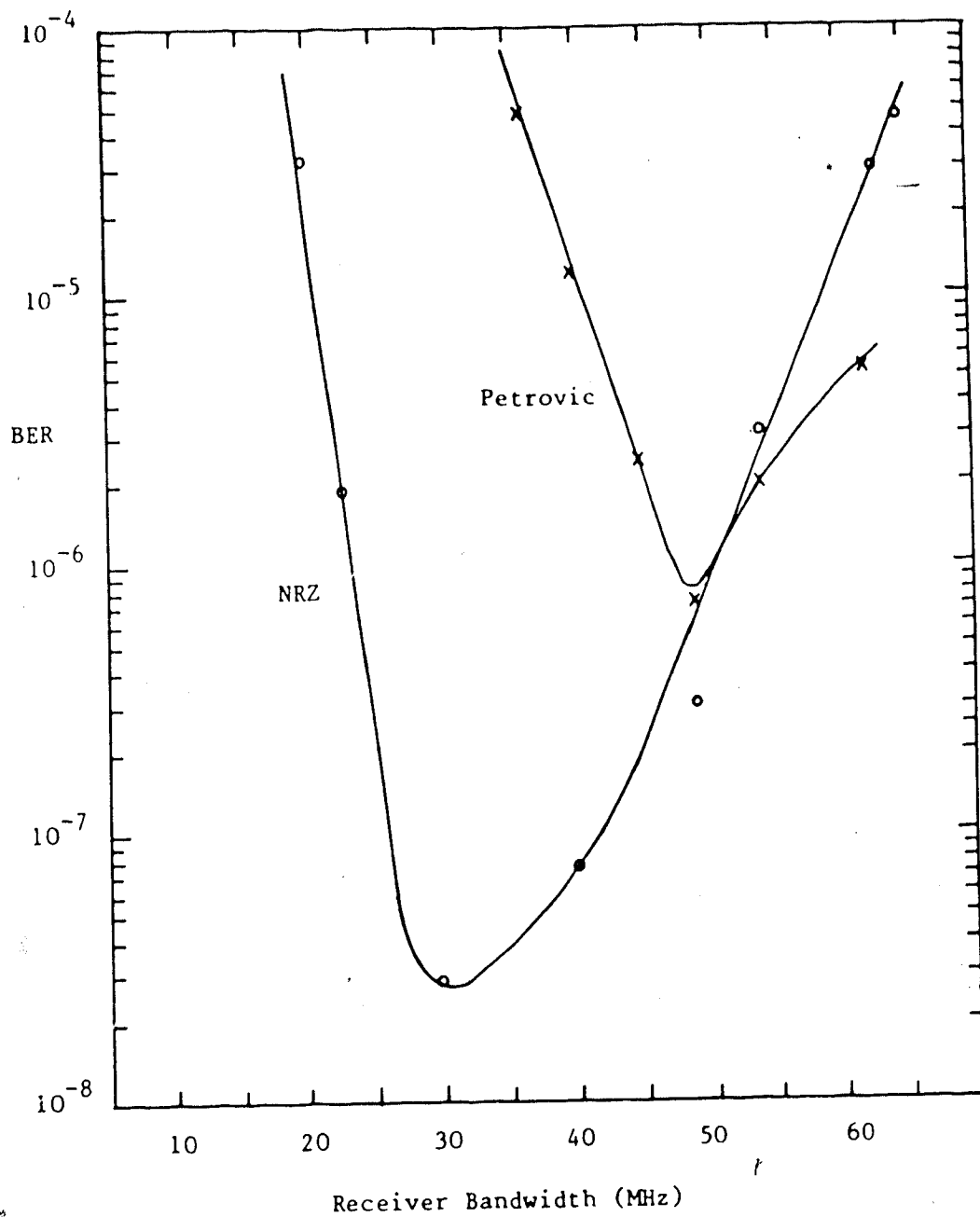


Fig. 5.10 Relationship between BER and Receiver Bandwidth for the NRZ and the Petrovic Codes.  
 (Received optical power for the NRZ code = -54 dBm, received optical power for the Petrovic code = -51 dBm.)

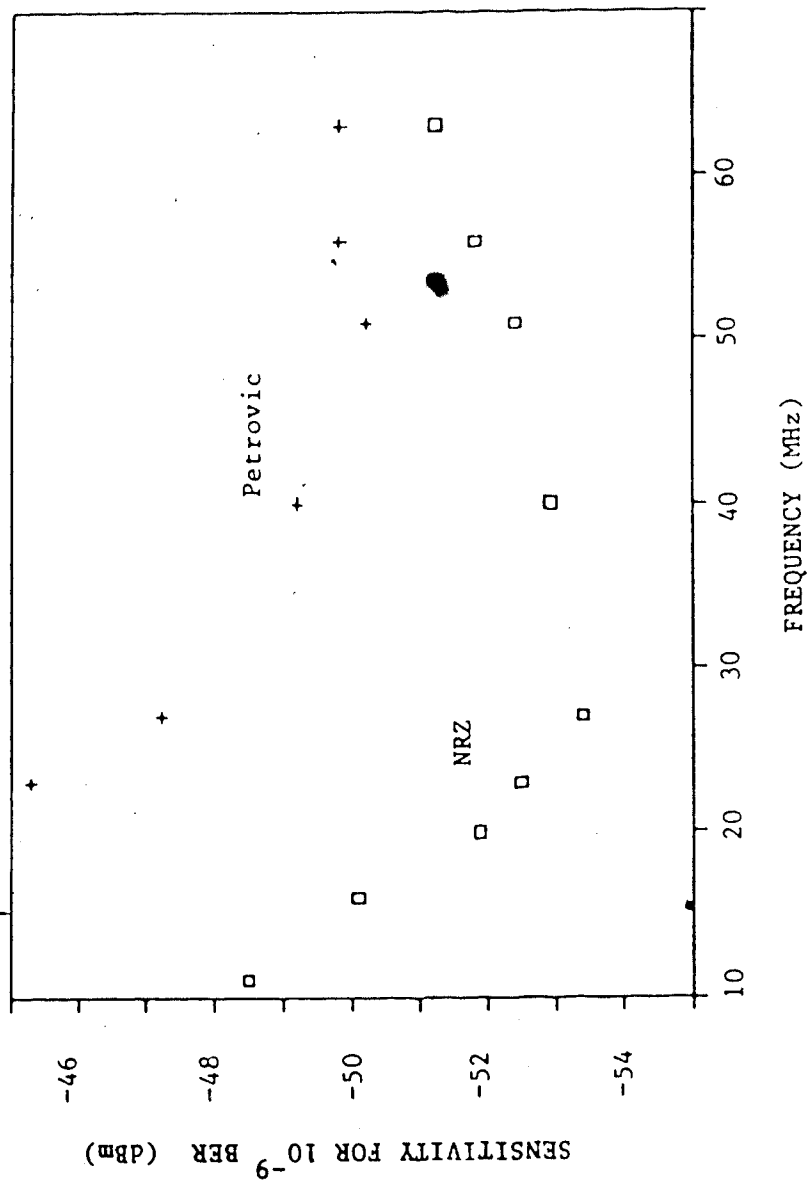


Fig. 5.11 Relationship Between Received Optical Power and Receiver Bandwidth, for  $10^{-9}$  BER.

This was obtained with a bipolar, high impedance APD-preamplifier. In the experimental system, a BER of  $10^{-9}$  was achieved for the NRZ code at a received power of -53.4 dBm. This sensitivity is only 2.6 dB below the best that has been obtained so far. The experimental sensitivity would be improved if a high impedance preamplifier had been used instead of the transimpedance type and the preamplifier is optimized with respect to noise.

### 5.3.3 BER Versus Bit Sequence

The BER for the experimental Petrovic system should be independent of the incoming bit pattern because the Petrovic code is bit sequence independent. The BER for the NRZ code, however, depends on the bit sequence because this code suffers from baseline wander. Table 5.1 shows the BER for the Petrovic and NRZ codes for various source bit sequences. For these measurements, the received power was held constant (-50.7 dBm for the Petrovic code and -52 dBm for the NRZ code), receiver bandwidth was 65 MHz, and the sampling instant and decoder threshold were fixed.

From Table 5.1, we see that for the Petrovic code, the BER remains relatively constant for any incoming bit pattern. (The small fluctuations in BER that do occur may be attributable to slight variations in optical



Table 5.1 BER versus Source Bit Sequence for the Petrovic and the NRZ code.  
 (Received Optical Power for the Petrovic and the NRZ code is -50.7 dBm and  
 -52.0 dBm respectively; receiver bandwidth = 65 MHz.)

Source Bit Pattern	BER	
	Petrovic Code	NRZ Code
10 <sup>23</sup> -1 Pseudorandom	1.3 X 10 <sup>-6</sup> to 1.7 X 10 <sup>-6</sup>	9.5 X 10 <sup>-7</sup> to 1 X 10 <sup>-6</sup>
10 <sup>15</sup> -1 "	1.4 X 10 <sup>-6</sup> to 1.7 X 10 <sup>-6</sup>	9.0 X 10 <sup>-7</sup> to 1.2 X 10 <sup>-6</sup>
10 <sup>10</sup> -1 "	1.3 X 10 <sup>-6</sup> to 1.8 X 10 <sup>-6</sup>	7.0 X 10 <sup>-7</sup> to 8.3 X 10 <sup>-7</sup>
1010101010...	4.0 X 10 <sup>-7</sup> to 4.8 X 10 <sup>-7</sup>	7.6 X 10 <sup>-7</sup> to 8.9 X 10 <sup>-7</sup>
111111111111...	4.9 X 10 <sup>-6</sup> to 6.1 X 10 <sup>-6</sup>	SYNC. LOSS
0000000000...	1.8 X 10 <sup>-6</sup> to 2.1 X 10 <sup>-6</sup>	" "
1000000000000000*	1.3 X 10 <sup>-6</sup> to 1.4 X 10 <sup>-6</sup>	" "
1100000000000000*	1.6 X 10 <sup>-6</sup> to 2.1 X 10 <sup>-6</sup>	" "
1110000000000000*	1.7 X 10 <sup>-6</sup> to 2.1 X 10 <sup>-6</sup>	1.6 X 10 <sup>-1</sup> to 3.2 X 10 <sup>-2</sup>
1111000000000000*	2.8 X 10 <sup>-6</sup> to 3.6 X 10 <sup>-6</sup>	1.1 X 10 <sup>-2</sup> to 4.2 X 10 <sup>-3</sup>
1111100000000000*	1.9 X 10 <sup>-6</sup> to 2.4 X 10 <sup>-6</sup>	1.1 X 10 <sup>-3</sup> to 3.2 X 10 <sup>-3</sup>
1111110000000000*	2.3 X 10 <sup>-6</sup> to 3.4 X 10 <sup>-6</sup>	4.6 X 10 <sup>-4</sup> to 8.9 X 10 <sup>-4</sup>
1111111000000000*	2.0 X 10 <sup>-6</sup> to 2.3 X 10 <sup>-6</sup>	3.4 X 10 <sup>-5</sup> to 4.0 X 10 <sup>-5</sup>
1111111100000000*	3.1 X 10 <sup>-6</sup> to 4.0 X 10 <sup>-6</sup>	9.8 X 10 <sup>-7</sup> to 1.0 X 10 <sup>-6</sup>

\* - 16 Bit Repeating Sequence

power, e.g., a change of 0.1 dB in the optical power will change the BER by a factor of 2, or by small static phase shifts in the decoder output from one pattern to the next). The BER for the NRZ code, however, is a strong function of the bit sequence; it fluctuates over 4 orders of magnitude.

#### 5.4 Jitter in the Recovered Clock

The spectrum of the self-sustaining monostable multivibrator clock recovery circuit, with the feedback delay parameter  $\Delta = 0.04$  ns ( $\Delta = T_1 - T/2$  where  $T_1 =$  feedback delay,  $T =$  incoming NRZ bit interval) is shown in Figure 5.12a; the clock spectrum of the modified circuit is shown in Figure 5.12b for  $\Delta = 0.04$  ns and  $\Delta' = 0.12$  ns ( $\Delta' = T/2 - T_2$ , where  $T_2 =$  outer feedback delay + monostable pulse width). For comparison, the spectrum of the transmitter clock is shown in Figure 5.12c. The recovered clock spectrum consists of a continuous spectrum and a discrete spectral line at the bit rate. The continuous spectrum arises due to the jitter in the clock signal. Quite often, the ratio between the clock spectral line amplitude to the continuous spectrum amplitude adjacent to the discrete line,  $R_{clk}$ , is used as a figure of merit [24]. One would like to have a large value of  $R_{clk}$ , i.e., a small continuous power spectrum. For the self-sustaining monostable circuit,

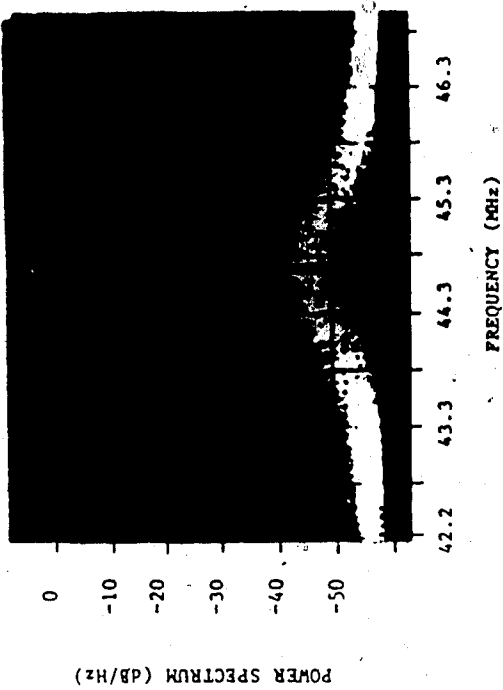
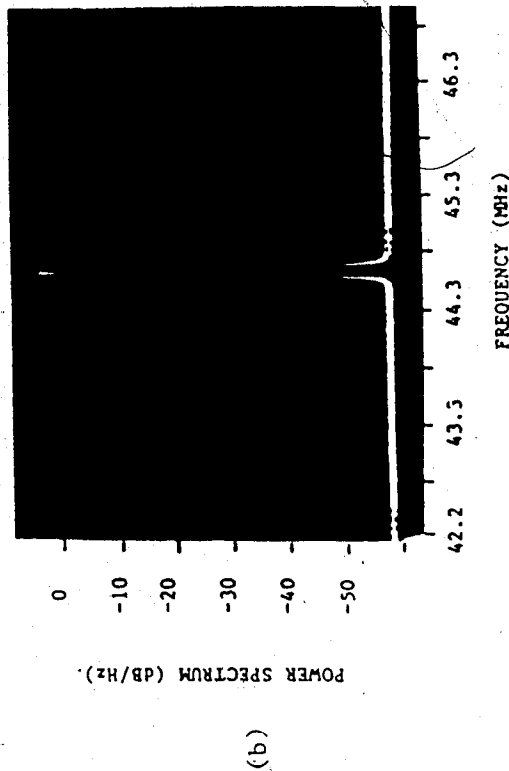
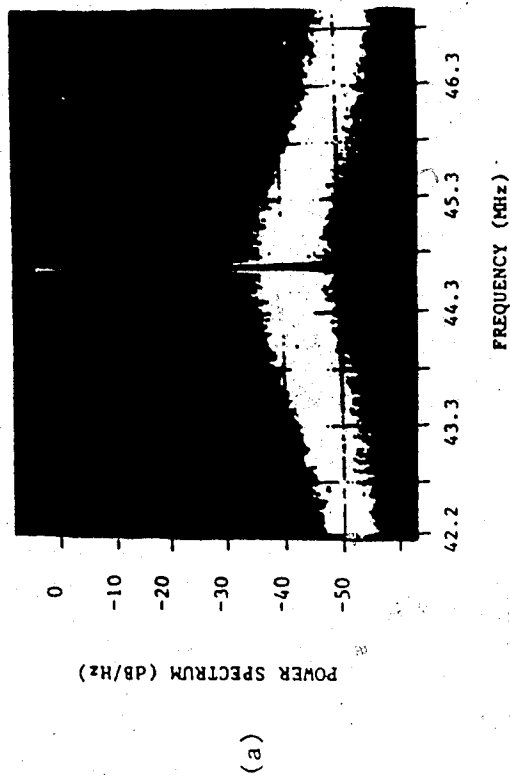


Fig. 5.12 Clock Spectrum

Received optical power = -48 dBm,  
 receiver bandwidth = 65 MHz,  
 spectrum analyzer resolution = 10 KHz.

- (a) Original Self-Sustaining Monostable Multivibrator Clock Recovery Circuit, for  $\Delta = 0.04$  ns.
- (b) Modified Clock Recovery Circuit, for  $\Delta = 0.04$  ns and  $\Delta' = 0.12$  ns.
- (c) Transmitter Clock

$R_{clk}$  is approximately 36 dB while for the modified self-sustaining monostable circuit, it is approximately 42 dB. Thus, the modification to the self-sustaining monostable clock recovery circuit does result in significant jitter reduction.

The clock jitter spectrum for both the self-sustaining monostable multivibrator clock recovery circuit and the modified self-sustaining monostable circuit were measured for various values of feedback delay. The jitter spectra were obtained by applying the transmitter clock and the recovered clock to a jitter measurer, which consisted of an EX-NOR gate followed by a first order LPF (see Section 4.6), and then monitoring the jitter output spectrum on a spectrum analyzer (HP8557A). Note that the 3 dB cutoff frequency of the LPF is approximately 20 MHz. Since this is much higher than the 3 dB cutoff frequency of the jitter spectrum (approx. 2 MHz), the LPF has a negligible effect on the jitter spectrum. The area under the jitter spectral curve is proportional to the clock jitter power,  $J_p$ . For a gaussian jitter pdf,  $J_p$  is equal to the jitter variance  $\sigma_p^2$ . If the jitter pdf is non-gaussian (as in the experimental system),  $J_p$  will be proportional to the jitter variance. Figure 5.13 shows the clock jitter spectrum of the original clock recovery circuit for various values of  $\Delta$ . The jitter power is simply the

area under the jitter spectral curve and is determined from the following equation:

$$J_p = KNB/R, \quad (5.1)$$

where  $N$  = spectral density at low frequency

$R$  = resolution of spectrum analyzer

$B$  = 3dB bandwidth of jitter spectral curve

$K$  = proportionality constant, which depends on the height of the pulses generated by the EX-OR gate of the jitter measurer and the shape of the spectral curves.

It is chosen to be 1, for convenience.

The jitter power corresponding to the spectrum shown in Figure 5.13 is given in Table 5.2. An examination of the jitter power reveals that it decreases as  $\Delta$  is reduced. This is to be expected because, as  $\Delta \rightarrow 0$ , the monostable multivibrator is triggered closer to the ideal time, thus reducing the positive portion of the clock jitter pdf (see Section 4.3), and decreasing its jitter variance. We also notice that the jitter power does not decrease by a large amount as  $\Delta$  is reduced. For example, changing  $\Delta$  from 0.11ns to 0.04ns decreases the jitter power by only a factor of 1.5. This is because, as  $\Delta$  is decreased, the positive portion of the input jitter pdf becomes smaller but the negative portion remains unchanged. The negative portion of the input jitter pdf

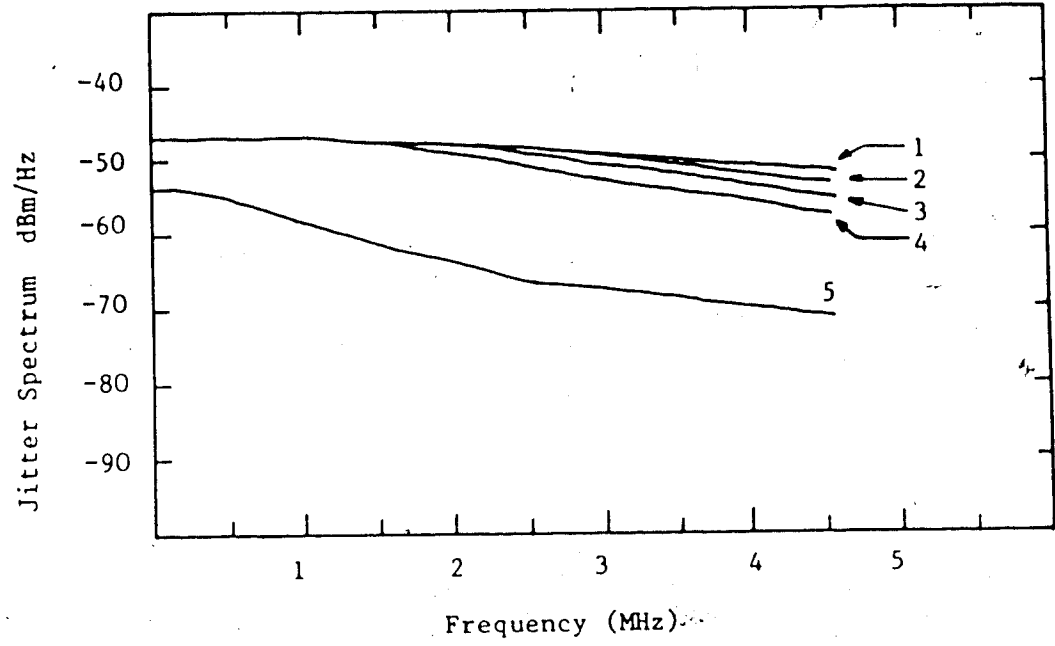


Fig. 5.13 Clock Jitter Spectrum of the Original Self-Sustaining Monostable Multivibrator Clock Recovery Circuit for various values of  $\Delta$ , with received optical power = -48 dBm, receiver bandwidth = 65MHz. (Resolution of Spectrum Analyzer = 30KHz.)

- 1 -  $\Delta = 0.11\text{ns}$
- 2 -  $\Delta = 0.08\text{ns}$
- 3 -  $\Delta = 0.06\text{ns}$
- 4 -  $\Delta = 0.04\text{ns}$
- 5 - Modified Clock Recovery Circuit with  $\Delta' = 0.12\text{ns}$  and  $\Delta = 0.04\text{ns}$

Table 5.2 Jitter Power corresponding to the Jitter Spectra shown in Fig. 5.13

$\Delta$ (ns)	Jitter Power (W)
0.11	$2.2 \times 10^{-6}$
0.08	$2.0 \times 10^{-6}$
0.06	$1.8 \times 10^{-6}$
0.04	$1.5 \times 10^{-6}$

---

Table 5.3 Jitter Power corresponding to the Jitter Spectra shown in Fig. 5.14  
( $\Delta = 0.04\text{ns}$ )

$\Delta'$ (ns)	Jitter Power (W)
1.95	$1.7 \times 10^{-6}$
0.88	$4.0 \times 10^{-7}$
0.12	$1.0 \times 10^{-7}$

will determine the lower limit of the output clock jitter power, which occurs when  $\Delta = 0$ . When the input jitter pdf is gaussian with a zero mean and a variance  $\sigma_i^2$ , the minimum output jitter variance will be  $0.341 \sigma_i^2$  (see Section 3.3). This corresponds to the maximum jitter power reduction of 2.9 that is possible with the self-sustaining monostable clock recovery circuit.

The clock jitter spectrum of the modified monostable clock recovery circuit is shown in Figure 5.14 for  $\Delta = 0.04$  ns and various values of the outer feedback parameter  $\Delta'$ . The jitter power corresponding to these spectra is given in Table 5.3. Notice that, when  $\Delta'$  is large, the jitter spectra is similar to that of the original clock recovery circuit. As  $\Delta' \rightarrow 0$ , the jitter power drastically reduces because the early primary pulses are prevented from triggering the MM. The clock jitter power for the modified circuit is considerably less than that of the original circuit. For example, with  $\Delta = 0.04$  ns and  $\Delta' = 0.12$  ns, the modification results in a factor of 15 reduction in jitter power.

The clock output of the original circuit was synchronized with the transmitter clock when  $\Delta$  was between 0.51 ns and 0.00 ns. When  $\Delta$  was outside these values, the clock recovery circuit oscillated at a



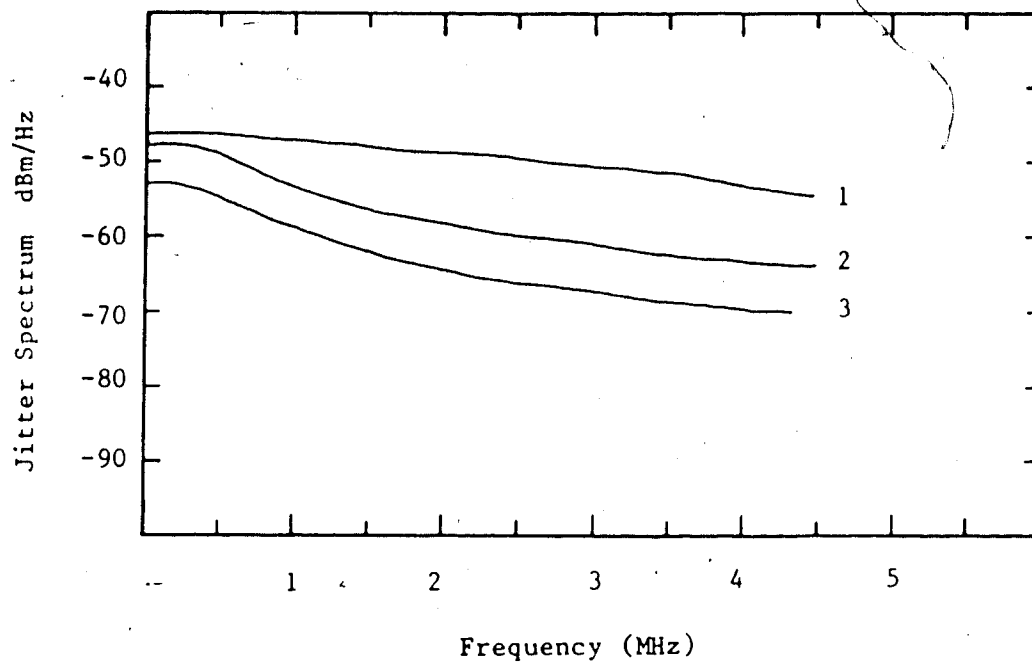


Fig. 5.14 Clock Jitter Spectrum of the Modified Self-Sustaining Monostable Multivibrator\_Clock Recovery Circuit for various values of  $\Delta'$ , with  $\Delta = 0.04\text{ns}$ , received optical power =  $-48\text{dBm}$ , receiver bandwidth =  $65\text{MHz}$ . (Resolution of Spectrum Analyzer =  $30\text{KHz}$ .)

1 -  $\Delta' = 1.95\text{ns}$

2 -  $\Delta' = 0.88\text{ns}$

3 -  $\Delta' = 0.12\text{ns}$

frequency of  $[1/(T/2 + \Delta)]$  Hz. The modified clock recovery circuit lost synchronization with the transmitter clock when  $\Delta' < 0.10$  ns (with  $\Delta = 0.04$  ns).

### 5.5 System BER With Recovered Clock

The experimental Petrovic system BER, as a function of received power, was difficult to obtain when the decoder clock was obtained from the original self-sustaining monostable circuit. This was because the clock signal experienced random 180 degree phase shifts at low power levels. (These phase shifts prevented the Error Detector from obtaining synchronization). For example, at a received power of -48.4 dBm and  $\Delta = 0.06$  ns, an average of 3 clock inversions, i.e. 180° phase shifts, were observed per second; at a received power of -49.0 dBm, 10 inversions occurred every second.

Clock inversions occur whenever the output of the MM (monostable multivibrator) is missing pulses. Since the output of the MM is divided by 2, these missing pulses result in 180 degree phase shifts in the clock signal. The MM output will be missing a pulse whenever a primary pulse arrives before the MM has recovered from the previous trigger pulse. Since jitter is proportional to SNR, the probability of a primary pulse arriving early increases as the signal power decreases. Thus, phase inversions occur only at low received power

levels. A BER of  $10^{-9}$  was achieved with the original clock recovery circuit at a received optical power of -48.2 dBm (2 errors were observed in a span of 30 seconds, which was the interval between clock inversions, giving a BER of  $10^{-9}$  at 44.7 Mb/s).

The clock signal from the modified clock recovery circuit did not suffer from 180 degree phase shifts because the outer feedback in this circuit inhibits the early primary pulses from triggering the MM. The experimental BER versus received power curve for the case when the sampling clock is obtained from the modified clock recovery circuit is shown in Figure 5.15. A  $10^{-9}$  BER was achieved at -49.6 dBm. This is 1.4 dB better than that obtained with the original clock recovery circuit and 0.2 dB poorer than when the delayed transmitter clock is used (see Section 5.3.1). Thus, only a small power penalty is incurred when the recovered clock from the modified self-sustaining monostable multivibrator clock recovery circuit is used to sample the received signal instead of the ideal transmitter clock. Also the modification to the self-sustaining monostable circuit by Witte and Moustakas [31] does result in significant jitter reduction and improved BER performance.

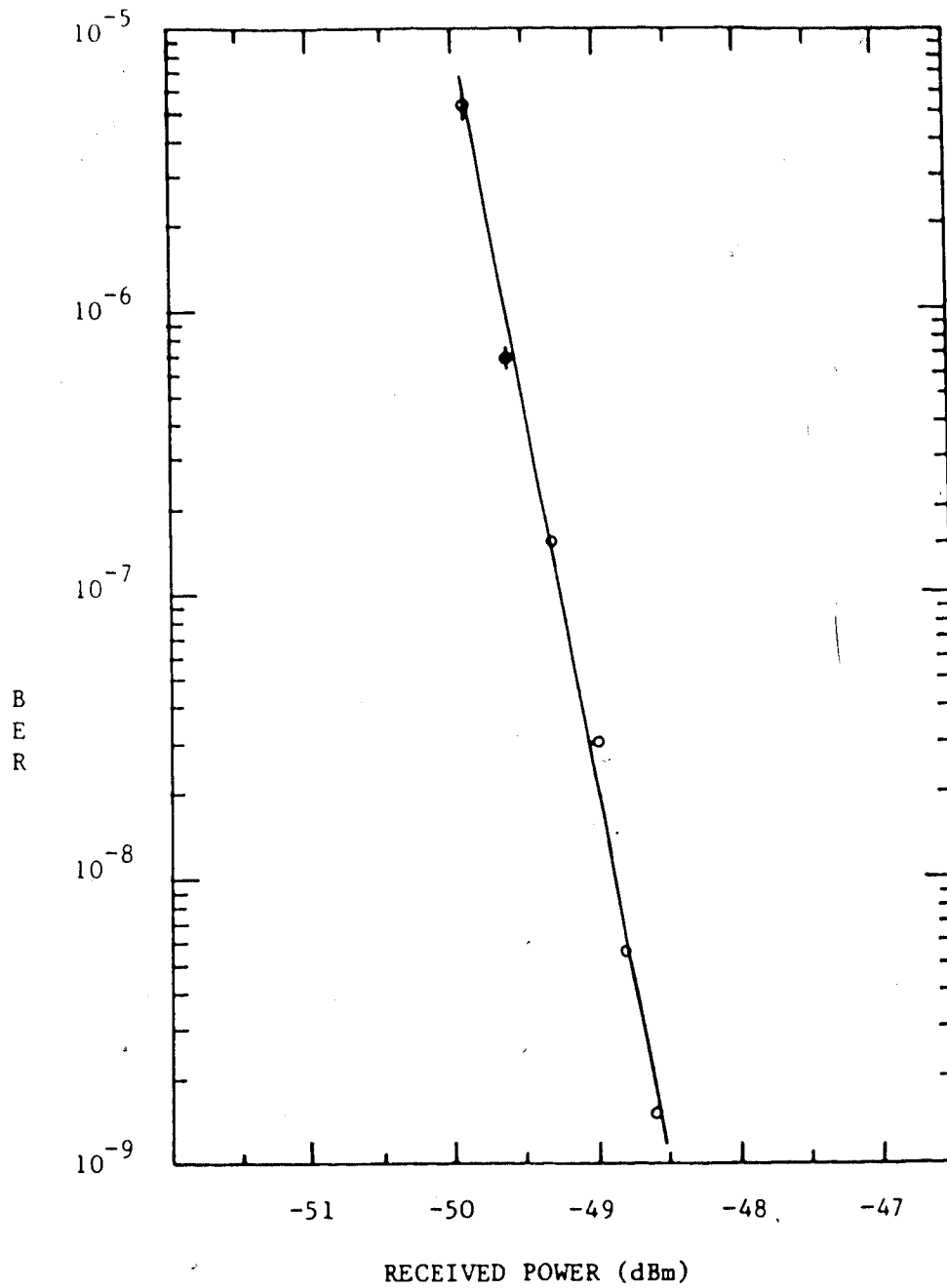


Fig. 5.15 BER versus Received Optical Power when the clock signal from the Modified Clock Recovery Circuit is used for the Decoder clock.  
( $\Delta = 0.04$  ns,  $\Delta' = 0.12$  ns, receiver bandwidth is 65 MHz.)

## CHAPTER 6

### SUMMARY AND CONCLUSIONS

A line code used in an optical fibre communication system should have the following characteristics:

- a) zero dc content and small low frequency content
- b) frequent transitions and the longest interval between transitions must be restricted.
- c) bit sequence independence
- d) error detection capability

The Petrovic code, which belongs to the 1B-2B family of line codes, has the above characteristics.

The bandwidth requirements of the Petrovic code were theoretically determined for an additive white gaussian noise channel with a first and second order Butterworth receiver transfer function. From this study it was determined that, even though the power spectral density (PSD) of the Petrovic code does not contain significantly larger high frequency components than the NRZ code, the Petrovic code requires twice the bandwidth of the NRZ code. The reason that the PSD of the Petrovic code does not contain large high frequency components is that due the encoding rules, the probability of a short pulse ( $T/2$  seconds long, where  $T$  is the source bit interval) being transmitted is small;

\*

the majority of the pulses that are transmitted are  $T$ ,  $3T/2$ , or  $2T$  seconds in duration. However, the receiver must contain sufficient bandwidth to reproduce the short pulse (in order to achieve a reasonable bit error rate) Since the shortest pulse length found in the Petrovic code is exactly half that of the shortest pulse length found in the NRZ code, the Petrovic code should require twice the bandwidth of the NRZ code.

If the system noise is white and gaussian, the Petrovic code will suffer from a 3 dB sensitivity penalty, when compared to the NRZ code since it requires twice the bandwidth. In a fibre optic receiver, where the noise is not white, the power penalty is approximately 3 dB when the front end is an APD-BJT or a PIN-BJT combination and the circuit is optimized to give minimum noise. For the case of a PIN-FET front end, the power penalty varies between 1.5 dB and 4.5 dB, and for an APD-FET, the power penalty varies between 2.3 dB to 3.8 dB.

The repeater spacing for the Petrovic code is smaller than the NRZ code by  $3/\alpha$  (where  $\alpha$  = fibre attenuation and the power penalty is 3 dB) when the system is attenuation limited. Under dispersion limited situations, the repeater spacing for the Petrovic code is smaller than the NRZ code by a factor of two. The difference in repeater spacing between the NRZ and

Petrovic codes is least when the system is attenuation limited. Hence, one should seriously consider employing the Petrovic code only for systems that are not dispersion limited, e.g., local area network applications.

Jitter analysis of the monostable clock recovery circuit, developed by Witte and Moustakas, showed that this circuit inhibits the late arriving data pulses from triggering the monostable multivibrator. The clock jitter variance is proportional to the difference between the feedback delay and the bit interval, denoted by  $\Delta$ . In the limiting case, when the feedback delay is equal to the bit interval, i.e.,  $\Delta = 0$ , the ratio between the output jitter variance to the input jitter variance is equal to 0.341 when the input jitter is a zero mean, gaussian process. When  $\Delta$  is non-zero and positive, a simple expression for the output jitter variance cannot be determined since the output jitter pdf is not time independent; it varies from one bit interval to the next.

The output jitter variance can be reduced further by also inhibiting the early arriving pulses from triggering the monostable. A simple modification to prevent the early arriving pulses, and hence reduce the jitter, was presented.

A 44.736 Mb/s optical fibre communication system employing the Petrovic code and the self-sustaining monostable clock recovery circuit was constructed and set up. Due to the simple encoding rules of the Petrovic code, the encoder and decoder circuitry consisted of only a few integrated circuits. The experimental Petrovic spectrum agreed with the theoretical spectrum obtained by Petrovic [7] and Lo Cicero [19]. A 3.2 dB power penalty was observed when the Petrovic code was used instead of the NRZ code. Since the front end device in the experimental receiver was a bipolar transistor, the theoretical power penalty is 3 dB. The 0.2 dB difference between the theoretical and experimental values occurs since the receiver was not optimized with respect to noise. The Petrovic code was found to require a receiver bandwidth 1.9 times greater than the NRZ code and was found to be bit sequence independent.

The self-sustaining monostable clock recovery circuit did not perform satisfactorily at low received power levels due to 180 degree phase shifts in the clock signal. These phase reversals were caused by primary pulses arriving before the recovery time of the monostable multivibrator had expired. The modification to prevent the early arriving pulses from triggering the monostable resulted in the following improvements:



- 1) A factor of 15 reduction in clock jitter power.
- 2) Elimination of the 180 degree phase shifts in the clock signal at low received power levels.
- 3) A 1.4 dB increase in the receiver sensitivity.

The receiver sensitivity with the delayed transmitter clock and with the clock signal from the modified monostable clock recovery circuit are virtually the same. This is partly due to the frequent transitions found in the Petrovic code and partly due to the substantial jitter reduction characteristics of the modified self-sustaining monostable clock recovery circuit.

Due to time constraints, this project was necessarily limited in scope. Some suggestions for further research include:

1. The computer simulation used to compare the bandwidth requirement of the Petrovic code with that of the NRZ code assumed a channel with an infinite bandwidth and additive white gaussian noise. It would be interesting to modify the software to cater for fibre dispersion and optical receiver noise characteristics and then determine the bandwidth requirements.
2. The jitter analysis of the self-sustaining monostable clock recovery circuit was mainly qualitative in nature. An analytical (or numerical) solution of

jitter variance as a function of feedback delay, taking into account the time dependent nature of the jitter pdf and the statistics of the line code, should be obtained.

3. The time delays used in the clock recovery circuit and the decoder were obtained with coaxial cables. This gives satisfactory performance in a laboratory environment but may not be suitable for field use, where large variations in temperature will result in variations in the propagation delay of the coaxial cables. An investigation into a more stable realization for the delay is required for field use.

4. The accumulation of jitter produced by the self sustaining monostable clock recovery circuit over several repeaters should be studied before this clock recovery circuit is used in a long haul fibre optic system.

5. The jitter produced by the self-sustaining monostable clock recovery circuit should be compared with the jitter produced by other clock recovery circuits, such as a: PLL, SAW filter, and an LC filter. This could be done for various line codes, and receiver bandwidth and noise characteristics.

It is sincerely hoped that this thesis has generated interest in the Petrovic code and in the modified self-sustaining monostable clock recovery circuit.

## REFERENCES

- [1] K.W. Cattermole, "Principles of Digital Line Coding", **Int. J. Electronics**, Vol. 55, No.1, 1983, pp. 3-33.
- [2] C. Game, A. Jessop, "Random Coding For Digital Systems", **Proceedings of the First European Conference on Optical Fibre Comm.**, Conference Publication No.132, 1975, pp 171-173.-
- [3] M. Rousseau, "Block Codes For Optical-Fibre Communications", **Electronic Letters**, Vol.12, No.18, Sept. 2 1976, pp.478-479.
- [4] Y. Takasaki, M. Tanaka, N. Maeda, K. Yamashita, K. Nageno, "Optical Pulse Formats for Optical Digital Communications", **IEEE Trans. on Commun.**, Vol. Com-24, April 1976, pp.404-413.
- [5] R. M. Brooks, A. Jessop, "Line Coding for Optical Fibre Systems", **Int. J. Electronics**, Vol. 55, No.1, 1983, pp. 81-126.
- [6] J.C. Lacroix, "Line Signals in Submarine Digital Telephone Links Using Optical Fibers", **IEEE** Vol. SAC-2, No.6, Nov. 1984, pp. 1038-1041.
- [7] R. Petrovic, "New Transmission Code For Digital Optical Communications", **Electronics Letters**, Vol. 14, No. 17, Aug. 17 1978, pp. 541-542.
- [8] R. Brooks, "7B8B Balanced Code With Simple Error Detecting Capability", **Electronics Letters**, Vol. 16, No. 12, June 5 1980, pp. 458-459.
- [9] Y. Takasaki, M. Tanaka, N. Maeda, "Optical Pulse Formats for Long Wavelength Fiber Optic Digital Transmission", **IEEE Conference on Communications**, 1979, pp. 53.2.2 - 53.2.5.
- [10] Y. Takasaki, Y. Yamashita, Y. Takahashi, "Two-Level AMI Line Coding Family For Optical Fibre Systems", **Int. J. Electronics**, Vol. 55, No.1, 1983, pp. 121-131.

- [11] S. Murakami, M. Shimodaira, M. Sugiyama, "Pulse Formats for Bandlimited Multimode Fibre Transmission", **Int. J. Electronics**, Vol. 55, No.1, 1983, pp. 133-140.
- [12] N. Yoshika, J. Yamada, S. Kawanishi, "Simple-In Service Method For Monitoring DMI Code Errors", **Electronics Letters**, Vol. 20, No. 23, Nov. 8 1984, pp. 452-453.
- [13] N. Yoshikai, K. Katagiri, T. Ito, "mB1C Code And Its Performance in an Optical Communication System", **IEEE Trans. on Commun.** Vol. COM-32, No. 2, Feb. 1984, pp. 163-168.
- [14] P. Radev, G. Stoyanov, "New 1B-2B Line Code For Digital Fibre Optic Transmission Systems", **Electronics Letters**, Vol. 20, No. 8, April 12th 1984, pp. 355-356.
- [15] K. Hagishima, J. Yamada, "400 Mbit/s CMI Transmission Experiment Using A 1.3 um LED", **Electronics Letters**, Vol. 21, No. 1, Jan. 3 1985, pp. 17-18.
- [16] T.V. Muoi, "Receiver Design For Digital Fiber Optic Transmission Using Manchester (biphase) Coding", **IEEE Trans. on Commun.**, Vol. COM-31, May 1983, pp. 608-619.
- [17] M Hecht, A. Guida, "Delay Modulation", **Proc. IEEE**, July 1969, pp. 1314-1316.
- [18] W. R. Hedeman, Jr., "Baseband Recording of Digital Data", **Amer. Nat. Standards Inst.**, X3B6/214, Aug. 10 1978, pp. 5-11.
- [19] J. L. Lo Cicero, D. J. Costello, Jr., L. C. Peach, "Characteristics Of The Hedeman H-1, H-2, and H-3 Codes", **IEEE Trans. on Commun.**, Vol. COM-29, No. 6, June 1981, pp. 901-908.
- [20] R. W. Wood, "Further Comments On The Characteristics Of The Hedeman H-1, H-2, And H-3 Codes", **IEEE Trans. on Commun.**, Vol. COM-31, No. 1, Jan. 1983, pp. 105-110.
- [21] P. Bylanski, D. G. W. Ingram, **Digital Transmission Systems**, Peregrinus Press Ltd., London, 1976.

- [22] J. J. O'Reilly, "Timing Extraction For Baseband Digital Transmission", **Mathematical Topics In Telecommunications, Non-Linear Operations In Stochastic Processes**, Digest of Colloquium held on 10th Feb. 1981, University of Essex.
- [23] Y. Takasaki, "Timing Extraction in Baseband Pulse Transmission", **IEEE Trans. on Commun.**, Vol. Com-20, No. 8, Oct. 1972, pp. 877-883.
- [24] T. Le-Ngoc, K. Feher, "A Digital Approach To Symbol Timing Recovery Systems", **IEEE Trans. on Commun.**, Vol. Com-28, No.12, Dec. 1980, pp. 1993-1999.
- [25] R. Gangopadhyay, "Timing Recovery In Optical Receivers For NRZ Signalling", **Electronics Letters**, Vol. 22, No. 1, Jan. 2 1986, pp. 38-39.
- [26] C. C. Cock, A. K. Edwards, A. Jessop, "Timing Jitter in Digital Line Systems",
- [27] D. L. Duttweiler, "The Jitter Performance Of Phase-locked Loops Extracting Timing From Baseband Data Waveforms", **BSTJ**, Vol. 55, No. 1, Jan. 1976, pp. 37-58.
- [28] E. Roza, "Analysis of Phase-locked Loops Extracting Circuits For Pulse Code Transmission", **IEEE Trans. on Commun.**, Vol. Com-22, 1974, pp. 1236-1249.
- [29] K. H. Teo, "Error Mechanisms and Clock Recovery On Four-level PWM Optical Fiber Systems", **M.Sc. Thesis**, University of Alberta, Spring 1985.
- [30] R. Rosenberg, D. G. Ross, P. R. Trischitta, D. A. Fishman, C. B. Armitage, "Optical Fiber Repeated Transmission Systems Utilizing SAW Filters", **IEEE Trans. on Sonics and Ultrasonics**, Vol. 30, No. 3, May 1983, pp. 119-125.
- [31] H. H. Witte, S. Moustakas, "Simple Clock Extraction Circuit Using A Self Sustaining Monostable Multivibrator Output Signal", **Electronics Letters**, Vol. 19, No. 21, 1983, pp. 897-898.
- [32] R. C. Houts, T. A. Green, "Comparing Bandwidth Requirements for Binary Baseband Signals", **IEEE Trans. on Commun.**, Vol Com-22, No. 6, June 1973, pp. 1236-1249.

- [33] D. R. Smith, **Digital Transmission Systems**, Van Nostrand Reinhold Co., New York, 1985, pp. 198-203.
- [34] M. G. Pelchat, J. M. Geist, "Surprising Properties of Two-level Bandwidth Compaction Codes", **IEEE Trans. on Commun.**, Vol. Com-23, No. 9, Sept. 1975, pp. 878-883.
- [35] D. J. Morris, **Pulse Code Formats For Fiber Optical Data Communications**, Marcel Dekker Inc., New York, 1983.
- [36] S. Haykin, **Communication Systems**, John Wiley and Sons, New York, 1978, pp. 481-488.
- [37] R. Petrovic, "On the Performance of Binary Coded Signals", **IEEE Trans. on Commun.**, Vol. Com-29, No. 9, Sept. 1981, pp. 1403-1405.
- [38] W. P. Stanley, G. R. Dougherty, R. Dougherty, **Digital Signal Processing**, Reston Publishing Company, 2nd ed., Reston, 1984, pp. 243-250.
- [39] D. R. Smith and I. Garret, "A Simplified Approach to Digital Optical Receiver Design", **Optical and Quantum Electronics**, Vol 10, 1978, pp. 211-221.
- [40] R. G. Smith, S. D. Personick, "Receiver Design for Optical Fiber Communication Systems", **Semiconductor Devices For Optical Communications**, Ed. by H. Kressel, Springer-Verlag, New York, 1980, Chapter 4, pp. 89-160.
- [41] P. Shumate, "Temperature Effects of Dispersion and Loss for High-Bit-Rate LED-Based Lightwave Systems", **Electronics Letters**, Vol. 22, No. 1, Jan 2 1986, pp. 1-2.
- [42] InGaAs/InP 1.3 $\mu$ m Wavelength Surface-Emitting LED's for High-Speed Short Haul Optical Communication Systems, **Journal of Lightwave Technology**, Vol. LT-3, Dec. 1985, pp. 1217-1222.
- [43] H. Fukinuki, T. Ito, M. Aki, "The FS-400M Submarine System", **Journal of Lightwave Technology**, Vol. LT-2, No. 6, Dec. 1984, pp. 754-760.
- [44] T. V. Muoi, "Optical Receiver Design", **Journal of Lightwave Technology**, Vol. LT-2, No. 3, June 1984, pp. 243-267.

- [45] R. D. Hall, H. A. Lancaster, "Prediction and Measurement of Jitter on Digital Line Links", pp. 41-44.
- [46] Ziemer, Tranter, **Principles of Communication**, Houghton Mifflin Co., Boston, 1976.
- [47] J. M. Wozencraft, I. M. Jacobs, **Principles of Communication Engineering**, John Wiley and Sons, 1965, pp. 60-61.
- [48] H. Taub, D. Schilling, **Digital Electronics**, McGraw-Hill, 1977, pp. 557-562.
- [49] Staff of Bell Northern Research and Northern Telecom, **Course Notes on Optical Fibre Communication and Technology**, 1984.
- [50] J. L. Hullet, T. V. Quoi, S. Moustakas, "High-Speed Optical Preamplifiers", **Electronic Letters**, Vol. 13, No. 23, Nov. 10 1977, pp. 688-689.
- [51] J. L. Hullet, S. Moustakas, "Optimum Transimpedance Broadband Optical Preamplifier Design", **Optical and Quantum Electronics**, Vol. 13, 1981, pp. 64-65.
- [52] M. Brain, T. P. Lee, "Optical Receivers for Lightwave Communication Systems", **Journal of Lightwave Technology**, Vol. LT-3, No. 6, Dec. 1985, pp. 1281-1300.
- [53] K. Ogawa, E. L. Chinnock, "GaAs FET Transimpedance Front End Design for a Wideband Optical Receiver", **Electronics Letters**, Vol. 15, No. 20, Sept. 27 1979, pp. 650-651.

## **APPENDIX A: COMPUTER PROGRAMS**

The computer programs used to determine the BER for an N bit filtered data sequence are given here. These programs contain ample documentation. Note that the programs used to convert a random bit sequence into the NRZ, CMI, and Manchester codes are omitted. These programs are identical to Program Petrovic with the exception of the program segment used to encode the incoming data.



```

1      1. PROGRAM RANDOM
2      2. .....
3      3. PROGRAM #1 - RANDOM (LOCATION - RAJU:RANDOM)
4      4. .....
5      5. PURPOSE - TO GENERATE A RANDOM SEQUENCE OF BINARY NUMBERS
6      6. OF LENGTH N.
7      7. .....
8      8. USAGE - A) COMPILATION: RUN *FORTRANVS SCARDS=RANDOM SPUNCH=OBJ.RANDOM SPRINT=L.RANDOM
9      9. B) EXECUTION: RUN OBJ.RANDOM 5=D.RANDOM 6=P.RANDOM T=1
10     10.
11     11. I/O - FILE #5 IS THE INPUT FILE AND IT CONTAINS VALUES
12     12. FOR N AND IX ((I3,I1,I2) FORMAT).
13     13. FILE #6 IS THE OUTPUT FILE: IT CONTAINS THE
14     14. RANDOM BIT SEQUENCE. ((' ',I2) FORMAT).
15     15.
16     16. DESCRIPTION OF VARIABLES:
17     17.
18     18.
19     19.
20     20. IX = ODD NUMBER TO START RANDOM NUMBER GENERATION
21     21. N = NUMBER OF RANDOM BITS TO BE GENERATED
22     22.
23     23. .....
24     24. INPUT VALUES FOR N AND IX
25     25.
26     26.
27     27. READ(5,10)N,IX
28     28. 10 FORMAT(I3,I1,I2)
29     29.
30     30. STORE THE VALUE OF N IN OUPPUT FILE #6
31     31.
32     32. WRITE (6,15) N
33     33. 15 FORMAT(' ',I4)
34     34.
35     35. THIS LOOP GENERATES A RANDOM BINARY BIT STREAM OF LENGTH
36     36. N AND STORES IT IN OUTPUT FILE #6.
37     37.

```

1

2 3

4 5

```
6      38.      DO 100 J=1,N
7      39.      IY=IX*65539
8      40.      IF(IY)5,6,6
9      41.      IY=IY+2147483647+1
10     42.      YFL=IY
11     43.      YFL=YFL*0.4656613E-09
12     44.      NB=YFL*0.5
13     45.      WRITE (6,20) NB
14     46.      FORMAT(' ',I2)
15     47.      IX=IY
16     48.      100 CONTINUE
17     49.      STOP
18     50.      END
```

```

1. PROGRAM PETROV
2. C.....|
3. C
4. C PROGRAM #2.1 - PETROVIC (FILE RAJU:PETROVIC)
5. C
6. C PURPOSE - TO INPUT A RANDOM BINARY STRING OF LENGTH N,
7. C WHICH WAS GENERATED BY PROGRAM #1, AND CONVERT IT TO A
8. C PETROVIC ENCODED SEQUENCE OF LENGTH 2*N.
9. C
10. C ENCODING RULES:
11. C
12. C 1 IS ENCODED BY 11 AND 00 ALTERNATELY.
13. C 0 IS ENCODED BY 10 AFTER 11 AND 01, AND BY 01 AFTER 00 AND 10.
14. C NOTE THAT THE PETROVIC CODE IS A 18-28 CODE. THUS IF
15. C IF T = INCOMING BIT INTERVAL, THEN THE OUTGOING
16. C BIT INTERVAL IS T/2.
17. C
18. C USAGE - A) COMPILATION: RUN *FORTRANVS SCARDS=PETROVIC SPUNCH=OBJ.PETROVIC SPRINT=L.PETROVIC
19. C B) EXECUTION: RUN OBJ.PETROVIC 5=P.RANDOM 6=P.PETROVIC T=1
20. C
21. C I/O - FILE #5 IS THE INPUT AND CONTAINS THE RANDOM BINARY
22. C SEQUENCE. FILE #6, THE OUTPUT, CONTAINS THE
23. C ENCODED PETROVIC SEQUENCE.
24. C
25. C
26. C DESCRIPTION OF VARIABLES:
27. C
28. C N - NUMBER OF INCOMING BITS
29. C M - NUMBER OF OUTGOING BITS. (N*2)
30. C F1 - FLAG FOR ONES
31. C F0 - FLAG FOR ZEROS
32. C IN = VALUE OF INCOMING BIT (0 OR 1)
33. C OUT1 = VALUE OF OUTGOING BIT FOR 1ST HALF OF THE BIT INTERVAL T
34. C OUT2 = VALUE OF OUTGOING BIT FOR 2ND HALF OF THE BIT INTERVAL T
35. C
36. C .....
37. C
38. C INTEGER N,M,F1,F0,IN,OUT1,OUT2
39. C

```

```

3      CHARACTER*15 CODE
41.
42. C INITIALIZE VARIABLES
43. C
44. READ(5,10) N
45. FORMAT(' ',I4)
46. M = N*2
47. F1 = 0
48. FO = 0
49. CODE = 'PETROVIC CODE'
50.
51. C STORE NAME OF CODE AND M IN OUTPUT FILE #6.
52. C
53. WRITE (6,15) CODE
54. FORMAT(' ',A15)
55. WRITE (6,20) M
56. FORMAT(' ',I4)
57. C
58. C THIS LOOP ENCODES THE INCOMING BIT STREAM.
59. C
60. DO 100 J = 1,N
61. READ (5,30) IN
62. FORMAT(' ',I2)
63. IF (IN .EQ. 1) THEN
64. C WE HAVE RECEIVED A 1
65. C
66. C IF (F1 .EQ. 1) THEN
67. C
68. C A 00 WAS SENT FOR THE LAST 1, THUS SEND 11
69. C
70. OUT1 = 1
71. OUT2 = 1
72. C
73. C SET FLAGS SO THAT A 00 WILL BE SENT FOR THE NEXT 1 AND
74. C A 10 WILL BE SENT IF THE NEXT RECEIVED BIT IS A 0.
75. C
76. F1 = 0
77. FO = 1
78. ELSE
79.

```

```

80. C
81. C A 11 WAS SENT FOR THE LAST INCOMING 1, THUS SEND OO
82. C
83. OUT1 = O
84. OUT2 = O
85. F1 = 1
86. FO = O
87. ENDIF
88. ELSE
89.
90. C A 0 IS RECEIVED, A 10 SHOULD BE SENT IF FO = 1, AND O1 SHOULD
91. BE SENT IF FO = O.
92. IF (FO EQ 1) THEN
93. OUT1 = 1
94. OUT2 = O
95. FO = O
96. ELSE
97. OUT1 = O
98. OUT2 = 1
99. FO = 1
100. ENDIF
101. ENDIF
102.
103. C THE INCOMING BIT HAS BEEN ENCODED: OUTPUT THE ENCODED BITS
104. C
105. 90 WRITE (6,65) OUT1,OUT2
106. 65 FORMAT('11.2X.11)
107. 100 CONTINUE
108. STOP
109. END

```

```

1. PROGRAM SPECTR
2. C
3. C
4. C PROGRAM #3 - SPECTRA (FILE RAJU:SPECTRA)
5. C
6. C PURPOSE - TO DETERMINE THE SPECTRAL CONTENT OF THE
7. C CODED SEQUENCE OF BINARY BITS GENERATED BY
8. C PROGRAMS 2.1 TO 2.5. FFT IS PERFORMED BY THE
9. C IMSL LIBRARY ROUTE FFTRC.
10. C
11. C USAGE - A) COMPILATION: RUN *FORTRANVS SCARDS*SPECTRA SPUNCH*OBJ SPECTRA SPRINT=L SPECTRA
12. C B) EXECUTION: RUN OBJ.SPECTRA*IMSLIB 5=P.PETROVIC 6=S.PETROVIC T=1
13. C
14. C I/C - FILE #5 IS THE INPUT FILE; IT IS GENERATED BY PROGRAM
15. C 2.1, 2.2, 2.3, 2.4, OR 2.5. FILE #5 IS THE OUTPUT
16. C FILE; IT CONTAINS THE SPECTRAL DISTRIBUTION
17. C
18. C DESCRIPTION OF VARIABLES:
19. C
20. C M - NUMBER OF BITS IN CODED SEQUENCE
21. C
22. C NDATA - NUMBER OF TIME DOMAIN DATA POINTS THAT WILL BE
23. C TRANSFORMED BY THE FFT ROUTINE
24. C
25. C NSPRO - THE FACTOR BY WHICH EACH DATA BIT WILL BE
26. C SPREAD OUT BY, I.E., EACH DATA BIT WILL BE REPRESENTED BY
27. C NSPRO POINTS. WE HAVE TO SPREAD OUT THE BITS SO THAT
28. C CAN GET FREQUENCY RESOLUTION
29. C
30. C TDATA - ARRAY THAT CONTAINS THE TIME DOMAIN DATA POINTS
31. C
32. C CFDATA - COMPLEX ARRAY CONTAINS THE FREQUENCY INFORMATION
33. C
34. C IWK, WK - WORK VECTORS REQUIRED BY THE FFTRC IMSLLIB
35. C ROUTINE
36. C
37. C
38. C
39. C DECLARATION OF VARIABLES

```

```

2      40.      C
3      41.      C   INTEGER IWK(20), IWC(20)
4      42.      C   REAL WK(1), TDATA(4096)
5      43.      C   COMPLEX CFDATA(4096), CONJG, CABS
6      44.      C   CHARACTER*15 CODE
7
8      45.      C   INITIALIZE VARIABLES
9      46.      C
10     47.      C
11     48.      C   NSPRD = 16
12     49.      C   READ (5,*) CODE
13     50.      C   FORMAT('A15')
14     51.      C   READ (5,15) M
15     52.      C   FORMAT('I4')
16     53.      C   NDATA = M*NSPRD
17     54.      C   DO 30 J = 1, M, 2
18     55.      C     J1 = J + 1
19     56.      C     READ (5,20) K1,K2
20     57.      C     FORMAT('I1,2X,I1')
21     58.      C     TDATA(J) = K1
22     59.      C     TDATA(J1)=K2
23     60.      C   CONTINUE
24     61.      C
25     62.      C   SPREAD OUT TDATA TO NSPRD POINTS PER SYMBOL
26     63.      C
27     64.      C   DO 60 K = 1, M
28     65.      C     KK = NSPRD*(M - K)
29     66.      C     N1 = M + 1
30     67.      C     XK1 = 1.0*TDATA(N1 - K)
31     68.      C     DO 70 JJ = 1, NSPRD
32     69.      C       TDATA(KK + JJ) = XK1
33     70.      C     CONTINUE
34     71.      C   CONTINUE
35     72.      C   PRINT55, (TDATA(I), I = 1,256)
36     73.      C   FORMAT('16F4.1')
37     74.      C
38     75.      C   OBTAIN THE FREQUENCY SPECTRA
39     76.      C
40     77.      C   CALL FFTRC(TDATA, NDATA, CFDATA, IWK, WK)
41     78.      C
42     79.      C   DIVIDE BY NDATA TO GET THE PROPER MAGNITUDES
43     80.      C   MIRROR TO OBTAIN THE SPECTRA FOR NEGATIVE FREQUENCIES

```

```

81. C ALSO, WE HAVE TO TAKE THE CONJUGATE OF THE POSITIVE
82. C FREQUENCY SPECTRA TO GET THE CORRECT SPECTRA
83. C
84. NDATA2 = NDATA/2
85. DO 80 KF = 2, NDATA2
86.   CFDATA(NDATA+2-KF) = CFDATA(KF)/NDATA
87. CONTINUE
88. NDTA21 = NDATA2 + 1
89. DO 90 I = 1, NDTA21
90.   CFDATA(I) = CONJG(CFDATA(I))/NDATA
91. CONTINUE
92. C
93. C THIS NEXT PART OF CODE IS FOR TEST PURPOSES ONLY.
94. C TAKE THE INVERSE TRANSFORM AND PRINT OUT THE FIRST
95. C 256 VALUES
96. C
97. C CALL FFT2C (CFDATA, 12, IWC)
98. C DO 110 J = 1, NDATA
99.   TDATA(J) = REAL(CFDATA(J))
100.  WRITE(*,120) (TDATA(I), I = 1, 256)
101.  FORMAT(' ', 16F5.1)
102. C
103. C DISCRETE FREQUENCY LINES OCCUR EVERY 1/TO HZ, WHERE TO IS
104. C THE PERIOD IN THE TIME DOMAIN. NSPRD POINTS CORRESPOND
105. C TO THE BIT INTERVAL T. FURTHERMORE THERE ARE NSPRD*M
106. C POINTS. THUS TO = M*T AND DF = 1/TO IS THE FREQUENCY
107. C INTERVAL BETWEEN DISCRETE LINES (NORMALIZE TO T).
108. C
109. C DF = 1./M
110. C
111. C WRITE NAME OF CODE, NDATA, NSPRD, DF AND SPECTRAL VALUES
112. C INTO OUTPUT FILE #6.
113. C
114.   WRITE (6,12) CODE
115.   WRITE (6,132) NDATA, NSPRD
116.   FORMAT(' ', 14.2X, 14)
117.   WRITE (6,130) DF
118.   FORMAT(' ', E14.7)
119.   DO 140 I = 1, NDATA
120.     WRITE (6,135) CFDATA(I)
121.     FORMAT(' ', E14.7, 2X, E14.7)
122.   CONTINUE
123.   STOP
124.   ENQ

```



```

1. PROGRAM FILE .....
2. C
3. C
4. C
5. C PROGRAM #4 - FILTER (FILE RAJU:FILTER)
6. C
7. C PURPOSE - TO WEIGHT THE SPECTRAL COMPONENTS GENERATED
8. C BY PROGRAM #3 (SPECTRA) BY A FILTER TRANSFER FUNCTION.
9. C FIND THE INVERSE FFT, AND SAMPLE THE RESULTING WAVEFORM
10. C TO DETERMINE THE PROBABILITY OF ERROR (BER).
11. C AT PRESENT, A NTH ORDER BUTTERWORTH
12. C TRANSFER FUNCTIONS IS EMPLOYED.
13. C
14. C USAGE - A) COMPILATION: RUN *FORTRANVS SCARDS=FILTER SPUNCH=OBJ.FILTER SPRINT=L.FILTER
15. C B) EXECUTION: RUN OBJ.FILTER**IMSLIB 5=S.PETROVIC 6=F.PETROVIC 7=IN.FIL T=2
16. C
17. C I/O - FILE #5 CONTAINS THE SPECTRAL CONTENT OF THE CODE
18. C FILE #7 IS ALSO AN INPUT FILE. IT CONTAINS PARAMETERS
19. C THAT THE USER WILL CHANGE OFTEN, E.G., NOISE SPECTRAL
20. C DENSITY, FILTER ORDER, FILTER 3DB BANDWIDTHS.
21. C FILE #6 IS THE OUTPUT; IT CONTAINS THE BER, FILTER
22. C ORDER AND 3DB FREQUENCY, NOISE SPECTRAL DENSITY,
23. C FILTERED TIME DOMAIN VALUES AND OTHER QUANTITIES OF
24. C INTEREST.
25. C
26. C DESCRIPTION OF VARIABLES:
27. C
28. C CFDATA - ARRAY THAT CONTAINS THE SPECTRAL COMPONENTS
29. C
30. C NDATA - NUMBER OF FREQUENCY COMPONENTS (POS AND NEG)
31. C
32. C MM - 2**MM = NDATA
33. C
34. C FBAUD - SYMBOL RATE (2*INCOMING BIT RATE)
35. C
36. C FO - 3DB CUTOFF FREQUENCY OF FILTER
37. C
38. C F - FREQUENCY
39. C

```

```

40. C      CBUTTR - FIRST ORDER BUTTERWORTH TRANSFER FUNCTION (COMPLEX VARIABLE)
41. C      ORDER - FILTER ORDER
42. C      = 1 IF 1ST ORDER BUTTERWORTH IS DESIRED
43. C      = 2 IF 2ND ORDER
44. C
45. C      NETA - WHITE GAUSSIAN POWER SPECTRAL DENSITY
46. C
47. C      SIGMA - SORT(NOISE POWER AT OUTPUT OF FILTER)
48. C
49. C      FC - ARRAY THAT CONTAINS THE FOLLOWING CONSTANT: (NOISE EQUIVALENT BANDWIDTH)/FILTER 3DB POIN
50. C
51. C      PE - PROBABILITY OF ERROR
52. C
53. C      Q(X) - THE Q FUNCTION (USED TO DETERMINE PE)
54. C
55. C
56. C
57. C
58. C      DECLARATION OF VARIABLES
59. C
60. C      INTEGER IWC(20), ORDER
61. C      REAL TDATA(4096), FO(25), FC(10), NETA
62. C      COMPLEX CFDATA(4096), CDATA(4096), CH, COMJG, CMLPX, CBUTTR
63. C      CHARACTER*15 CODE
64. C
65. C      INPUT VALUE FOR VARIABLES AND PRINT THEM IN OUTPUT FILE
66. C
67. C      READ (5,11) CODE
68. C      FORMAT(' ',A15)
69. C      WRITE (6,12) CODE
70. C      FORMAT(' ',A15)
71. C      READ (5, 10) NDATA, NSPRD
72. C      FORMAT(' ',14.2X,14)
73. C      WRITE(6,14)NDATA, NSPRD
74. C      NDATA2 = NDATA/2
75. C      NDT21 = NDATA2 + 1
76. C      READ (5,15) DF
77. C      FORMAT(' ',E14.7)
78. C      WRITE (6,16) DF
79. C

```

2  
3  
4  
5  
6  
7  
8  
9  
10  
11  
12  
13  
14  
15  
16  
17  
18

```

19      80.      16      FORMAT(' ',DF = ',E14.7)
      81.      C
      82.      C READ THE SPECTRAL DATA
      83.      C
      20      DO 30 I = 1, NDATA
      21      READ (5,20) CFDATA(I)
      22      FORMAT(' ',E14.7,2X,E14.7)
      23      30      CONTINUE
      88.      C
      89.      C CALCULATE MM: 2**MM = NDATA (MM IS REQUIRED FOR THE FF2C ROUTINE).
      90.      C
      24      XNDATA = NDATA
      25      MM = INT( LOG(XNDATA)/LOG(2.))+ 0.5)
      26      WRITE (6,28)MM
      27      FORMAT(' ',MM = '.13)
      28      READ (7,25)NSAMPL, INC
      29      FORMAT(12.1X,12)
      30      WRITE(6,27)NSAMPL, INC
      31      FORMAT(' ',SAMPLING TIME IS ',12.'/16*T . INC = '.12)
      32      READ (7,35) ORDER, NFO
      33      FORMAT(12.1X,12)
      34      35      READ (7,55) FBAUD
      102.      C
      103.      C INPUT THE NOISE POWER SPECTRAL DENSITY
      104.      C
      35      READ (7,55) NETA
      36      WRITE(6,57)NETA
      37      FORMAT(' ',NETA = ',E14.7)
      108.      C
      109.      C READ THE DESIRED FILTER 3DB FREQUENCIES
      110.      C
      38      DO 50 I = 1, NFO
      39      READ (7,55) FO(I)
      40      FORMAT(E14.7)
      41      50      CONTINUE
      42      PI = 3.141592654
      43      FC(1) = PI/2.
      44      FC(2) = 1.111
      45      FC(3) = 1.047
      119.      C
      120.      C WRITE THE FILTER CONSTANT
      121.      C
      46      WRITE (6,58) FC(ORDER)
      47      FORMAT(' ', 'FILTER NOISE CONSTANT = ',F7.3)

```

```

124. C
125. C
126. C THIS MAIN LOOP DOES THE FILTERING AND ERROR CALCULATIONS.
127. C
128. C
129. C DO 500 I = 1, NFO
130. C
131. C NORMALISE THE FILTER 3DB FREQ. TO THE SYMBOL RATE
132. C
133. C F3DB = FO(I)/FBAUD
134. C
135. C COPY CONTENTS OF CFDATA INTO CDATA. THE CONTENTS OF THE
136. C ARRAY CONTAINING THE FREQUENCY COMPONENTS WILL BE REPLACED
137. C BY THE TIME DOMAIN POINTS WHEN THE INVERSE FFT IS INVOKED.
138. C THUS, WE HAVE TO USE TWO ARRAYS.
139. C
140. C DO 100 J = 1, NDATA
141. C CDATA(J) = CFDATA(J)
142. C CONTINUE
143. C
144. C MULTIPLY POS. FREQUENCY POINT BY THE FILTER TRANSFER FUNC.
145. C AT THAT POINT (CF)
146. C THE NEG. FREQUENCY PART IS MULTIPLIED BY THE CONJUG(CF)
147. C
148. C DO 120 J = 2, NDATA2
149. C F = (J-1)*DF
150. C
151. C DEPENDING UPON THE ORDER, EVALUATE THE BUTTERWORTH TRANSFER
152. C FUNCTION AT FREQUENCY F.
153. C FOR ORDER 1, H(F) = 1/(1 + JF/F3DB):
154. C FOR ORDER 2, H(F) = 1/(1 + J1.41421*F/F3DB + (JF/F3DB)**2)
155. C
156. C IF (ORDER .EQ. 1) THEN
157. C CH = CMPLX (1. , F/F3DB)
158. C END IF
159. C IF (ORDER .EQ. 2) THEN
160. C HR = 1. - (F/F3DB)**2
161. C CH = CMPLX(HR , 1.4142136*F/F3DB)
162. C END IF
163. C IF (ORDER .EQ. 3) THEN
164. C HR = 1. - 2.*(F/F3DB)**2

```

```

64      HI = 2.*F/F3DB - (F/F3DB)**3
65      CH = CMLPX (HR, HI)
66      END 15
67      IF (ORDER .GT. 4) THEN
68          C
69          ORDER IS NOT 1, 2, 3. AT THIS TIME THE PROGRAM DOES NOT
70          CATER FOR ANYTHING ELSE, THUS PRINT ERROR MESSAGE AND
71          TERMINATE THE PROGRAM.
72          WRITE (6, 122)
73          FORMAT (' ', '*ERROR* : ORDER IS > 3. CANNOT SOLVE')
74          STOP
75          END IF
76          CDATA(J) = CDATA(J)/CH
77          CDATA(NDATA + 2 - J) = CDATA(NDATA + 2 - J)/CONJG(CH)
78          CONTINUE
79          F = NDATA*DF
80          C
81          CDATA(NDT21) STILL REMAINS TO BE WEIGHTED
82          IF (ORDER .EQ. 1) THEN
83              CH = CMLPX(1., F/F3DB)
84              ELSE
85              HR = 1. - (F/F3DB)**2
86              CH = CMLPX(HR, 1.4142136*F/F3DB)
87              END IF
88              CDATA(NDT21) = CDATA(NDT21)/CH
89          C
90          OBTAIN THE FILTERED TIME DOMAIN RESPONSE BY TAKING THE
91          INVERSE FOURIER TRANSFORM
92          CALL FFT2C(CDATA, MM, IWC)
93          STORE THE REAL PART OF THE SIGNAL IN TDATA
94          DO 150 J = 1, NDATA
95              TDATA(J) = REAL(CDATA(J))
96              CONTINUE
97          C
98          WRITE THE FIRST 256 POINTS OF THE FILTERED TIME DOMAIN
99          SIGNAL INTO FILE #6
100         ALSO WRITE THE FILTER ORDER AND THE 3DB FREQUENCY.
101         WRITE (6, 209)
102
103
104
105
106
107
108
109
110
111
112
113
114
115
116
117
118
119
120
121
122
123
124
125
126
127
128
129
130
131
132
133
134
135
136
137
138
139
140
141
142
143
144
145
146
147
148
149
150
151
152
153
154
155
156
157
158
159
160
161
162
163
164
165
166
167
168
169
170
171
172
173
174
175
176
177
178
179
180
181
182
183
184
185
186
187
188
189
190
191
192
193
194
195
196
197
198
199
200
201
202
203
204
205
206
207

```

```

88      208.  FORMAT('-',',', 'FILTERED TIME DOMAIN SIGNAL')
89      209.  WRITE (6,212) ORDER
90      210.  FORMAT('-',',', 'ORDER = ',I2,', (BUTTERWORTH)')
91      211.  WRITE (6,214) FO(I)
92      212.  FORMAT('-',',', 'FILTER 3DB FREQUENCY = ',E14.7)
93      213.  WRITE (6,211) (TDATA(K), K=1,256)
          214.  FORMAT('-',',',16F7.3)
          215.  C
          216.  C  ERROR CALCULATIONS
          217.  C
          218.  C  PE = O.O
          219.  C  PEMAX = O.O
          220.  C  SIGMA = SQRT(NETA * FC(ORDER) * F3DB * FBAUD)
          221.  C
          222.  C  STORE THE VALUE OF SIGMA IN OUTPUT FILE
          223.  C
          224.  C  WRITE (6,244) SIGMA
94      224.  FORMAT('-',',', 'SIGMA = ',F7.3)
95      225.  DO 300 K = NSAMPL, NDATA, INC
96      226.  C
          227.  C  SAMPLE THE SIGNAL: THE SIGNAL IS SAMPLED STARTING WITH
          228.  C  T = NSAMPL/16*T AND EVERY INC/16 * T SECONDS LATER, WHERE T =
          229.  C  1/FBAUD.
          230.  C
          231.  C  XM = TDATA(K)
          232.  C  X = ABS((O.5 - XM)/SIGMA)
          233.  C
          234.  C  Q(X) IS THE PROBABILITY OF ERROR FOR A GIVEN NOISE POWER
          235.  C  (SIGMA**2). DECISION THRESHOLD (O.5 IN THIS CASE). AND
          236.  C  HEIGHT OF THE SIGNAL AT SAMPLING TIME (XM)
          237.  C
          238.  C  PE1 = Q(X)
          239.  C
          240.  C  PEMAX IS THE MAXIMUM BIT ERROR PROBABILITY
          241.  C
          242.  C  IF (PE1 .GT. PEMAX) THEN
          243.  C    PEMAX = PE1
          244.  C  END IF
          245.  C
          246.  C  KEEP A RUNNING SUM OF PE
          247.  C

```

```

106      PE = PE + PE1
107
108
248      PE = PE + PE1
249      CONTINUE
250
300      C
301      C   PE = PE / NDATA * INC
302      C
303      C   WRITE THE PEMAX AND PE INTO FILE #6
304      C
305      C   WRITE (6,348) PEMAX
306      C   FORMAT (' ', 'MAXIMUM BIT ERROR PROBABILITY IS ', E14.7)
307      C   WRITE (6, 350) PE
308      C   FORMAT (' ', 'AVERAGE PROBABILITY OF ERROR = ', E14.7)
309      C   CONTINUE
310      C   STOP
311      C   END

```

```

266      C
267      C   THE Q FUNCTION
268      C   FOR X > 3 THE Q FUNCTION CAN BE APPROXIMATED BY THE EXPRESSION:
269      C   Q(X) ~ EXP( -(X**2/2) ) / ( SORT(2*PI)*X )
270      C
271      C   REAL FUNCTION Q(X)
272      C   FORMAT(' ', 'HELLO')
273      C   PI = 3.141592654
274      C   Q = EXP( -(X**2/2) ) / ( SORT(2*PI)*X )
275      C   RETURN
276      C   END

```

**END**

**28.03.88**

**FIN**